

Image Cover Sheet

CA001524

CLASSIFICATION

UNCLASSIFIED

SYSTEM NUMBER

513477

**TITLE**

Investigation of Decoupling Material Performance with a Transmission Loss Model
and Acoustic Intensity Measurements

System Number:**Patron Number:****Requester:****Notes:****DSIS Use only:****Deliver to:**



INVESTIGATION OF DECOUPLING MATERIAL PERFORMANCE WITH A TRANSMISSION LOSS MODEL AND ACOUSTIC INTENSITY MEASUREMENTS

K. Klein – Q. Liu – J. Y. Guigné

DEFENCE RESEARCH ESTABLISHMENT ATLANTIC

Contractor Report
DREA CR 1999-127
September 1999



National
Defence

Défense
nationale

Canada



National Defence
Research and
Development Branch

Défense nationale
Bureau de recherche
et développement

DREA CR 1999-127

**INVESTIGATION OF DECOUPLING MATERIAL
PERFORMANCE WITH A TRANSMISSION LOSS MODEL
AND ACOUSTIC INTENSITY MEASUREMENTS**

K. Klein, Q. Liu, and J.Y. Guigné

GUIGNÉ INTERNATIONAL LIMITED
685 St. Thomas Line
Paradise, Newfoundland
A1L 1C1

Scientific Authority

Jeffrey P. Szabo
JP Szabo

W7707-7-5409
Contract Number

September 1999

CONTRACTOR REPORT

Prepared for

**Defence
Research
Establishment
Atlantic**



**Centre de
Recherches pour la
Défense
Atlantique**

Canada

Abstract

The complex dilatational moduli of three closed cell foam materials and one elastomeric material were determined by mechanical excitation of thin samples. The neoprene/EPT/SBR, polyvinylchloride, and ethylvinylacetate foams had moduli that ranged from 0.2 MPa to 3 MPa in the 100 – 900 Hz frequency range. The decoupling performance of these materials was then determined by applying them to steel substrates that were mechanically excited, and measuring the effect of the coatings on the radiated sound. Unlike previous studies where the test plates were supported at the corners and semi-submerged, in this study the plates were clamped at the edges and backed by an air filled concrete enclosure. This "concrete box" was submerged into a water filled tank and the radiated sound was determined by intensity mapping in the near field of the plate. Because the net radiated acoustic power was not uniformly positive across the frequency range studied (100 – 900 Hz), a quantity related to the near field acoustic power, $\sum |\tilde{I}| dA$, was used to quantify the effect of the coating. The experimental decoupling

behaviour of the coatings was compared to that predicted by a one dimensional transmission loss model for the 4 layer system: air/ steel/ coating/ water; or for the 5 layer system that included the finite dimensions of the water layer in the tank: air/ steel/ coating/ water/ air. Several of the substrate/ coating combinations were predicted to have large decoupling amplification peaks based on their measured material properties and the one dimensional model. Experimentally, these peaks were either much smaller than predicted or not observed at all. This discrepancy was explained by the fact that edges of the steel substrate were clamped, precluding a mass-spring resonance effect which is responsible for the amplification.

Résumé

On a déterminé le module de dilatation complexe de trois mousses à alvéoles fermés et d'un matériau élastomère par excitation mécanique d'échantillons minces. Les modules des trois mousses, soit le néoprène/EPT/SBR, le poly(chlorure de vinyle) et l'acétate éthylvinyle, se situaient entre 0,2 et 3 MPa, pour l'intervalle de fréquence de 100-900 Hz. On a ensuite déterminé la performance de découplage de ces matériaux en revêtant des substrats en acier qui étaient ensuite excités mécaniquement, puis en mesurant l'effet du revêtement sur l'onde acoustique émise. À la différence des études antérieures, où les plaques mises à l'essai étaient fixées par les coins à l'aide de pinces et étaient à moitié submergées, la présente étude a été réalisée avec des plaques dont les bords étaient fixés par des pinces et qui étaient soutenues par une enceinte en béton remplie d'air. Ce « coffre en béton » était submergé dans un réservoir rempli d'eau et l'onde acoustique émise était mesurée en cartographiant l'intensité dans le champ proche de la plaque. La puissance acoustique nette émise n'étant pas uniformément positive dans tout l'intervalle de fréquence étudié (100-900 Hz), on a utilisé une valeur associée à la puissance acoustique du champ proche, $\Sigma |f| dA$, pour quantifier l'effet dû au revêtement. On a comparé le comportement de découplage des revêtements mis à l'essai au comportement prévu par un modèle unidimensionnel de perte par transmission, et ce, pour le système à quatre couches (air/acier/revêtement/eau) et pour le système à cinq couches qui comprend les dimensions finies de la couche d'eau dans le réservoir (air/acier/revêtement/eau/air). Les prévisions basées sur les propriétés mesurées du matériau et le modèle unidimensionnel suggéraient que plusieurs combinaisons substrat/revêtement présenteraient d'importants pics d'amplification de découplage. D'après les résultats expérimentaux, ces pics, lorsqu'ils étaient observés, étaient beaucoup plus petits que les pics prévus. On explique cette divergence par le fait que les bords du substrat d'acier étaient fixés, ce qui empêchait l'effet de résonance masse-ressort responsable de l'amplification.

DREA CR 1999-127

Investigation of Decoupling Material Performance with a Transmission Loss Model and Acoustic Intensity Measurements

K. Klein, Q. Liu, and J.Y. Guigné

EXECUTIVE SUMMARY

Background The use of decoupling tiles attached to the exterior of a ship's hull can be a very effective means of reducing ship radiated noise. It has been observed in both reduced scale tests¹ and in full scale tests² that the coating may actually increase the radiated noise below a critical "cut-off" frequency. This has been explained in terms of a simplified one dimensional transmission loss model¹ of the air/ steel/ coating/ water system. The purpose of this work was to measure the dynamic plate modulus of several foam materials, and to predict the decoupling performance of these materials on various substrates using the one dimensional model. The predicted performance was compared to the experimental decoupling performance, which was determined using a method based on the use of sound intensity and a "concrete box" measurement platform.

Principle Results Several of the substrate/ coating combinations were predicted to have large decoupling amplification peaks (see above) based on their measured material properties and the one dimensional model. Experimentally, these peaks were either much smaller than predicted or not observed at all. This discrepancy was explained by the fact that edges of the steel substrate were clamped, precluding a mass-spring resonance effect which is responsible for the amplification.

Significance of Results The use of a one dimensional model to predict the performance of decoupling materials for ship hull tiles must be undertaken with care at frequencies below the cut-off frequency. This model would be expected to better represent floating structures than plates whose edges are clamped or simply supported. At frequencies well above the cut-off frequency, the one dimensional model gives similar results to the VIBRO code³, which assumes simply supported boundary conditions.

Future Work This study raises some interesting questions on the applicability of various models to tile design for surface ships. Future experimental and modelling work on hull tiles should attempt to address the issues raised in this report, including the effect of boundary conditions on the predicted decoupling performance.

J. Szabo September 1999

¹ J.R.C. House, "Considerations for Underwater Decoupling Treatments", Proceedings of the Institute of Acoustics, Volume 13, Part 3 (1991).

² Minutes of Meetings, Visit of Dr. Jeff Szabo to TNO-TPD, TNO-TPD Reference HAG-MOM-990037, 14 June 1999

³ Based on calculations done at DREA.

Table of Contents

Abstract.....	i
Executive Summary	iii
1.0 Introduction.....	1
2.0 Transmission Loss Model.....	3
2.1 Four Layer Model	3
2.2 Five Layer Model.....	5
3.0 Dilatational Modulus Measurement.....	8
3.1 Modulus Measurements of Elastomers.....	8
3.2 Experimental setup for infinite backing mass.....	9
3.3 Experimental setup for finite backing mass.....	12
4.0 Decoupling Performance Prediction	19
4.1 Example Prediction.....	19
4.2 Model Comparison - Four Versus Five Layers.....	20
5.0 Acoustic Measurements.....	22
5.1 Concrete Enclosure	22
5.2 Experimental Configuration.....	26
5.3 Measured Plates and Coatings	31
5.4 Measured Frequency Response.....	32
6.0 Quantifying The Radiated Field	34
6.1 Examining the Net Radiated Power.....	34
6.2 Absolute Power.....	37
6.3 Comparison of Bare and Coated Plates	38
6.4 Examining The Spatial Distribution of Measured Intensity	40
7.0 Experimental and Modelled Decoupling Performance	43

7.1 Experimental Decoupling Performance 43

7.2 Observed Decoupling Performance -Tank and Barge Configurations 45

7.3 Example of a Partially Coated Plate 47

7.4 Example of Reversing the Coating to the Air Side..... 48

7.5 Comparison of Experimental and Modelled Performance..... 49

8.0 Discussion 53

REFERENCES..... 56

List of Figures

Figure 2.1: Geometry for 4 layer transmission loss model.....	3
Figure 2.2: Geometry for 5 layer transmission loss model.....	5
Figure 3.1: Infinite backing mass measurement configuration.....	9
Figure 3.2: Diverging values of Dilatational modulus with rigid backing mass.	12
Figure 3.3: Finite backing mass measurement configuration.....	13
Figure 3.4: Values of the Dilatational modulus with the finite backing mass configuration.....	14
Figure 3.5: Measured dilatational modulus for V710 foam with bonded surfaces... 15	
Figure 3.6: Measured dilatational modulus for SC4116 foam with bonded surfaces.	16
Figure 3.7: Measured dilatational modulus for VA80 foam with bonded surfaces..	17
Figure 4.1: Decoupling performance (3mm plate with 3mm V710 foam) - 4 versus 5 layer model.....	19
Figure 4.2: Decoupling performance (9.5 mm plate with 25mm SC4116 foam) - 4 versus 5 layer model.....	21
Figure 5.1: Concrete enclosure design.	23
Figure 5.2: Steel plate secured to concrete box.	24
Figure 5.3: View of plate suspended above concrete enclosure.	25
Figure 5.4: Acoustic intensity measurement grid.	26
Figure 5.4: View of the apparatus positioning the hydrophones over the plate.	27
Figure 5.5: Measurement equipment setup.....	28
Figure 5.6: Measured intensity spectra for 4 hydrophone spacings.	30
Figure 5.7: Example of intensity spectra as a function of height above plate.	31
Figure 5.8: Measured FRF of 9.5mm thick bare plate.	33
Figure 6.1: Net radiated power for 9.5mm bare plate.....	35
Figure 6.2: The calculated net acoustic power versus the quantity of measurement positions.....	36
Figure 6.3: Normalized net and absolute power from bare 9.5mm plate.....	37
Figure 6.4: Normalized net and absolute power from a 9.5mm plate coated with 25mm of SC-4116.	38
Figure 6.5: Comparison of 9.5mm plate (bare vs 25mm SC4116 coated) using absolute power normalized to square force.....	39
Figure 6.6: Comparison of 9.5mm plate (bare vs 25mm SC4116 coated) using absolute power normalized to input power.	40
Figure 6.7: The spatial distribution of intensity from the bare 9.5mm plate in a modal band.	41
Figure 6.8: The spatial distribution of intensity from the 9.5mm coated plate (25mm of SC-4116) in the same modal band.	41
Figure 7.1: Experimental decoupling performance for a 23mm coating of SC4116 on a 9.5mm steel plate.....	44
Figure 7.2: Experimental decoupling performance for a 23mm coating of SC4116 on a 9.5mm steel plate suspended with vibration supports.	46
Figure 7.3: Comparison of decoupling performance for a 23mm coating of SC4116 on a 9.5mm steel plate – Barge configuration vs Tank configuration.....	47

Figure 7.4: Experimental decoupling performance for a partially coated 9.5mm steel plate with 23mm SC4116. 48

Figure 7.5: Experimental and modelled decoupling performance for 3mm of V710 on 3mm plate..... 50

Figure 7.6: Experimental and modelled decoupling performance for 12mm of VA80 on 9.5mm plate..... 51

Figure 7.7: The effect of a 50% increase in the dilatational modulus..... 52

List of Tables

Table 2.1: Properties of layered media. 4

Table 3.1: Fitted Modulus Expressions..... 18

Table 5.1: Plate and coating combinations. 32

Table A.1 Elastomer and foam descriptions..... 57

1.0 INTRODUCTION

The tactical use of military naval vessels often demands a degree of acoustic stealth. Consequently, there is a need to make ships and submarines acoustically quiet in the marine environment. One means of reducing the sound transmitted into water by a vessel is to coat its hull with special tiles that suppress underwater sound radiation.

The selection of the most suitable tile for the application is not an easy process. There are many choices of tile, with differing principles of operation⁴ and the cost of full scale performance trials is a factor. The hull of a vessel has a large surface area. Full scale tests for each tile type means the purchase and installation of a coating over a large area, an expensive proposition. The full scale cost is the incentive to develop a method that compares tile performance at a reduced scale, to identify the best candidate tile before proceeding to a full scale assessment.

It might appear that the preferred setting for conducting a small scale performance test of a coating would be an open water environment so that the necessary measurements could be made in the acoustic far field⁵ where the radiated energy could be obtained simply from the amplitude of acoustic pressure measurements. The relative merit of different coatings would then reduce to a comparison of their far field pressures. However, open water is typically an uncontrolled environment with an ambient noise level. The ambient noise level is problematic because it limits the sensitivity of pressure measurements. The combination of limited measurement sensitivity, the spreading losses that all acoustic fields suffer in the far field and the introduction of a coating intended to reduce radiated energy increase the difficulty of successful measurements.

An alternative to open water testing is to consider conducting the test in a tank facility where the environment can be controlled. Tank testing requires the measurements of radiated energy to take place much closer to the test specimen, in the near field. The tank boundaries introduce complications in the form of reflection and scattering from the walls, bottom and the water-air interface. The question arises whether a performance assessment can legitimately be made in such an environment.

In both test scenarios it is the measurement of radiated energy that is of interest. The direct measurement of radiated energy is acoustic intensity, and involves paired measurements of acoustic pressure at different positions to get directional energy flow. The advantage of acoustic intensity is that the measurement can be made in the near or far field. Consequently acoustic intensity becomes a potentially useful tool for measuring coating tile performance.

Flexural vibrations are typically the main contributor to the radiation of sound from a structure. For this reason, a coating's performance tends to be judged by its ability to

⁴For example, damping tiles operate by absorbing vibrational energy to directly reduce the amount of vibration in the hull, while decoupling tiles operate by reducing the vibrational coupling between the hull and the water. Both methods lessen the amount of hull vibration radiated into the water. Other types of tiles exist as well.

⁵The far field is the region many wavelengths from the source where the radiated waves tend to follow the relationships for plane waves (see for example, Morse and Ingard, p 310-311). In this region, the acoustic energy is all outward flowing and is proportional to the square of acoustic pressure.

reduce the sound radiated by flexural waves in a plate. The finite boundaries of the plate⁶ introduce modal behaviour (preferred vibrational response at select frequencies with unique operational deflection patterns). This behaviour complicates performance testing because meaningful data tends to be acquired only in regions where there is appreciable response. In addition, the introduction of a coating alters the modal response of the system, and different coatings result in different modal responses. Consequently, data collected for different coatings tends to generate performance data in different frequency regions which can complicate the comparison of relative performance.

It is believed that the performance should be related to how much acoustic energy is radiated into the water for each coating as a function of input excitation. However, because of the nature of the application, it is not clear how the excitation should be judged. The different action of the coatings (damping versus decoupling) on the structure raises the possibility of introducing additional quantities that acknowledge the effect of the coating on the vibrational response of the plate substrate.

This study was a continuation of a program⁷ to investigate experimental methods for quantifying coating performance in a tank. Several new directions were pursued. A theoretical model was implemented to develop a capability for predicting the level of performance of different coatings on steel plates. The model was a very simplified description of a complex process, but it provided a means of making quantitative predictions for comparison with experiment. Also a method was developed to measure the material properties of the foam coatings. The performance of the coatings depended on their properties which were frequency dependent. Material property measurements provided the data for comparing coatings on the basis of their relative properties, and also the information required by the model in order to make performance calculations. Also, several modifications were made to the experimental test apparatus to improve the test conditions. Several plate and coating combinations were tested in a tank to obtain experimental coating performance. In addition, the theoretical performance calculated with the measured coating properties was compared with the observed experimental performance.

⁶Only an infinite plate will support flexural waves at all frequencies

⁷Klein K and Hamm, C (1997)

2.0 TRANSMISSION LOSS MODEL

The transmission loss model provided a means of theoretically examining how the sound radiated by a plate would be affected by the addition of a coating. In particular it took into account the thicknesses of the base plate and coating, as well as their respective material properties. The output of the transmission loss model was the ratio of output power to input power. The theoretical performance of the coating would be judged on the ability to minimize this ratio.

The particular model selected for this study was based on normally incident plane waves⁸. The assumption of normally incident plane waves simplified the complexity of the problem and facilitated exact equations. It was an appropriate model for the level of effort of this study.

2.1 Four Layer Model

Figure 2.1 illustrates the geometry that was initially assumed for the transmission loss model.

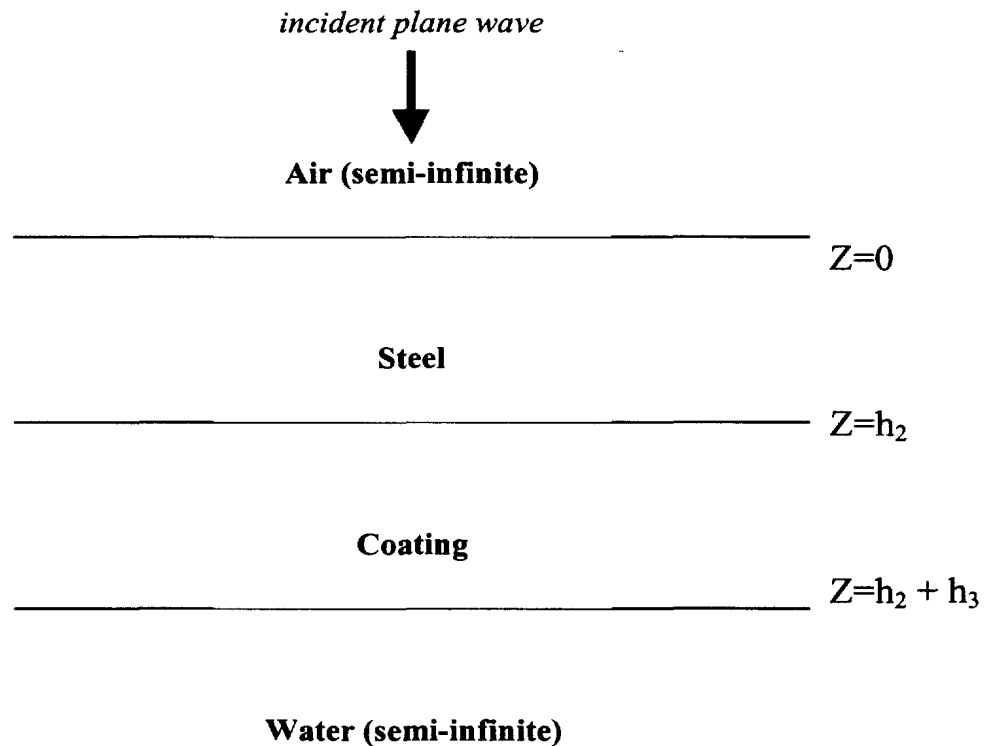


Figure 2.1: Geometry for 4 layer transmission loss model.

⁸ Of the form $A \exp[i(\omega t - kz)]$ for forward propagating waves and $A \exp[i(\omega t + kz)]$ for backward propagating waves

Single frequency plane waves were assumed to be normally incident onto the air side of a steel plate of thickness h_2 . The opposing side of the steel plate was attached to a coating of thickness h_3 . A semi-infinite layer of water bounded the far side of the coating. Only outgoing plane waves were assumed to be present in the semi-infinite water layer. The properties of the media, with the exception of the foam coatings, are listed in table 2.1.

Table 2.1: Properties of layered media.

Medium	Density (kg/m ³)	C _{compressional} (m/sec)
Air	1.29	331.5
Steel	7,860	5,960
Water	1,000	1,450

The properties of the coating varied with each coating material. The compressional wave velocities were calculated from experimental measurements of the density (ρ) and dilatational modulus (L) of each foam coating. These measurements are described separately in section 3. Once the values of L and ρ were established, the foam compressional wave velocity (C_{foam}) was calculated via,

$$C_{\text{foam}} = \sqrt{\frac{L}{\rho}} \quad (2.1)$$

The transmission loss (T.L.) was characterized in terms of the ratio of the amplitude (A_1) of the original plane wave incident on the steel plate, and the amplitude (A_4) of the outgoing plane wave propagating in the water.

$$T.L. = \left| \frac{A_1}{A_4} \right| \quad (2.2)$$

A closed form expression for the amplitude ratio was used,

This expression can be obtained by applying the usual boundary conditions for acoustics

$$\left[\frac{A_1}{A_4} \right] = \frac{e^{(-ik_4(h_2+h_3))}}{2} \left[\left(1 + \frac{Z_1}{Z_4} \right) \cos(k_2 h_2) \cos(k_3 h_3) - \left(\frac{Z_2}{Z_3} + \frac{Z_1 Z_3}{Z_2 Z_4} \right) \sin(k_2 h_2) \sin(k_3 h_3) \right. \\ \left. + i \left(\left(\frac{Z_2}{Z_4} + \frac{Z_1}{Z_2} \right) \sin(k_2 h_2) \cos(k_3 h_3) + \left(\frac{Z_3}{Z_4} + \frac{Z_1}{Z_3} \right) \cos(k_2 h_2) \sin(k_3 h_3) \right) \right] \quad (2.3)$$

where,

$$Z_1 = \rho_{\text{air}} c_{\text{air}},$$

$$Z_2 = \rho_{\text{steel}} c_{\text{steel}},$$

$$Z_3 = \rho_{\text{foam}} c_{\text{foam}},$$

$$Z_4 = \rho_{\text{water}} c_{\text{water}}$$

at the interfaces between the media. Apart from a leading exponential phase factor, this expression is identical to that given by House (1991).

2.2 Five Layer Model

The four layer model assumed the water layer to be semi-infinite. However, the actual experimental measurements used to estimate transmission loss took place in a tank, with the coated plate situated near the bottom of the tank, facing upwards. The height of the water above the foam coating was finite, typically 1.3 meters. The four layer model was modified to include the finite thickness of this water layer, which produced a 5 layer model. This revised model incorporated a finite thickness water layer in contact with a semi-infinite layer of air. Comparison of the predictions from the four and five layer models was used to examine the effect of the finite thickness of the water above the coating. Figure 2.2 illustrates the geometry assumed for the five layer transmission loss model.

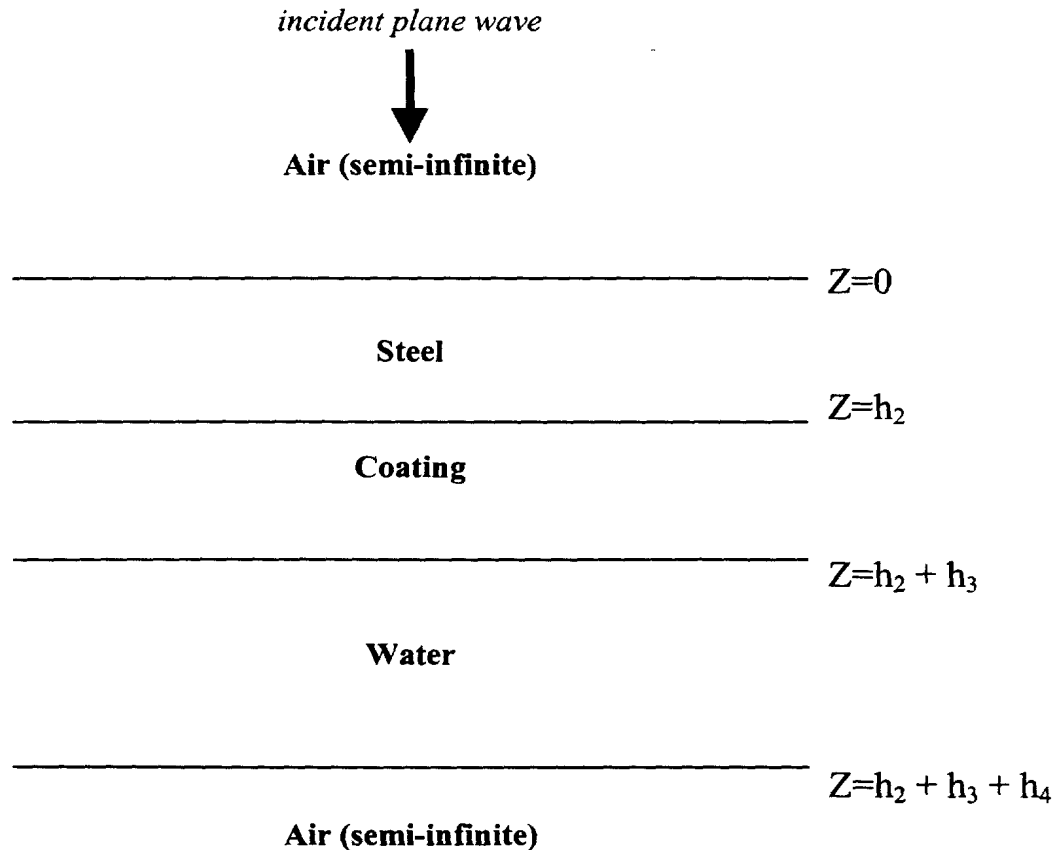


Figure 2.2: Geometry for 5 layer transmission loss model.

The equations relating the amplitude of the incident plane wave to the amplitude of the outgoing plane wave were derived from the usual acoustic boundary conditions at the media interfaces. The coefficients of the outgoing and reflected waves are related by the following equations,

$$\frac{A_4}{A_5} = \frac{1}{2} \left(1 + \frac{Z_4}{Z_5} \right) e^{-i(k_5 - k_4)(h_2 + h_3 + h_4)} \quad (2.4)$$

$$\frac{B_4}{A_5} = \frac{1}{2} \left(1 - \frac{Z_4}{Z_5} \right) e^{-i(k_5 + k_4)(h_2 + h_3 + h_4)} \quad (2.5)$$

$$A_3 = \frac{1}{2\omega^2 \rho_3} \left(- \left(\frac{Z_3}{Z_4} + 1 \right) e^{-i(k_4 - k_3)(h_2 + h_3)} A_4 + \left(\frac{Z_3}{Z_4} - 1 \right) e^{i(k_4 + k_3)(h_2 + h_3)} B_4 \right) \quad (2.6)$$

$$B_3 = \frac{1}{2\omega^2 \rho_3} \left(\left(\frac{Z_3}{Z_4} - 1 \right) e^{-i(k_4 + k_3)(h_2 + h_3)} A_4 - \left(\frac{Z_3}{Z_4} + 1 \right) e^{i(k_4 - k_3)(h_2 + h_3)} B_4 \right) \quad (2.7)$$

$$A_2 = \frac{1}{2\rho_2 c_3} \left((Z_3 + Z_2) e^{-i(k_3 - k_2)h_2} A_3 + (Z_3 - Z_2) e^{i(k_3 + k_2)h_2} B_3 \right) \quad (2.8)$$

$$B_2 = \frac{1}{2\rho_2 c_3} \left((Z_3 - Z_2) e^{-i(k_3 + k_2)h_2} A_3 + (Z_3 + Z_2) e^{i(k_3 - k_2)h_2} B_3 \right) \quad (2.9)$$

$$A_1 = \frac{\omega^2}{2c_2} \left(- (Z_1 + Z_2) A_2 + (Z_1 - Z_2) B_2 \right) \quad (2.10)$$

$$B_1 = \frac{\omega^2}{2c_2} \left((Z_1 - Z_2) A_2 - (Z_1 + Z_2) B_2 \right) \quad (2.11)$$

where ,

$$Z_5 = \rho_{air} c_{air}$$

A_5 = amplitude of outgoing wave in air

Transmission loss was calculated from,

$$T.L. = \left| \frac{A_1}{A_5} \right| \quad (2.12)$$

The amplitude ratio A_1/A_5 was obtained by starting with equations 2.4 and 2.5 to obtain the ratios of A_4/A_5 and B_4/A_5 and then iterating sequentially through equations 2.6 through 2.10.

3.0 DILATATIONAL MODULUS MEASUREMENT

The model in section 2 needed the compressional wave velocity (C) and density (ρ) of each of the materials involved to calculate transmission loss. The compressional wave velocities for air, water and steel were well documented. They could be assumed to be independent of frequency in the range of interest (100 to 1,000 Hz). These values could also be taken to be real (i.e. no attenuation). Likewise their material densities were well documented and could also be measured. Consequently, the velocity and density values for air, water and steel to input into the model were readily obtained.

On the other hand the foam coatings were soft, porous elastomers. (A description of the elastomers used in this study is given in Appendix A.) Elastomers could not be expected to exhibit real compressional wave velocities independent of frequency. Rather, frequency dependent, attenuative behaviour was expected. In order to apply the model described in section 2, the behaviour of the foam's dilatational modulus needed to be measured in the frequency range of interest.

3.1 Modulus Measurements of Elastomers

The propagation of plane compressional waves through infinite uniform media is described by,

$$C_{\text{compressional}} = \sqrt{\frac{\lambda + 2\mu}{\rho}} \quad (3.1)$$

where (λ , μ) are the Lamé constants. The Dilatational modulus (L) is defined from,

$$L = \lambda + 2\mu \quad (3.2)$$

If the value of L is known along with the material density, then the compressional wave velocity can be calculated.

Most of the published experimental methods for measuring the physical modulus' of elastomeric materials have focussed on Young's modulus (Edwards and Hicks (1971), Jones and Parin (1972), Jones (1974), Cannon et al (1968), Nashif (1967)) and to a lesser degree on the Bulk modulus (Burns et al (1990)). Methods for directly measuring the Dilatational modulus were found to be relatively non-existent.

The sample measurement geometry for obtaining the Dilatational modulus in this study was suggested by Snowden (1979). Snowden noted that a thin layer of material subjected to a static compressive stress across its thickness, exhibits a mechanical response governed by L . This comment suggested a dynamic mechanical measurement of L could be made in a fashion similar to a dynamic measurement of Young's modulus (E), the only difference being the geometric proportions of the material being tested. The dynamic stress would still be applied along the sample thickness. However, for L measurements the sample's lateral dimensions would have to be much greater than its thickness, instead

of the sample's lateral dimensions being much less than its thickness as for E measurements.

Mechanical measurements of E (or G) of rubberlike materials have been obtained from resonance tests. The method makes use of a mechanical shaker to excite a layer of material supporting a dead mass via compression (or via shear). Input and output accelerations are measured. This type of measurement is referred to as the "classical technique" (Jones, 1973). However, measurements are only obtained at the resonant frequency⁹; the dead mass is varied in order to shift the resonant frequency. An array of different masses would be required to span the frequency range of interest, and yet only values at discrete frequencies would be obtained.

Alternatively, a mechanical non-resonant method of measuring E had been described by Edwards and Hicks (1971). This technique was of interest because its measurements provided continuous results across a frequency band. It was this latter technique that was adopted for Dilatational modulus measurements using the geometric profile suggested by Snowden.

3.2 Experimental setup for infinite backing mass

The first modulus measurement geometry that was utilized is shown in Figure 3.1. The foam under test was sandwiched between a solid, stiff driving plate and an aluminum plate resting on a concrete floor (assumed to be a rigid surface)

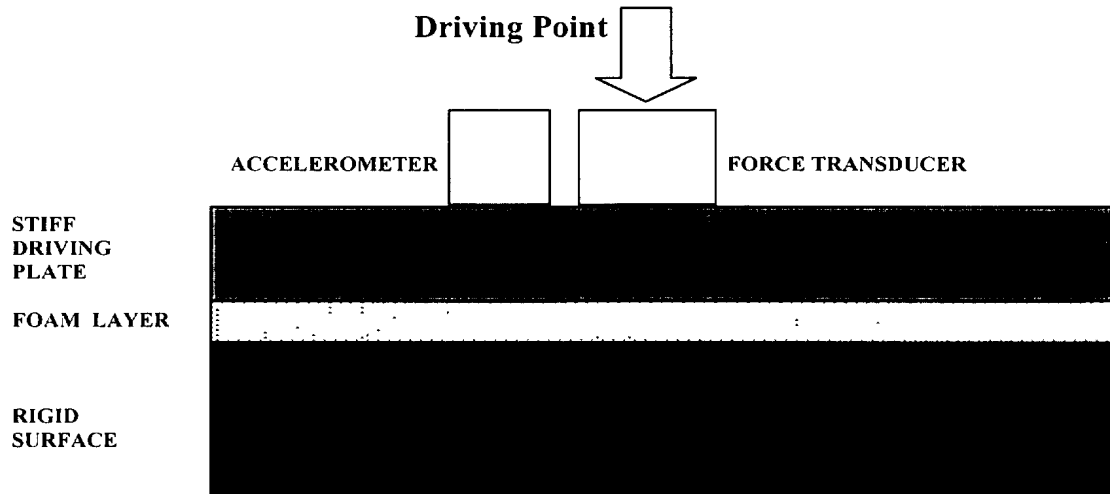


Figure 3.1: Infinite backing mass measurement configuration.

⁹ The reason why measurements are restricted to the resonance condition is not clear. One reason may be the measurement configuration is very similar to a SDOF (single degree of freedom) harmonic oscillator, e.g. a mass on a damped spring. The degree of damping of such a system is only easily measureable around resonance where damping governs the amplitude of response. Away from resonance, the amplitude of response is governed mostly by the separation between the driving and resonant frequencies. In this vein, the limitation of measurements to resonance conditions may have been hardware related. The time of publication seems to predate the advent of digital instrumentation capable of performing fine phase resolution at small phase angles.

A vibration shaker was used to apply a broad band force at one end of a force transducer attached to the centre of the driving plate. An accelerometer was mounted on the driving plate adjacent to the force transducer.

The governing equation for L_{foam} was developed in terms of the ratio of measured acceleration to applied force. The assumption was made that the sample was sufficiently thin such that its deformation could be described by plane compressional waves (i.e. edge effects could be ignored). With forward and backward propagating plane waves in the foam as a result of the applied force described by,

$$\begin{aligned}\Phi_1 &= A_1 e^{i(\omega t - kz)} \quad (\text{forward propagating}) \\ \Phi_2 &= A_2 e^{i(\omega t + kz)} \quad (\text{backward propagating})\end{aligned}\quad (3.3)$$

the displacement vector U_{foam} in the foam was described by,

$$\vec{U}_{\text{foam}} = -\vec{\nabla}(\Phi_1 + \Phi_2) \quad (3.4)$$

The stress-strain equation connected the displacement in the foam to the material properties (λ , μ) and the stress (σ),

$$\sigma_{ij} = \lambda \frac{\partial U_k}{\partial x_k} \delta_{ij} + 2\mu \left(\frac{\partial U_i}{\partial x_j} + \frac{\partial U_j}{\partial x_i} \right) \quad (3.5)$$

Application of the usual boundary conditions at the foam surfaces yielded,

$$\frac{U}{F} = \frac{1}{kS(\lambda + 2\mu)} \tan(kh) \quad (3.6)$$

where,

F = amplitude of applied force at upper foam surface,

S = contact area of foam sample,

h = thickness of foam sample.

Equation 3.6 is equivalent to the form described by Edwards and Hicks (1971)¹⁰. Equation 3.6 was rewritten in terms of the force applied to the driving plate, and the acceleration of the driving plate yielding,

¹⁰ Equation (1) with β set to zero ($M=\infty$) representing the rigid surface backing the foam sample

$$\frac{\omega}{S\sqrt{\rho}} \left(M - \frac{1}{H_1(\omega)} \right) - \sqrt{L(\omega)} \cot \left(\sqrt{\frac{\rho}{L(\omega)}} h \right) = 0 \quad (3.6)$$

where,

M = driving plate mass, and

$H_1(\omega)$ = measured ratio of acceleration to force at angular frequency ω .

This transcendental equation was solved numerically using the Newton-Raphson method to obtain the values of L as a function of frequency from experimentally measured values of H_1 .

The driving plate was designed to minimize its modal response up to a frequency well above the highest frequency of interest (1,000 kHz). It could therefore be considered as a rigid piston. The driving plate was 28 mm thick aluminum with a diameter of 150 mm. Experimental measurements were conducted with foam samples of varying thickness. Most tests were limited to a driving plate diameter/foam thickness ratio of 13 or greater. With this ratio, theory suggested the measured L would be within 10 % of the true value (foams with a minimum air content of 90%, DREA (1998)).

The measurement method was judged on its ability to obtain results that were independent of the thickness of the foam sample being tested. Figure 3.2 illustrates the values¹¹ of L for tests with the same foam in sample thicknesses of 3, 6 and 9mm. The results were in fact dependent on sample thickness. The values for |L| overlapped up to approximately 400 Hz but then they diverged. The phase of L diverged above 200 Hz. The diverging values suggested there were problems with the experimental apparatus.

¹¹ calculated with an approximate solution to equation 3.6

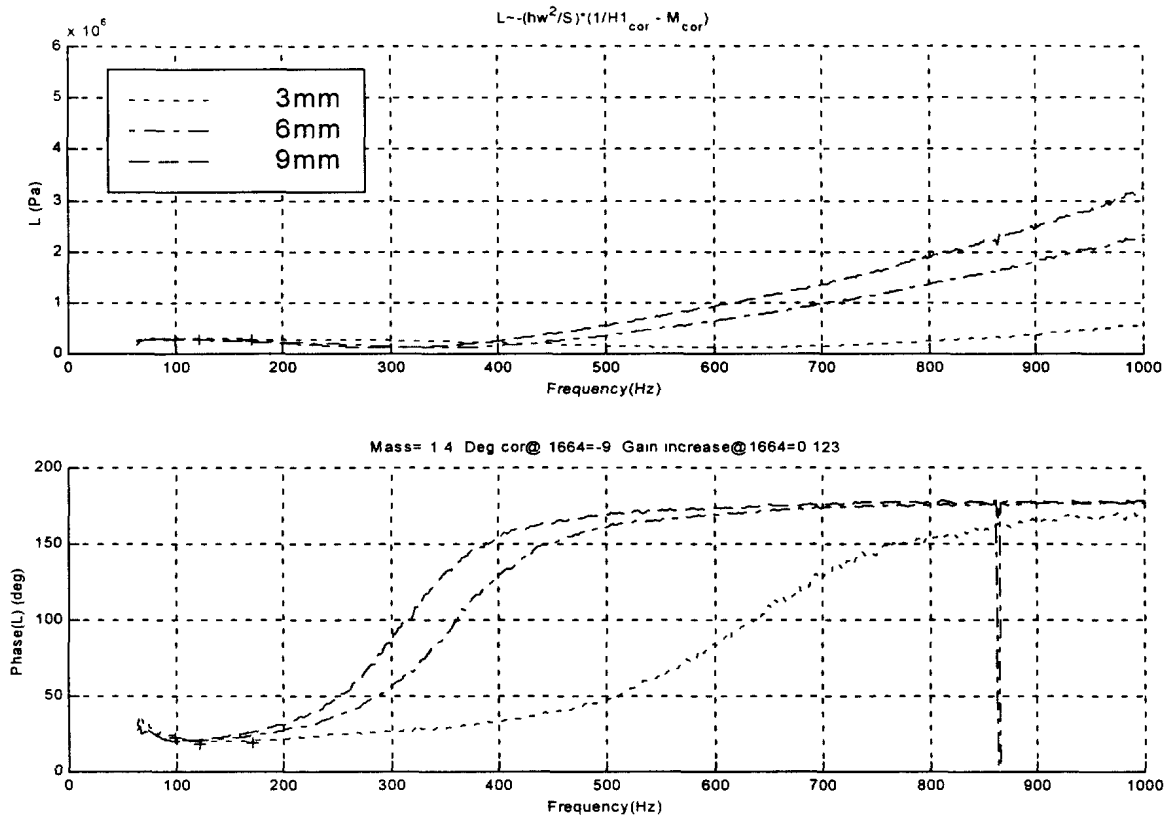


Figure 3.2: Diverging values of Dilatational modulus with rigid backing mass.

The problem was indeed found to be in the experimental configuration. The aluminum plate/concrete floor was not a truly rigid surface backing the foam. Measurements of the frequency response of the driving plate in direct contact with the aluminum plate resting on concrete exhibited an increasingly mobile surface above 200 Hz. This mobility suggested imperfect contact between the aluminum plate and concrete surfaces. There was a need to better define the effective mass acting on the far side of the foam.

3.3 Experimental setup for finite backing mass

The mechanical arrangement was changed to place the foam between two finite masses. The arrangement is shown in Figure 3.3.

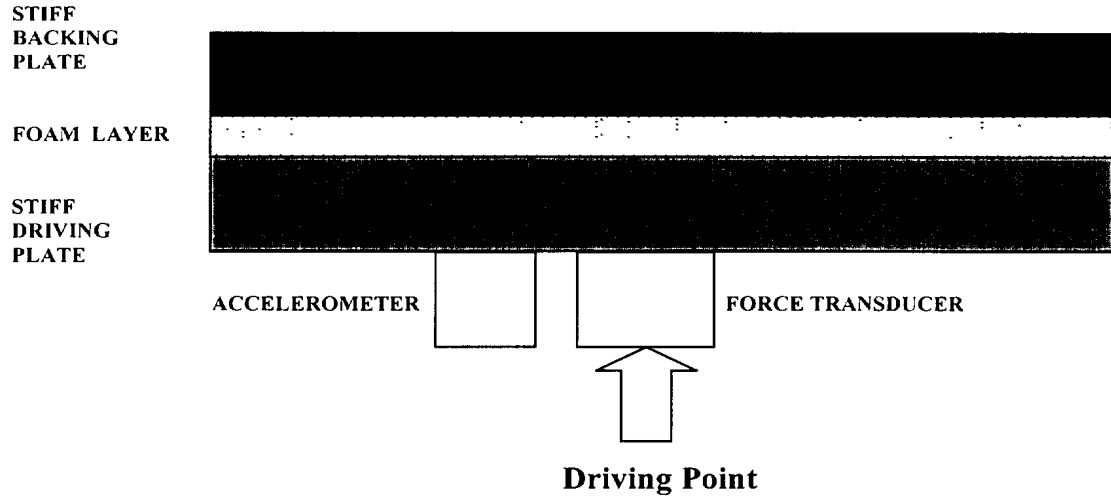


Figure 3.3: Finite backing mass measurement configuration.

The governing equation for this configuration was calculated to be,

$$\tan\left(\frac{\omega h}{c}\right) = i \left(\frac{Q(D + M_2)}{Q^2 + DM_2} \right)$$

where,

$$\begin{aligned} M_1 &= \text{mass of driving plate,} \\ M_2 &= \text{mass of backing plate,} \end{aligned} \tag{3.7}$$

$$D = \left(M_1 - \frac{1}{H_1} \right)$$

$$Q = \frac{\rho S c}{i \omega}$$

This equation was solved for the value of c , the complex velocity of the foam, and L then calculated from,

$$L = \rho c^2 \tag{3.8}$$

Measurements were made in this new configuration with the same foam as in the previous example. Valid measurements were expected to be indicated by results that were independent of the thickness. Figure 3.4 illustrates the observed values of L for tests with sample thicknesses of 3 and 9mm. From 64 to 700 Hz the results for the two sample thicknesses were reasonably close in both amplitude and phase. Beyond 700 Hz the values diverged.

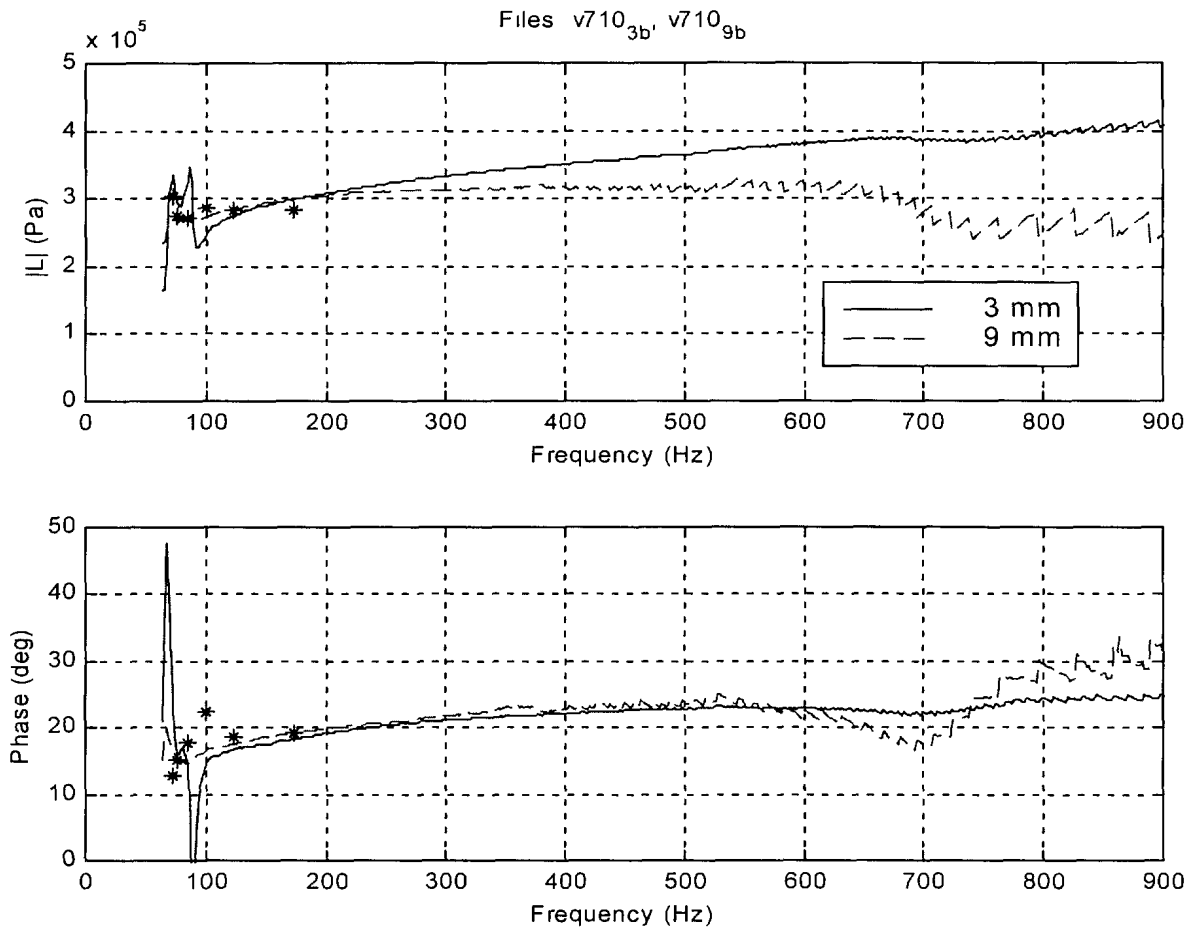


Figure 3.4: Values of the Dilatational modulus with the finite backing mass configuration.

Up to this point the foam samples had not been glued to the contact surfaces of the plates because the measurement configuration was subject to change. The availability of the foam samples was limited. Once glued, a foam sample could not be removed intact. However, the latter configuration was now producing results out to 700 Hz that were reasonably independent of thickness. It was now possible to remove the measurement uncertainty that was associated with the lack of bonded surfaces. The foam surfaces were bonded with adhesive¹² to the driving and backing plates. Measurements were repeated. The results for the same foam, bonded with adhesive, are shown in Figure 3.5. The calculated modulus was found to be reasonably independent of sample thickness from 64 to 800 Hz. The modulus had an approximate value of 0.2 MPa in this region with a phase of 10 to 15 degrees.

¹² Foam samples were adhesive backed on one side. Lepage Pres-tite Contact Cement 1543-1 was used on the opposing side.

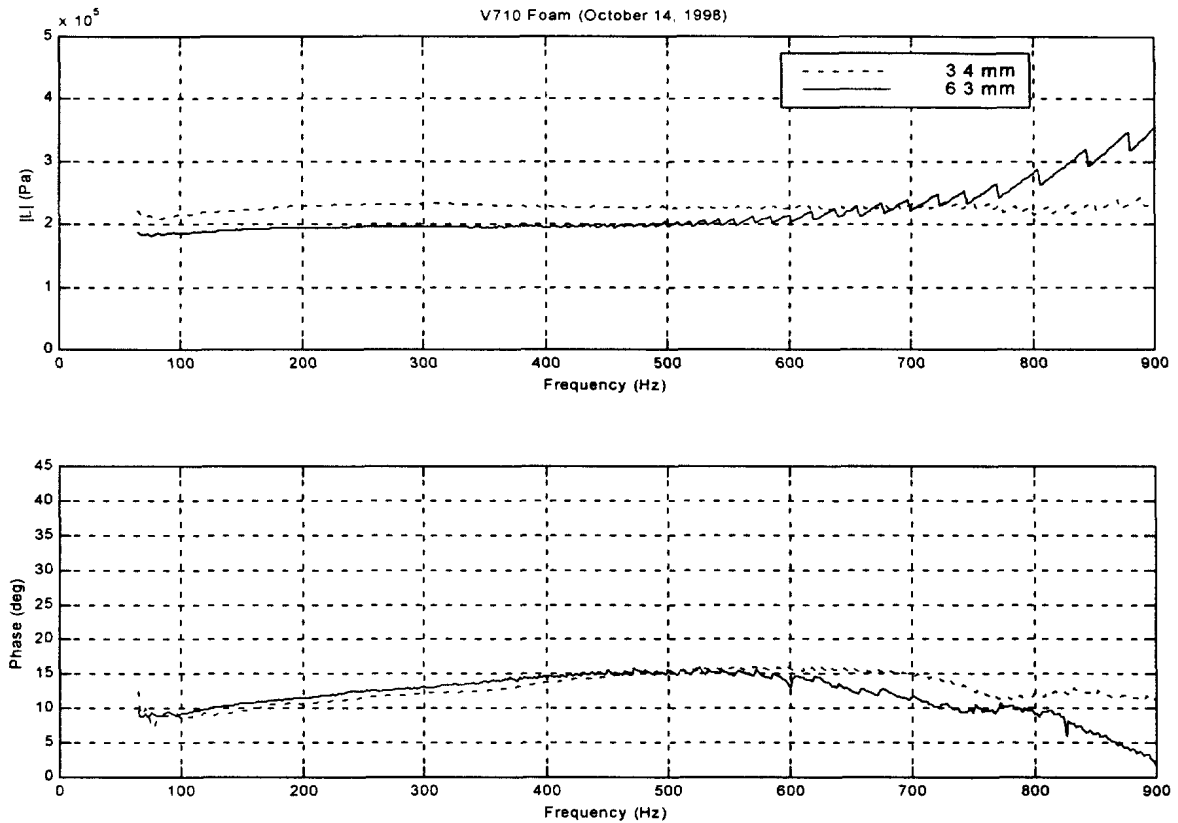


Figure 3.5: Measured dilatational modulus for V710 foam with bonded surfaces.

Measurements were made on two additional types of foam, SC4116 and VA80. The measurement configuration was the same as for the V710 foam. Foam surfaces were bonded with adhesive to the driving and backing plates. The results for the SC4116 foam, bonded with adhesive, are shown in Figure 3.6.

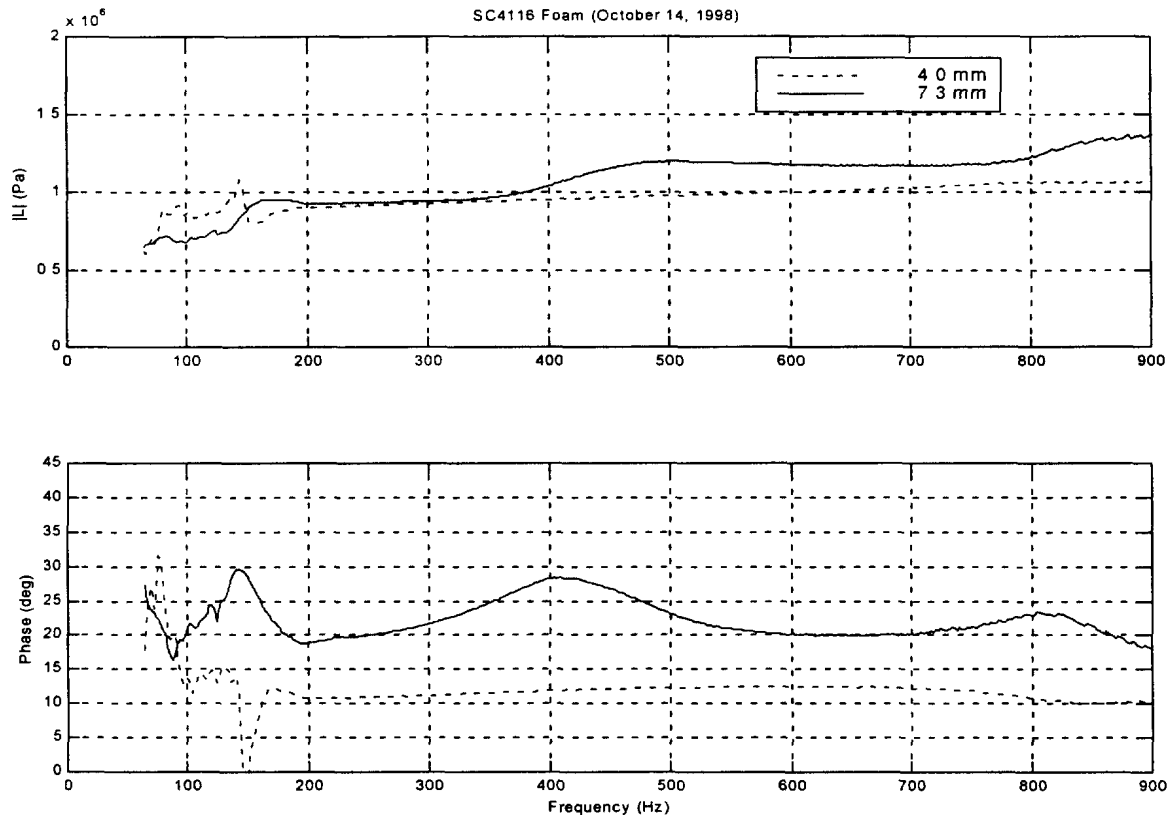


Figure 3.6: Measured dilatational modulus for SC4116 foam with bonded surfaces.

The magnitude of the calculated modulus for SC4116 was found to be reasonably independent of sample thickness from 64 to 900 Hz. The modulus exhibited a steadily increasing amplitude with frequency. It had an approximate value of 1 MPa. The phase was not totally independent of sample thickness. The thinner sample exhibited a phase of approximately 12 degrees, while the thicker sample exhibited a phase of approximately 25 degrees.

The results for the VA80 foam, bonded with adhesive, are shown in Figure 3.7.

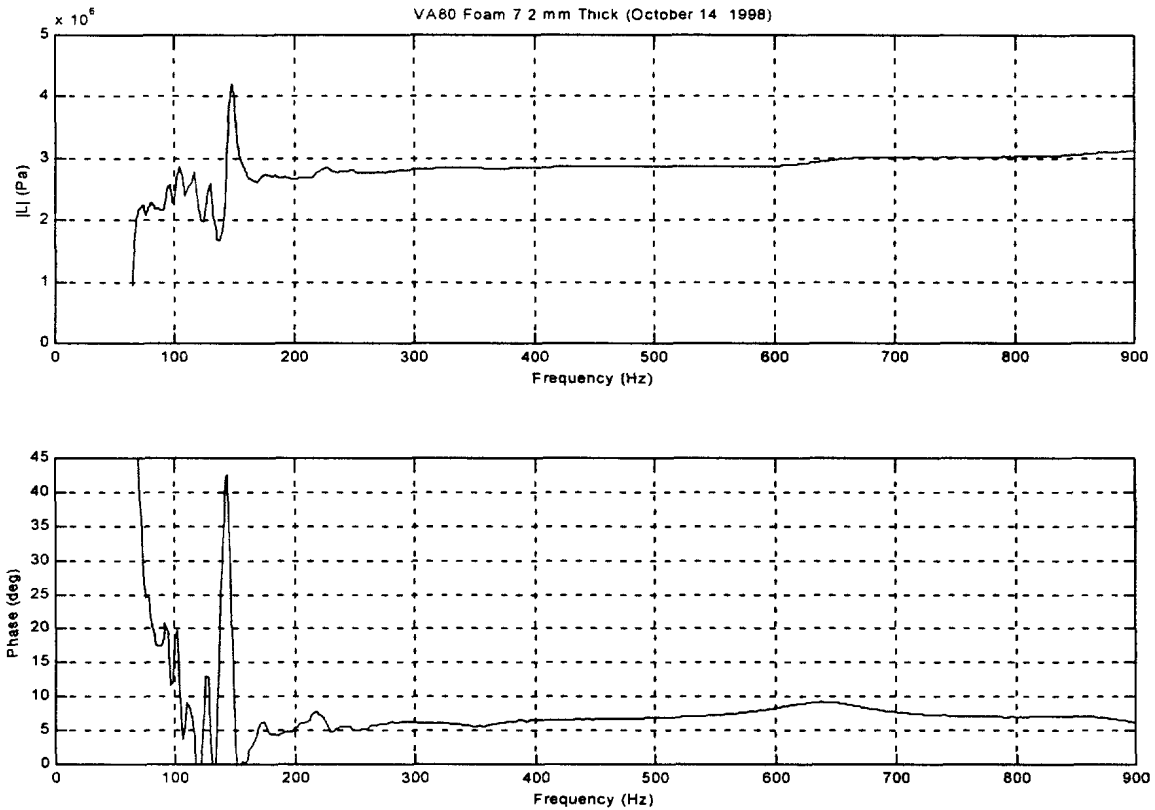


Figure 3.7: Measured dilatational modulus for VA80 foam with bonded surfaces.

Only one thickness of VA80 was provided for measurement. The modulus exhibited a steadily increasing amplitude with frequency. It had an approximate value of 3 MPa. A phase of approximately 7 degrees was exhibited.

Smooth curves were fitted to the measured values of the dilatational modulus for each foam. Where two thicknesses had been measured, the data from the thinner sample was used. The order of the curves were either constant, linear or quadratic, selected to best fit the shape of the data. On average, the fitted curves followed the calculated values within a few percent, above some minimum frequency value (above 100 Hz for V710 foam, above 175 Hz for SC4116 and VA80 foams). Below these frequencies the measured modulus suffered obvious irregularities that the fitted curves tended to ignore. The fitted expressions are provided in table 3.1, written as functions of the frequency (f) in Hz. The fitted curves were used by the transmission loss model described in section 2.

Table 3.1: Fitted Modulus Expressions

Foam Type	Real(L) (Pa)	Imag(L) (Pa)
V710	0.22×10^6	$-0.13 \times f^2 + 144 \times f + 0.02 \times 10^6$
SC4116	$243 \times f + 0.84 \times 10^6$	$0.25 \times f^2 + 330 \times f + 0.10 \times 10^6$
VA80	$439 \times f + 2.65 \times 10^6$	$260 \times f + 0.22 \times 10^6$

4.0 DECOUPLING PERFORMANCE PREDICTION

Decoupling performance (DP) was calculated from the ratio,

$$DP = \frac{TL_{coated}}{TL_{bare}} \quad (4.1)$$

Predictions of decoupling performance were made using the plane wave transmission loss model described in section 2. The model used the dilatational modulus curves obtained in section 3 to describe the properties of the foam coatings.

4.1 Example Prediction

An example of modelled decoupling performance is provided in the upper graph of Figure 4.1. This example models a 3mm steel plate coated with 3mm of V710 foam. The steel plate is backed by semi-infinite air. The coating is in contact with semi-infinite water. The squared amplitude of the dimensionless decoupling performance is plotted versus frequency. A value above unity indicates a reduction in radiated sound due to the addition of the coating while a value below unity indicates an increase in radiated sound due to the coating.

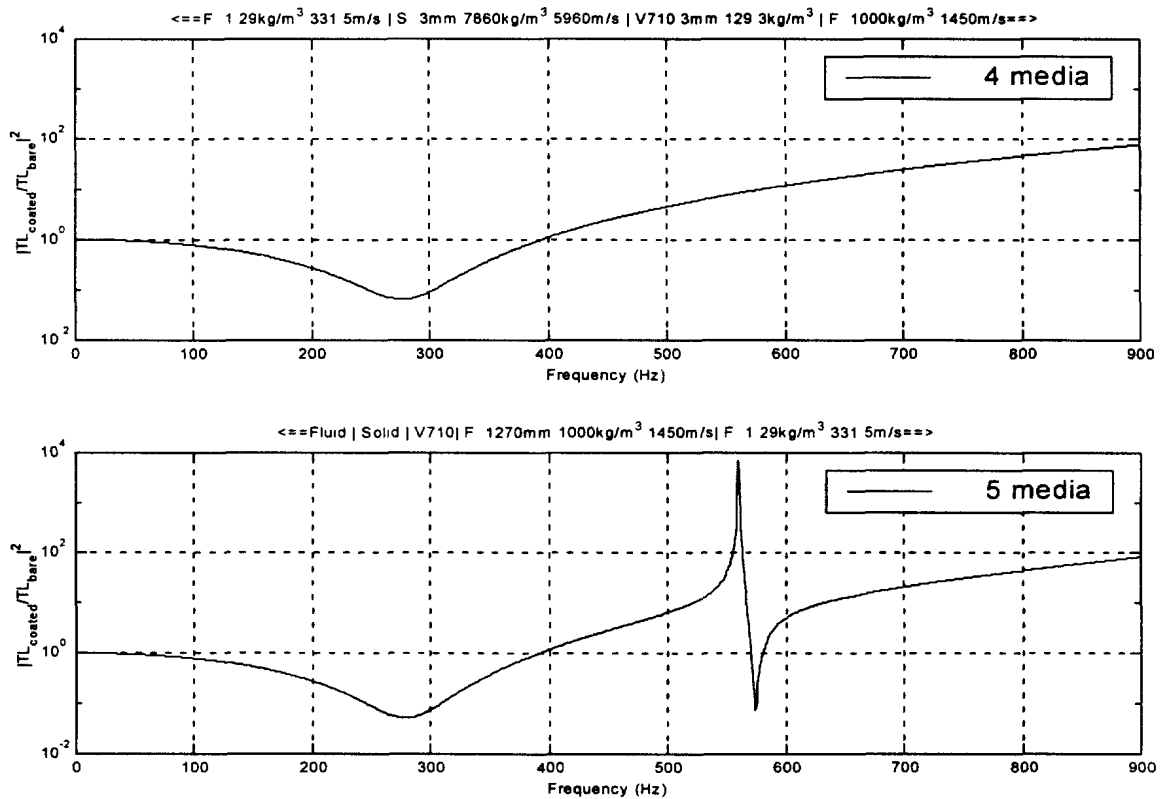


Figure 4.1: Decoupling performance (3mm plate with 3mm V710 foam) - 4 versus 5 layer model.

The trough in the performance (around 280 Hz in this example) was a feature that was found in all the modelled cases. It corresponded to the situation where the foam acted as a spring and the plate as a rigid mass. The center frequency of the trough could be accurately obtained from ,

$$f = \frac{1}{2\pi} \sqrt{\frac{L_{foam}}{h_{foam} h_{plate} \rho_{plate}}} \quad (4.1)$$

where L is the magnitude of the dilatational modulus, h refers to thickness and ρ is density. The trough corresponds to a sprung mass resonance. In this case the plate moves as a whole, the amplitude is large and the decoupling ability of the foam is defeated. This situation could happen theoretically in the plane wave model. However, it was not clear that this situation could take place with the experimental setup because the plate was clamped along its boundaries. To achieve a sprung mass situation would require a unique combination of foam and plate to align the sprung mass frequency with a plate modal frequency where the plate had adequate flexibility. This would be difficult to achieve in practice.

4.2 Model Comparison - Four Versus Five Layers

One of the unknowns within this study was the effect that the finite dimensions of the tank had on the experimentally observed decoupling performance. The model was used to examine this effect in two dimensions by comparing the theoretical decoupling performance for the case of a finite thickness water layer versus the case of a semi-infinite layer of water¹³. The cases examined by the model were selected from the combinations of plate thickness and coating thickness used experimentally during the study.

The lower graph in Figure 4.1 illustrates the modelled decoupling performance for a 3mm steel plate coated with 3mm of V710 foam where the water layer is assumed to have finite thickness 1270mm¹⁴, and is in contact with a semi-infinite layer of air. Comparison of the calculated decoupling performances for the two cases, finite and semi-infinite water, showed the two are very similar except for the 550 to 650 Hz region, where an apparent maxima occurred at 560 Hz and a minima occurred at about 575 Hz.

Figure 4.2 illustrates the modelled decoupling performance for a 9.5mm steel plate coated with 25mm of SC4116 foam. The steel plate is backed by semi-infinite air. The coating is in contact with water. In the upper graph the water layer is assumed to be semi-infinite. In the lower graph, the water layer is 1270mm thick and in contact with a semi-infinite layer of air. Comparison of the calculated decoupling performances shows the two are very similar except for the 450 to 700 Hz region, where an apparent maxima occurs at 540 Hz and again a minima occurs at 575 Hz.

¹³ From section 2, it will be recalled that the transmission loss (TL) was developed with both a 4 layer model and a 5 layer model. The 4 layer model assumed the foam coating was in contact with a semi-infinite water layer. The 5 layer model assumed the foam coating was in contact with a layer of water of specified thickness, which in turn was in contact with a semi-infinite layer of air.

¹⁴ Typical water depth to foam coating during experimental measurements

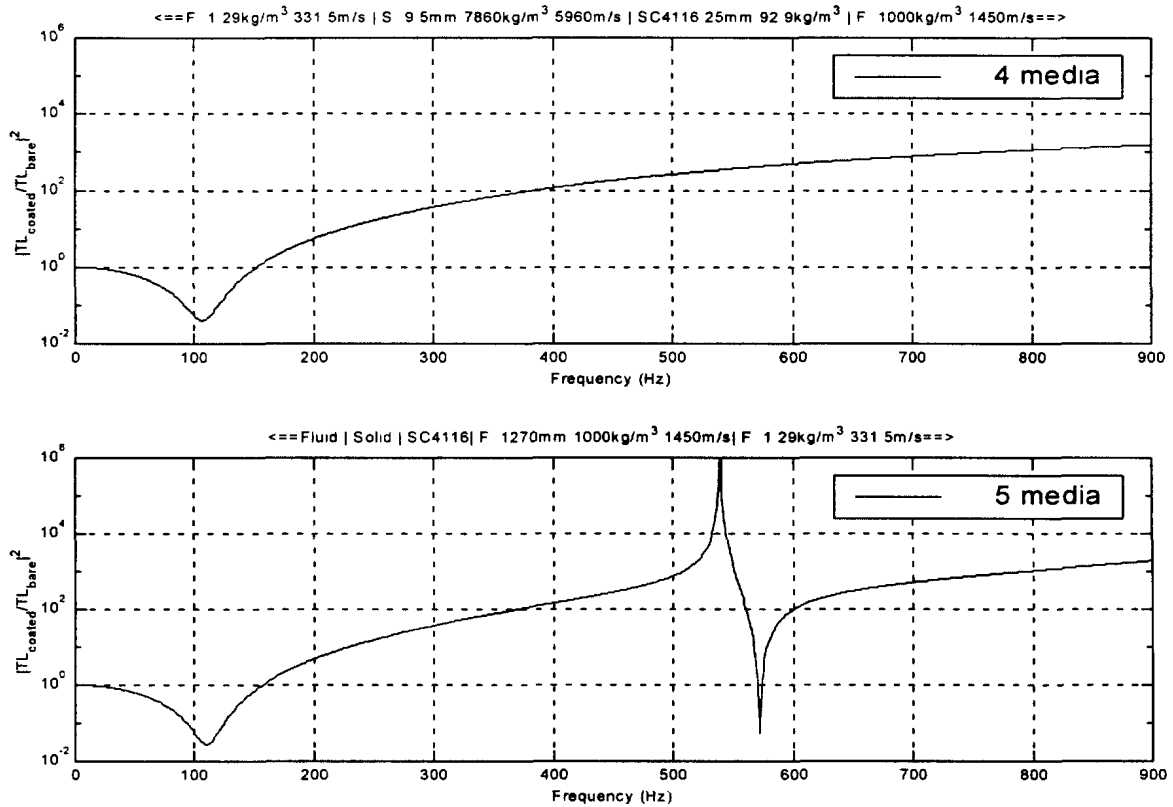


Figure 4.2: Decoupling performance (9.5 mm plate with 25mm SC4116 foam) - 4 versus 5 layer model.

Both cases exhibited their minima at 575 Hz, where the half-wavelength corresponds to the thickness of the water layer in the 5 layer model. This suggested that the main difference between the two models was associated just with the standing wave condition for the water thickness. (The nearby maxima was assumed to be related to the same phenomenon.)

Theoretically the 5 layer model was more representative of the finite extent of the experimental tank environment. The coated plate resided in a finite volume of water, not a semi-infinite medium. However, the real apparatus also involved a finite size plate which radiated diverging non-planar waves in all directions as opposed to plane waves. The 5 layer model did not take into account that the standing wave phenomenon could not be easily created by the existing apparatus. Consequently the 4 layer model was considered to be the better tool for comparison with experimental measurement.

5.0 ACOUSTIC MEASUREMENTS

The purpose of the measurements was to document the acoustic behaviour of bare and foam coated steel plates submerged inside the water filled tank. These measurements documented the mechanical power forcing the plate into vibration and the acoustic field that resulted from this vibration. The measurements also documented the characteristic frequency response of each plate-coating combination tested. The experimental measurements in this study were made in the same manner as the previous study (Klein and Hamm, 1997). The main difference between the experimental setup in this study and the previous study was the type of structure used to support the plate being tested.

5.1 Concrete Enclosure

In the previous study, a square steel¹⁵ plate had been suspended from its four corners with vibration mounts that were attached to a stiff frame positioned just above the water level of the tank. The coated side of the plate faced down into the tank, submerged a few cm below the water surface. A flexible shroud around the perimeter of the plate kept the air side of the plate from being flooded. The plate was mechanically excited from the air side and the acoustic field radiated into the tank measured with hydrophones positioned below the plate in the tank.

The study had subsequently recommended a change to the method of supporting the plate, to make the support conditions more reproducible from plate to plate, and in order to minimize the possibility of exciting undesirable frame vibrations that would contribute radiated sound. A concrete box had been suggested for mounting the plate, that could be placed on the bottom of the tank. Such a box was constructed for this program. Figure 5.1 shows the geometry of this concrete enclosure. Embedded in the concrete was a steel frame with regularly spaced protruding bolts. Every plate that was tested had been drilled with this bolt pattern along its edges. This configuration allowed each plate to be securely attached to the box. An o-ring seal kept the box watertight. During installation the nuts securing the plate to the box were torqued to a fixed amount, which made the plate clamping conditions reproducible. The stiffness of the concrete box walls and characteristics of concrete reduced the possibility of undesirable vibration. Because the concrete enclosure was watertight the entire box could be placed on the bottom of the tank, plate side up. This arrangement facilitated making measurements of the acoustic field relative to the plate. The hydrophone positions relative to the plate could be visually determined. Also, any air bubbles attached to the plate surface could be seen and their removal could be visually confirmed.

¹⁵ 604 x 604 x 9.5 mm

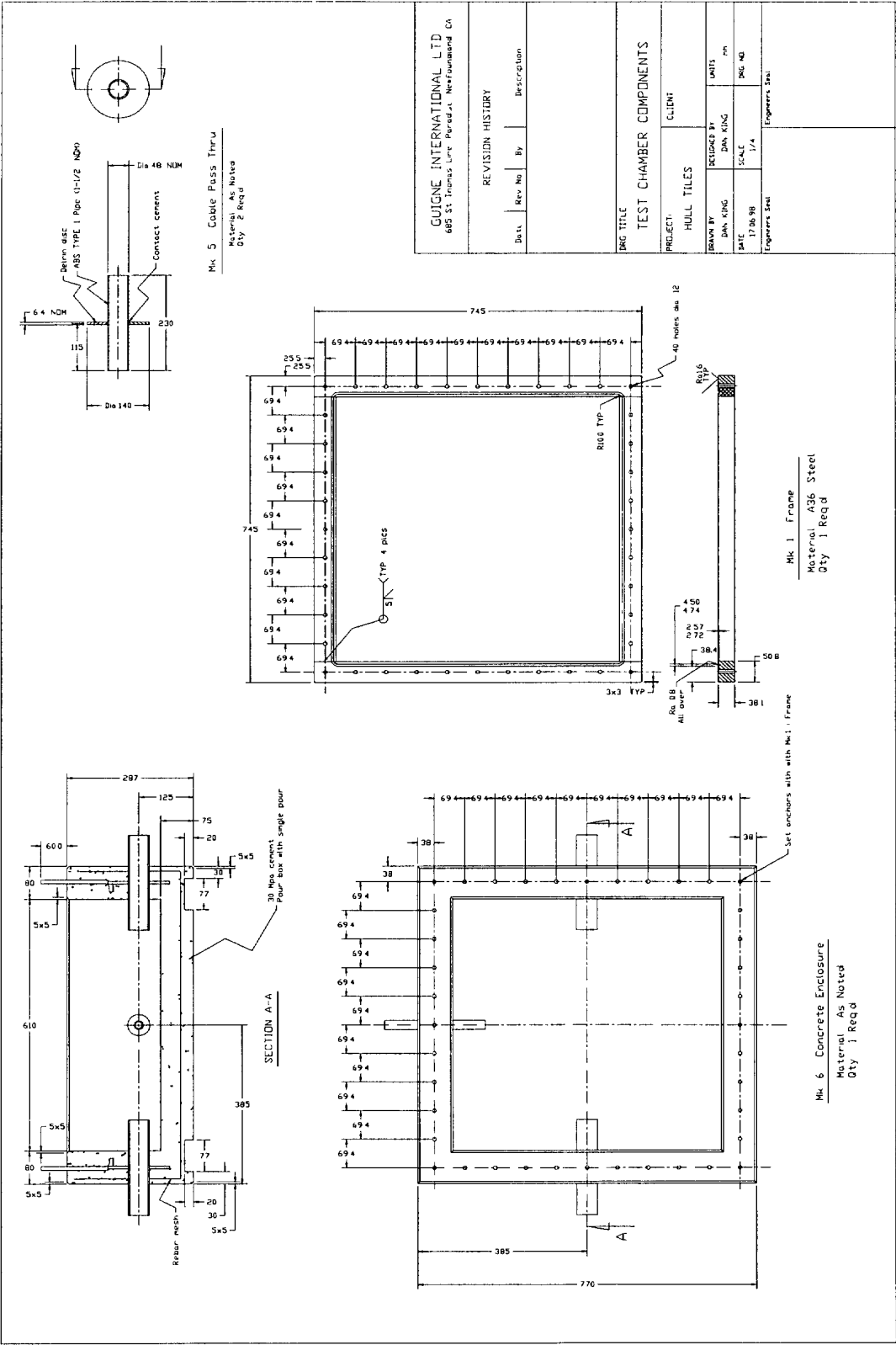


Figure 5.1: Concrete enclosure design.

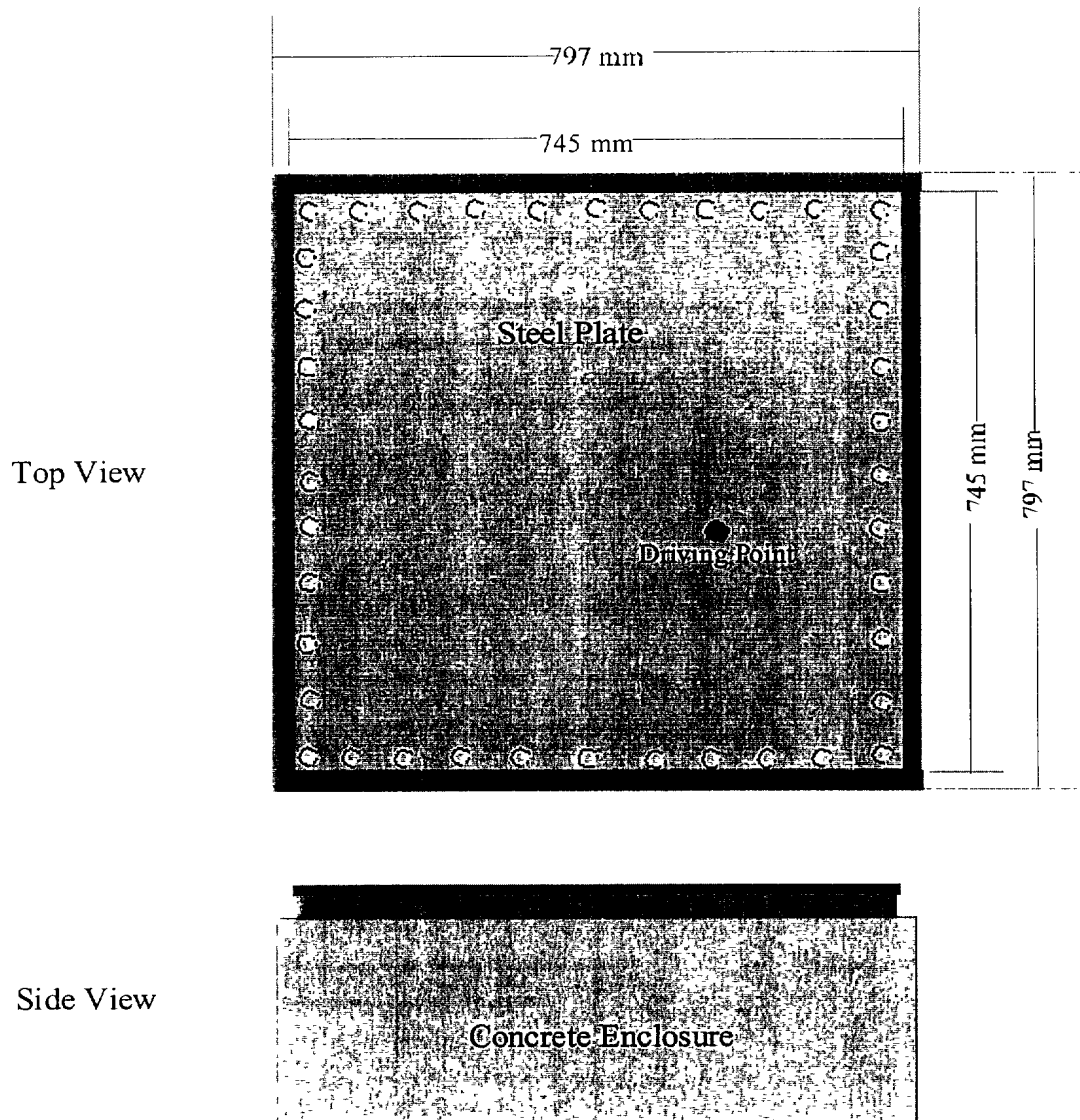


Figure 5.2: Steel plate secured to concrete box.

Figure 5.2 illustrates the appearance of the plate when secured to the box. The side dimensions of each plate tested were 745mm x 745mm. The interior area of the plate that was free to vibrate within the clamped boundaries was approximately 610mm x 610mm. This interior area had been selected to match the area of vibration of the plates in the previous study.

Figure 5.3 shows a photo of the underside of a plate suspended above the concrete enclosure prior to installation. A mechanical shaker was attached to the plate interior. The shaker was positioned relative to the plate's clamped edges to match the shaker position in the previous study. This driving point position had been selected in order to excite as many modes as possible within the frequency band of interest. The shaker was

part of a Wilcoxin Research vibration system which included a matching network and a power amplifier (models N7C and PA7D).



Figure 5.3: View of plate suspended above concrete enclosure.

Tests were conducted with the box interior air pressurized¹⁶ to balance the hydrostatic head acting on the plate, plus a fraction of a psi. The fraction of a psi over-pressure was to mitigate the presence of any leaks, by pushing air out, rather than letting water in. The over pressure also made it easy to spot leaks with a bubble trail¹⁷.

¹⁶ At 3 psi, 0.5 psi greater than the hydrostatic head on the plate

¹⁷ The setup was leak tested and the leaks sealed prior to measurements. The interior of the concrete box remained dry during the entire suite of measurements.

5.2 Experimental Configuration

The mechanical shaker housed an impedance head (in-line force transducer and accelerometer) that measured the applied force to, and resultant acceleration of, the air side of the plate at the driving point. The frequency response function (FRF) of the plate at the driving point was calculated from the ratio of acceleration to force as a function of frequency. The spectrum of input mechanical power to the plate was calculated from the cross spectrum of acceleration with force.

The acoustic power radiated into the water was described with acoustic intensity measurements. Acoustic intensity was measured using two hydrophones, P_a and P_b , positioned above the plate. The measurement was calculated from the cross spectrum of the two hydrophone pressures and constructed the component of acoustic power flowing in the direction normal to the plate's surface (along the line joining P_a to P_b). The position of the measurement was taken to be the midpoint lying between P_a and P_b . Acoustic intensity was measured at each point on a 5 x 5 grid in a plane above the coated plate. Figure 5.4 illustrates the measurement grid above the plate.

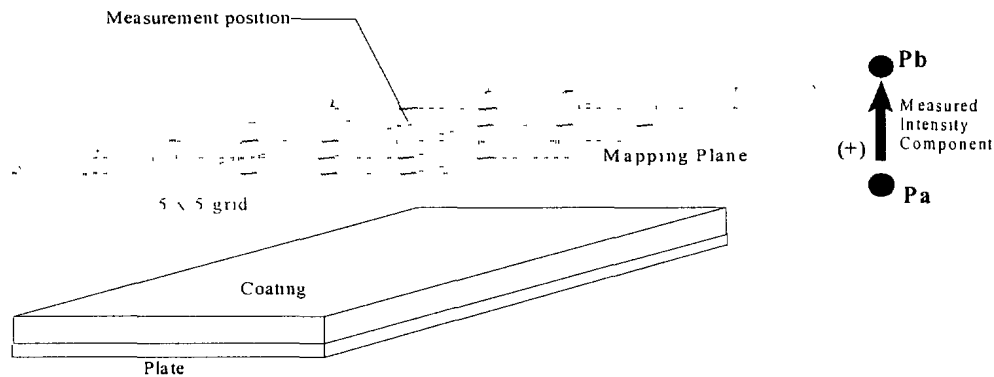


Figure 5.4: Acoustic intensity measurement grid.

The mapping plane was approximately 121 mm above the surface of the coating (or plate if no coating present). This configuration assumed that most of the acoustic power was radiated by the upper surface of the coating, and passed through the mapping plane.

A positioning frame was used to suspend the hydrophones above the plate. Figure 5.4 illustrates a view of the frame positioning the hydrophones over the plate (mounted on the concrete box).

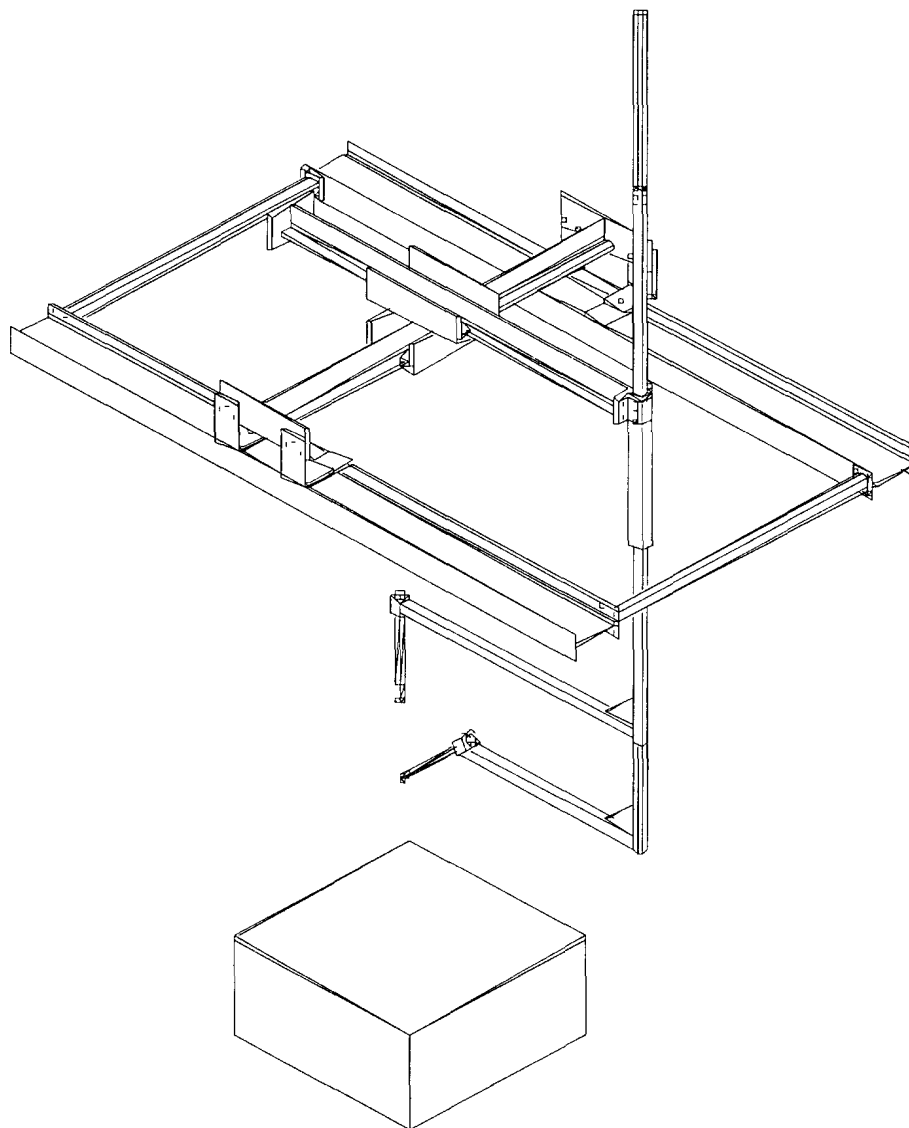


Figure 5.4: View of the apparatus positioning the hydrophones over the plate.

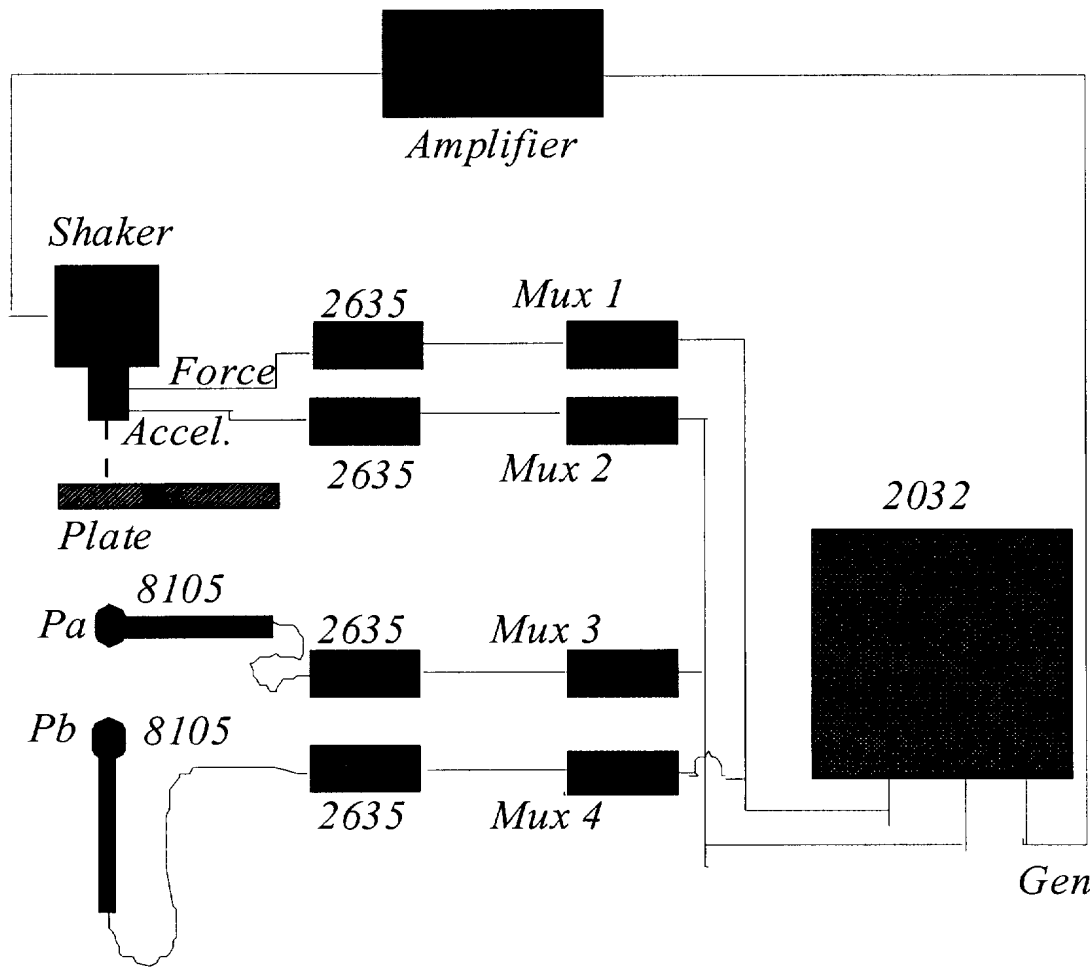


Figure 5.5: Measurement equipment setup.

Figure 5.5 shows the configuration of equipment used for measurements of FRF's, input mechanical power and radiated acoustic intensity. Acoustic measurements of pressure above the plate were made with underwater hydrophones¹⁸. All four transducers were piezoelectric in nature, with scale factors of charge per unit measurement. Charge amplifiers¹⁹ were used to convert the transducer charge outputs to voltage. A dual channel signal analyzer²⁰ was used to measure the cross spectra and transfer functions²¹ of two signals at a time.

¹⁸ Bruel and Kjaer type 8105

¹⁹ Bruel and Kjaer type 2635

²⁰ Bruel and Kjaer type 2032

²¹ The measurement of FRF's required just the existing two channel capability of the analyzer. The analyzer was typically used to average 100 instantaneous spectra into one final average H1 spectrum (a Hanning window was used with 50% overlap between instantaneous spectra)

Measurements of the mechanical power into the plate and the net radiated power out of the plate for essentially the same time interval required a multiplexer. There were four signals to be processed, applied force at the driving point, resultant acceleration at the driving point, and two acoustic pressures at differing positions above the plate. The object was to obtain both the mechanical input power to the plate and the acoustic intensity radiated from the plate for the same time interval. Practically this was accomplished with the introduction of a multiplexer²². The multiplexer was used to pass force and acceleration to the analyzer to obtain a mechanical input power spectrum and then to pass the two hydrophone pressures to the analyzer to obtain an acoustic intensity spectrum. This sequence was then repeated several times. In this way, a time series of spectra of the input mechanical power and of the output radiated intensity could be obtained for essentially the same measurement interval. This was the same method of data collection applied in the previous study²³.

Measurements of acoustic intensity required a choice of hydrophone spacing appropriate to the frequency range of interest. The highest frequency of interest was approximately 1,000 Hz. Far field calculations based on plane waves suggested a nominal hydrophone spacing of 46 to 92 mm would be appropriate. As measurements were to be in the near field, the spacing needed to be tested. Measurements of acoustic intensity were repeated four times keeping the midpoint of the hydrophones constant while varying their spacing. Similar intensity spectra were expected for each spacing if the range of spacing used was appropriate for the sound field. The resulting intensity spectra are shown in Figure 5.6 and were indeed reasonably similar. The similarity confirmed that this range of spacing would be appropriate up to about 900 Hz. The mid-point value, 90 mm, was used as the hydrophone spacing for all intensity mappings. This hydrophone spacing had been used in the previous study.

22 HP 34970A Data Acquisition/Switch Unit

23 Each spectrum in the timeseries represented an average of several instantaneous spectra. For example, each mechanical power spectrum in the timeseries from the dual channel analyzer was produced from a linear average of 20 instantaneous spectra. The final calculated mechanical power spectrum was obtained from a timeseries of 5 of these spectra. The final calculated acoustic intensity power spectrum was obtained using the same format as for mechanical power. Although 5 constituted a statistically small number, this approach allowed the calculation of the standard deviation associated with each spectral coefficient. While a statistically larger number would have been preferable, the length of measurements had to be balanced with the long data collection time interval required to map a grid of radiated intensity for one plate. One measurement of mechanical input power and acoustic radiated power, as described above took approximately 15 to 20 minutes. A mapping of a 5 by 5 grid of intensity required a full day.

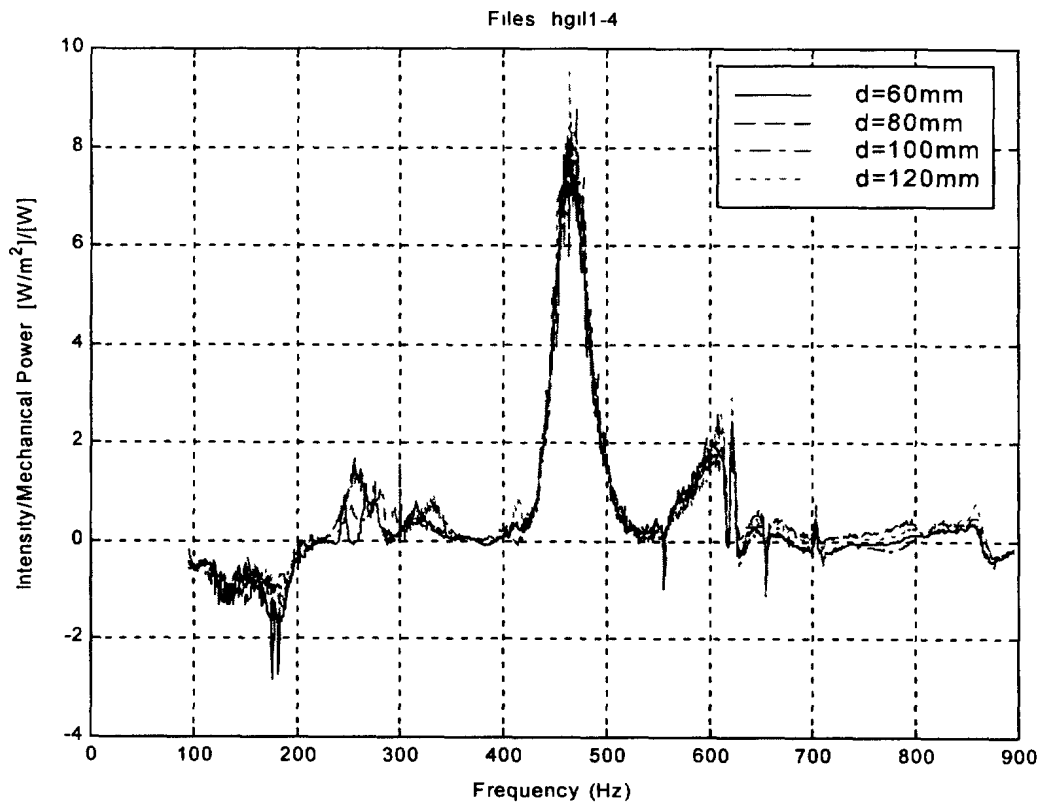


Figure 5.6: Measured intensity spectra for 4 hydrophone spacings.

The height of the mapping plane above the plate was examined. The mapping plane needed to be close to the vibrating surface of the plate in order to be able to assume that most of the radiated field crossed the plane. However, the height could be varied somewhat. Figure 5.7 illustrates an example of the measured intensity spectra for 4 heights above the same plate position. The results were dependent on the distance to the plate. After collecting several data sets versus height a mapping plane height of 121 mm was selected. Throughout the program the mapping plane height was adjusted carefully to maintain a similar height for all mappings.

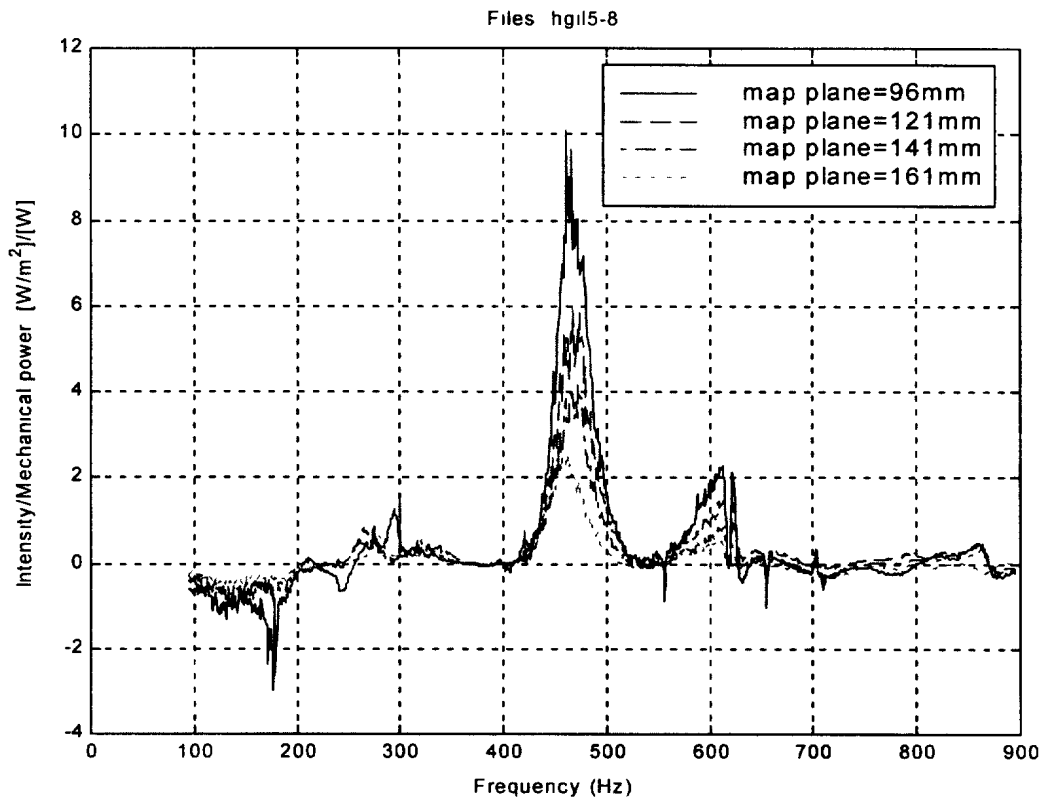


Figure 5.7: Example of intensity spectra as a function of height above plate.

The repeatability of acoustic intensity measurements was examined at various opportunities throughout the program. Typically a measurement taken at a position earlier in a mapping was repeated at a later time or the next day. Overall the repeatability was found to be quite good.

5.3 Measured Plates and Coatings

Two thicknesses of steel plates were used during the program, 3mm and 9.5 mm. Each plate thickness was tested in the bare condition. Each plate thickness was subsequently tested with different thicknesses and types of foam coatings as specified by DREA. The tested combinations of plate thickness and foam coating are listed in Table 5.1. The first column (ID) indicates the letter given to each plate and coating combination for ease of identification. The third column indicates the short name used to identify the coating material. Additional information on each coating material can be found in Appendix A. The last column indicates the approximate range of frequency over which the measured FRF appeared to exhibit relatively distinct separated peaks.

Table 5.1: Plate and coating combinations.

ID	Plate Thickness (mm)	Foam Type	Foam Thickness (mm)	Water Temp (deg C)	Modal Range (Hz)
h	9.5	none	0	15	100-900
i	9.5	SC4116	25 ²⁴	14	100-900
j	9.5	SC4116	25	13	100-900
k	3.0	none	0	13	100-900
l	3.0	V710	3	11	100-150
m	3.0	EAR	3	12	100-900
n	3.0	VA80	12	12	100-400
o	-	-	-	-	-
p	9.5	VA80	12	13	100-300
q	3.0	VA80	23	12	100-300
r	3.0	EAR	3 ²⁵	12	100-900
s	3.0	V710	3 ²⁶	12	100-900

5.4 Measured Frequency Response

The FRF (Frequency Response Function) for each coating and plate combination was obtained from the ratio of acceleration to force at the shaker driving point²⁷. An FRF was recorded prior to the start of intensity measurements and again at their conclusion. In all cases, the FRF's before and after data collection were very similar if not identical. Thus it could be assumed that the test setup had not changed appreciably during the intensity mapping. Figure 5.8 illustrates the FRF measured for the 9.5mm thick bare plate. This plate exhibited well separated modes from 100 to 900 Hz.

The FRF's are useful for examining the change in the vibrational response due to the addition of a coating. Appendix B contains graphs of the FRF amplitude ($|H1|$). Each graph shows two curves, the FRF for a coated plate and the corresponding FRF for a bare plate of the same plate thickness. Of the three foams examined, the V-710 seemed to exhibit the best ability to smooth out modal behaviour in the FRF (see plates K and L).

²⁴ Edge coated only along clamped boundary

²⁵ Coating facing into concrete enclosure

²⁶ Coating facing into concrete enclosure

²⁷ Calculated from the spectra of acceleration and force

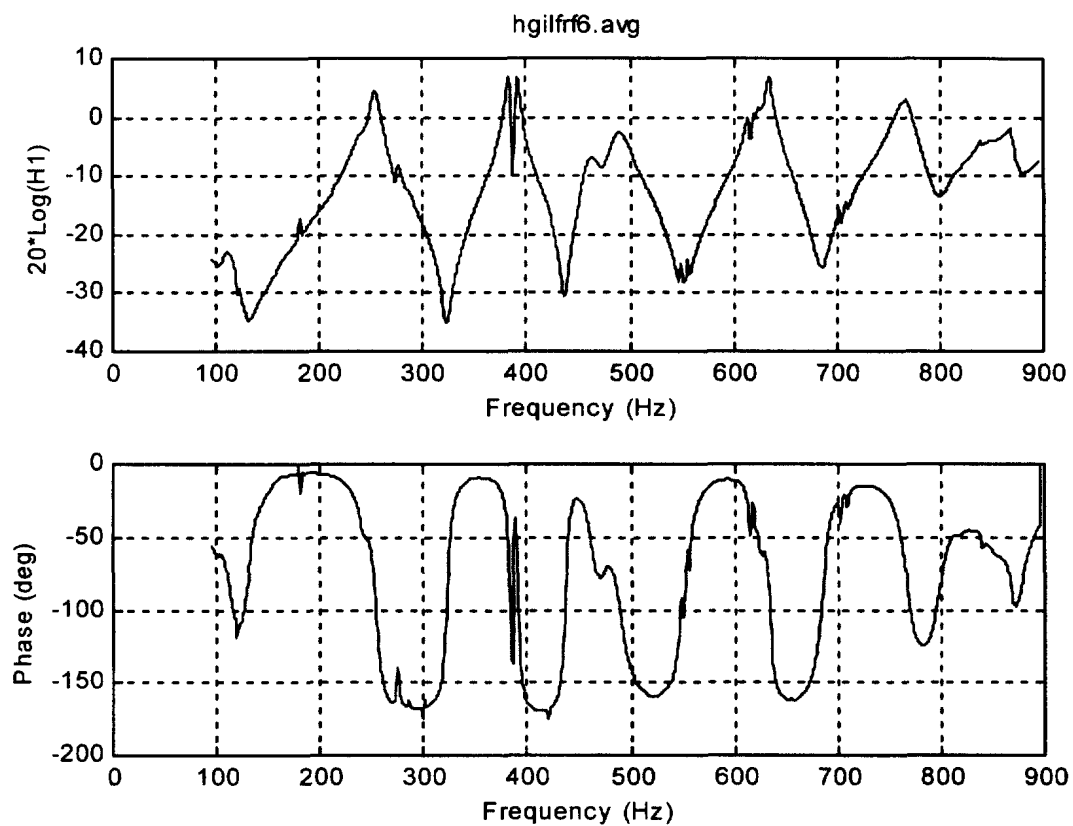


Figure 5.8: Measured FRF of 9.5mm thick bare plate.

6.0 QUANTIFYING THE RADIATED FIELD

This study, like the previous one, started by assuming that the majority of the acoustic power was radiated by the exposed surface of the plate or coating. It was assumed that the bulk of the radiated acoustic field passed through the mapping plane (positioned only a few centimetres from the surface of the coating). A positive outflow of net energy was anticipated at all frequencies.

In the previous study, there was an apparent influx of net power into the plate in some frequency regions, but the experimental setup had not excluded the possibility of external vibrations causing a second acoustic field. Also the standard deviation in the measurements had been comparable to the net observed power. So it was possible that the apparent influx of power was a combination of error and external contamination.

The concrete enclosure had been intended to significantly reduce the possibility of external vibration because of its relative stiffness and mass. Measurements on the 9.5mm thick bare plate were used to re-examine the net radiated acoustic power with the revised setup.

6.1 Examining the Net Radiated Power

The net radiated power was estimated by summing over the 5 x 5 grid, the product of each normalized intensity measurement with the cross sectional area represented by the measurement in the mapping plane. Two types of normalization were used. Intensity was normalized with respect to square force. Intensity was normalized with respect to mechanical input power. Both forms of normalization are indicated below. These calculations used the measured frequency spectra of intensity, force and velocity, and performed these calculations at each discrete frequency.

$$\frac{P_{\text{net}}}{[F^2]} = \sum_{i=1}^{25} \frac{I_i}{F_i^2} \times A_i, \quad (6.1)$$

$$\frac{P_{\text{net}}}{[F \times v]} = \sum_{i=1}^{25} \frac{I_i}{[F_i \times v_i]} \times A_i, \quad (6.2)$$

where ,

I = intensity measured at i th grid point,

A = area at i th grid point,

F = force measured for i th measurement,

v = velocity measured for i th measurement

The net power measured for the bare 9.5mm plate is shown in Figure 6.1.

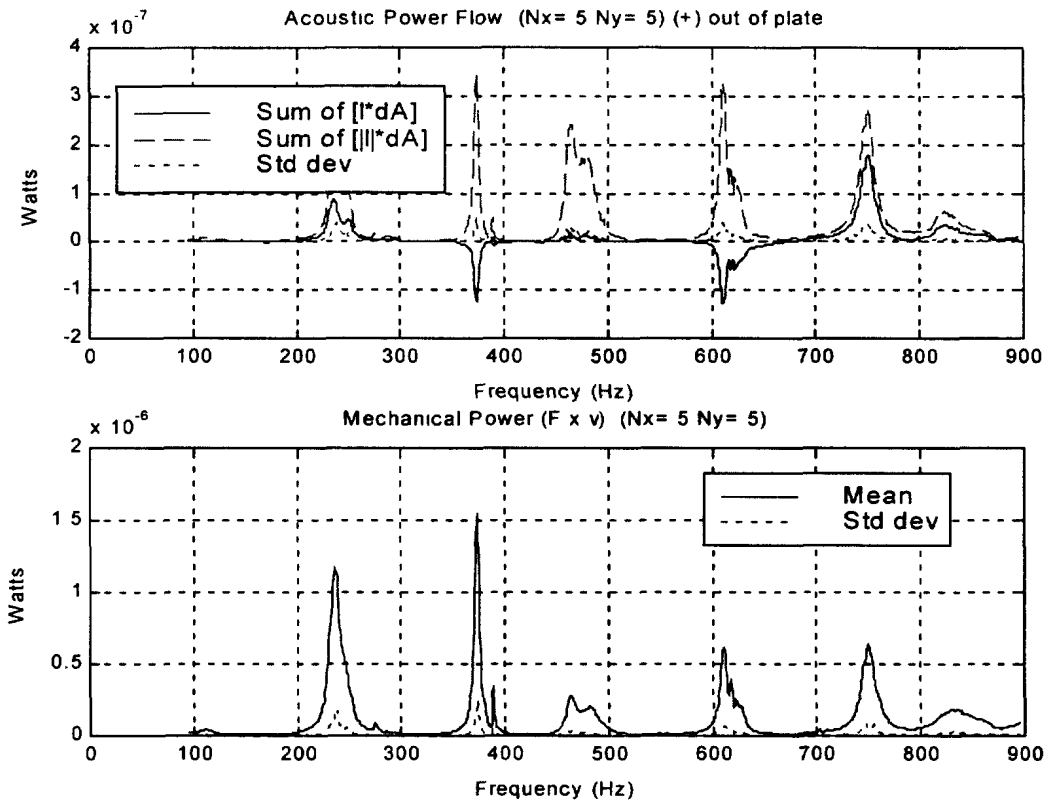


Figure 6.1: Net radiated power for 9.5mm bare plate.

The upper graph shows the net power crossing the mapping plane (sum of $[I \cdot dA]$) and its calculated error (std dev). Unlike the previous study, the net power now typically exceeded its error estimate comfortably. However, negative net radiated power was still indicated in some frequency regions.

It was speculated that perhaps the mapping plane was not being sufficiently sampled and some of the power crossing the plane was being missed. To investigate this hypothesis, additional data was collected at positions in between the existing 5 by 5 grid point positions, generating a 9 by 5 grid. A comparison of the net radiated power versus the number of grid points in the mapping plane is given in Figure 6.2. The curve of net power stabilized once a 5 by 5 point grid was established. Increasing the grid density to 9 by 5 did not appreciably change the curve. Consequently it did not appear that the mapping plane was being undersampled.

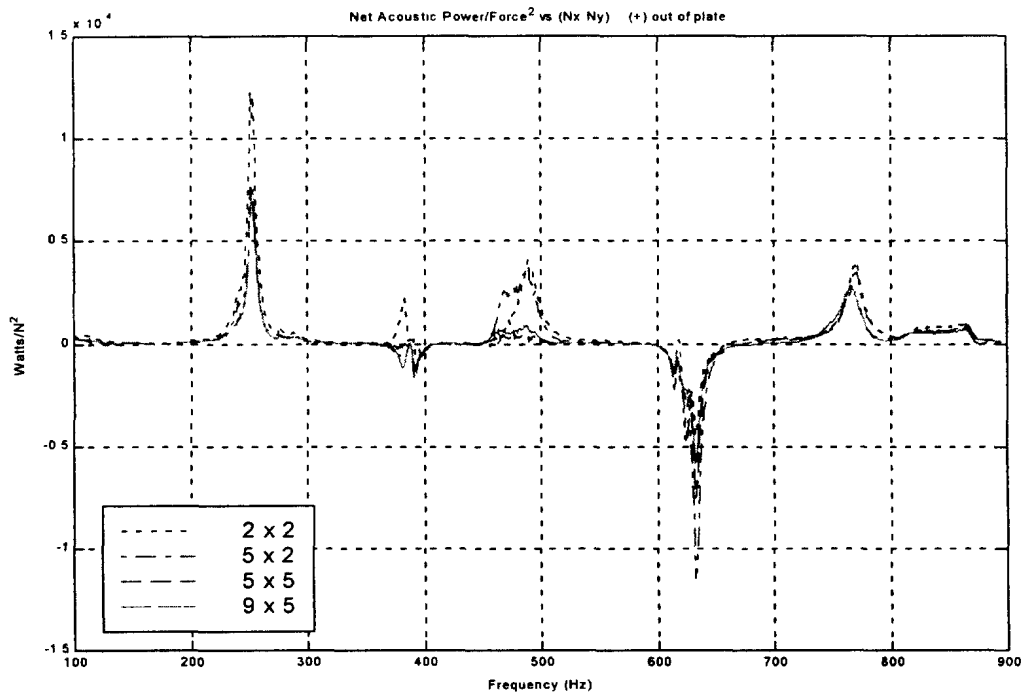


Figure 6.2: The calculated net acoustic power versus the quantity of measurement positions.

It was speculated that perhaps the acoustic energy was circulating in a complex pattern that did not fully intersect the mapping surface as expected, and perhaps the mapping plane should be enlarged. To investigate this hypothesis, additional measurements were made along a 5 by 2 grid that effectively extended one side of the mapping plane. However the net power crossing this strip was observed to be a small fraction (~5%) of the net power crossing the original 5 by 5 grid. While the possibility of a complex flow pattern could not be ruled out²⁸, it did not appear that enlarging the mapping plane would alter the experimental results appreciably.

The presence of isolated regions in the frequency spectrum of negative radiated power remained unresolved. Appendix C shows the corresponding graphs of input mechanical power and output radiated power for each coating and plate combination tested. The tests with the 9.5mm plates exhibited negative radiated power more so than the tests with the 3mm plates. Nonetheless there were isolated regions in almost every plot where the power appeared to be negative. An alternate approach was required to proceed with the experimental data analysis.

²⁸ Measurements could not be continued all across the tank. The hydrophone arms were only designed to cover the original grid.

6.2 Absolute Power

The alternate approach was to make use of the absolute value of the measured intensity as had been done in the previous study. The absolute value of measured intensity was integrated over the mapping plane, as an indicator of the level of acoustic power circulating in the near field. The operating premise was that a coating that reduced radiated sound would also reduce the amount of energy circulating in the near field. Comparison of the absolute intensity integrated over the mapping plane for the bare plate and coated conditions would provide a measure of the ability of the coating to reduce the radiated field. This approach was used as a means of estimating coating performance.

Mathematically the same expressions were used with the absolute value of intensity replacing the signed value.

$$\frac{P_{abs}}{[F^2]} = \sum_{i=1}^{25} \frac{|I_i|}{F_i^2} \times A_i \quad (6.3)$$

$$\frac{P_{abs}}{[F \times v]} = \sum_{i=1}^{25} \frac{|I_i|}{[F_i \times v_i]} \times A_i \quad (6.4)$$

Figure 6.1 illustrates, in addition to the net radiated power, a curve of the integrated absolute power. The magnitude of the absolute power always exceeds that of the net power as it should. Figure 6.3 illustrates the normalized absolute and net power for the 9.5mm bare plate.

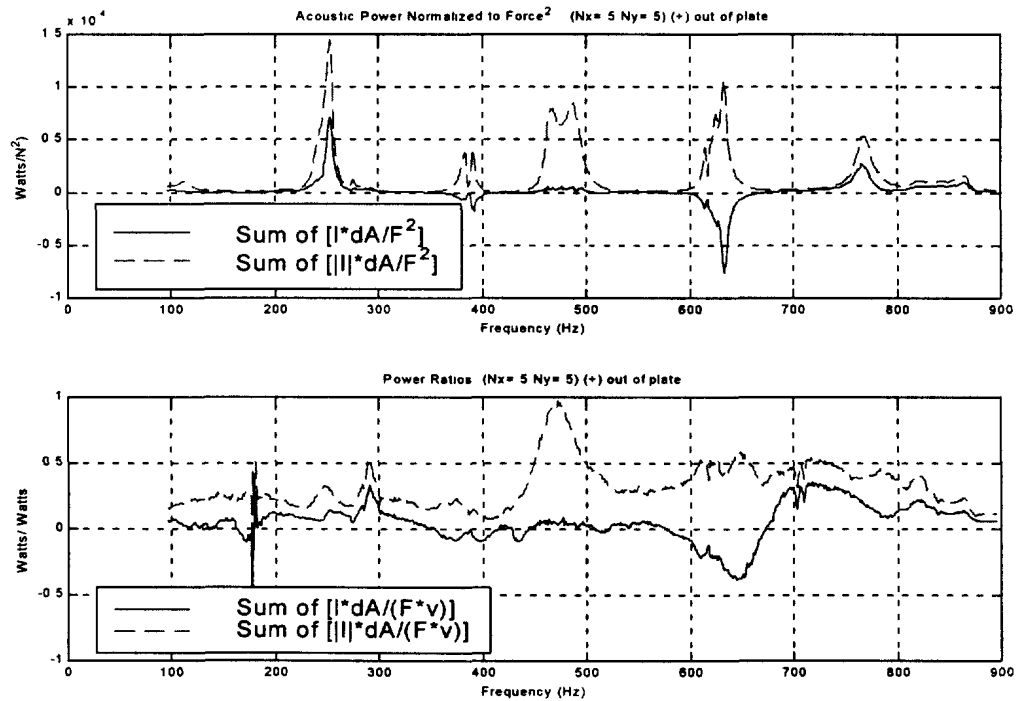


Figure 6.3: Normalized net and absolute power from bare 9.5mm plate.

Figure 6.4 illustrates the normalized absolute and net acoustic power for a 9.5mm plate coated with of 25mm of SC-4116.

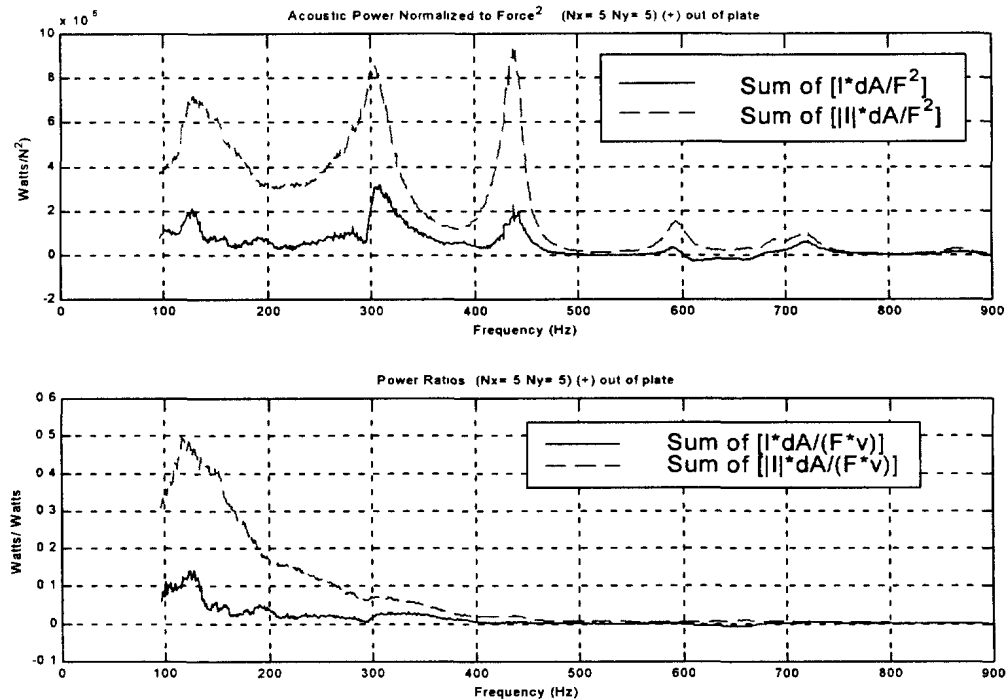


Figure 6.4: Normalized net and absolute power from a 9.5mm plate coated with 25mm of SC-4116.

Different vertical scales were used for the graphs of the bare and coated plates to get better detail of the curves. For the bare plate, the power normalized to force is presented on a scale of 1.5×10^{-4} while the coated plate is presented on a much smaller scale of 10×10^{-6} . Just from the differing scales it was apparent that the coating had reduced the radiated field. (Appendix D contains graphs of the normalized net and absolute power for each plate and coating combination tested.)

6.3 Comparison of Bare and Coated Plates

A visual comparison of the absolute acoustic power calculated for each bare and coated plate combination was made by plotting both curves on the same graph. Appendix E contains these graphs with the absolute power normalized to square force and with the absolute power normalized to mechanical input power. Figures 6.5 and 6.6 illustrate these two different normalizations for the 9.5mm plate, bare versus coated with 25mm SC-4116. From figure 6.5 it was seen that both curves had pronounced peaks and troughs, showing the emphasis that the normalization to force placed on modal response.

By comparison, figure 6.6 exhibited far fewer peaks and troughs showing the lack of emphasis that the normalization to input power placed on the modal nature of the plate.

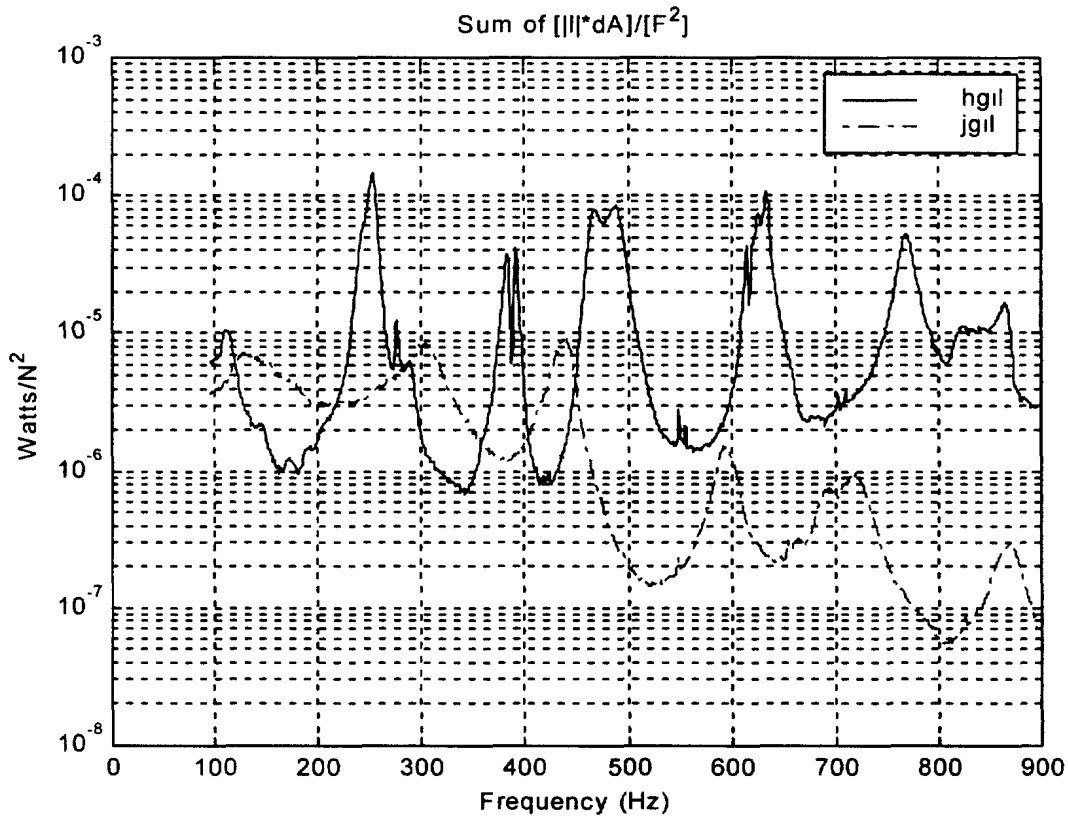


Figure 6.5: Comparison of 9.5mm plate (bare vs 25mm SC4116 coated) using absolute power normalized to square force

In both cases the trend of the coating was to decrease the amount of power with increasing frequency, relative to the bare plate. However this trend was more obvious with the normalization to input power where the curves tended to be smoother.

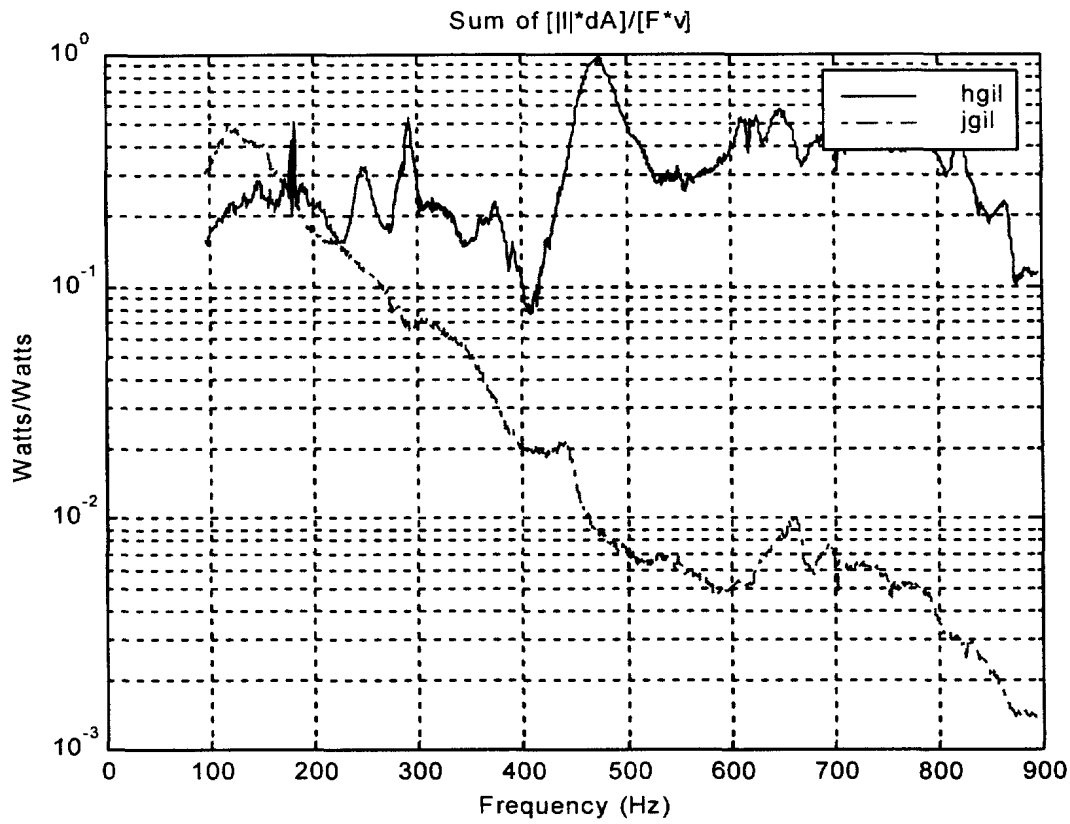


Figure 6.6: Comparison of 9.5mm plate (bare vs 25mm SC4116 coated) using absolute power normalized to input power.

6.4 Examining The Spatial Distribution of Measured Intensity

The change in spatial distribution of measured intensity in the mapping plane as a result of coating the bare plate had also been investigated. The measurements on the bare 9.5mm plate and the 9.5mm plate coated with 25mm of SC-4116 were used for this examination. The spectra of intensity measurements were separated into frequency bands corresponding to individual modes of vibration²⁹. A plot was then made of the measured net amplitude of intensity in each frequency band as a function of measurement position. Figure 6.7 illustrates the spatial distribution of the measured intensity of the bare plate in the 200 to 300 Hz band. The height of the arrows in the plot are proportional to the intensity magnitude. The direction of the arrows indicate positive (out of plate) or negative (into plate) power flow. The axis scales are indicated on the graph. Figure 6.8 illustrates the spatial distribution of the measured intensity of the coated plate for the same mode as that of the bare plate, which in this case corresponded to the 230 to 330 Hz band.

²⁹ For each plate the FRF's were used to identify the frequency bands that enclosed single modes

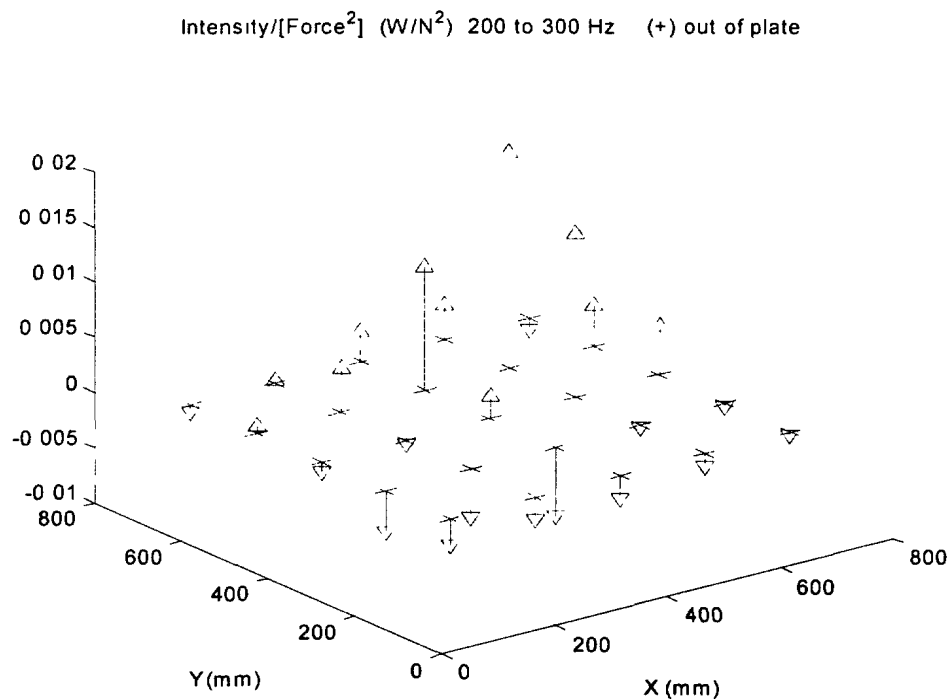


Figure 6.7: The spatial distribution of intensity from the bare 9.5mm plate in a modal band.

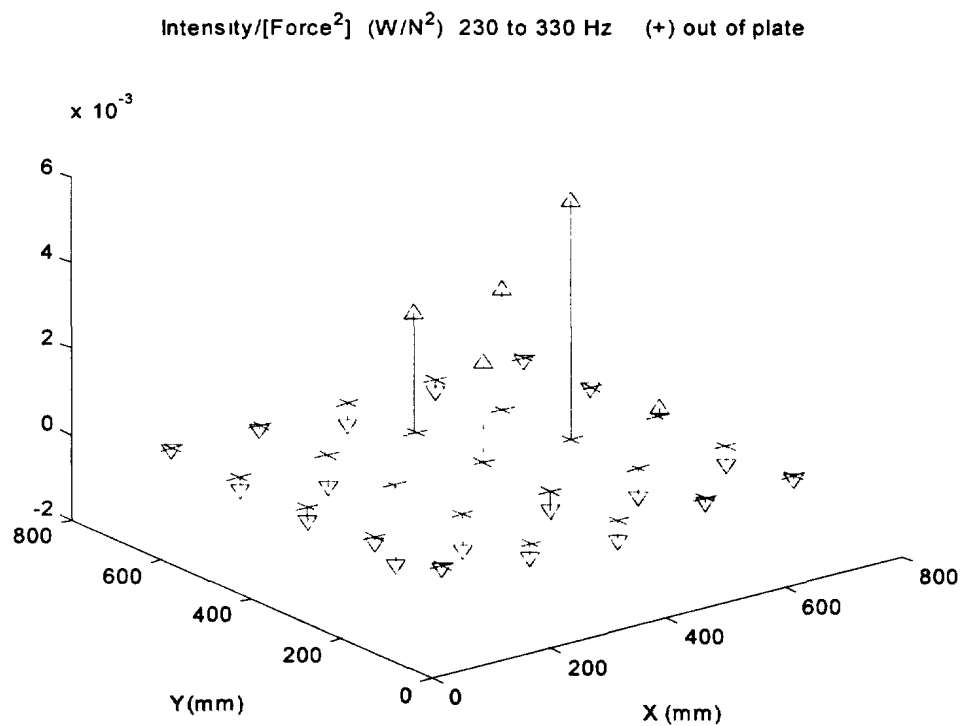


Figure 6.8: The spatial distribution of intensity from the 9.5mm coated plate (25mm of SC-4116) in the same modal band.

Similar plots were examined for each modal band common to both plates to provide some insight into the effect of the coating. In general, the spatial energy flow was both into and out of the plate in all bands, for both plates. The pattern of radiated power was not easily interpreted. Consequently it was difficult to attach physical significance to a change in the pattern of radiation from the bare to the coated condition. No new information was acquired by this route.

7.0 EXPERIMENTAL AND MODELLED DECOUPLING PERFORMANCE

7.1 Experimental Decoupling Performance

The experimental decoupling performance (DP) was estimated from the absolute value of the measured intensity integrated over the mapping plane. Calculations were made using normalization with respect to force,

$$DP = \frac{\left[\frac{P_{abs}}{F^2} \right]_{bare}}{\left[\frac{P_{abs}}{F^2} \right]_{coated}} \quad (7.1)$$

and also using normalization with respect to input power,

$$DP = \frac{\left[\frac{P_{abs}}{F \times v} \right]_{bare}}{\left[\frac{P_{abs}}{F \times v} \right]_{coated}} \quad (7.2)$$

The formulae for the individual ratios in square brackets have been given in equations 6.1 to 6.4. Figure 7.1 plots the calculated value of DP for a 23mm coating of SC4116 on a 9.5mm plate. Each data point represents the average value over a 50 Hz wide frequency window. With either normalization, the calculated DP showed the same trend of increased performance with increasing frequency. However the normalization to input power exhibited a much smoother curve with less variation than the normalization to force. The lack of smoothness of the DP calculated with the normalization to force was attributed to the tendency of that normalization to emphasize the modal nature of the plate. Appendix F contains the graphs of the estimated experimental decoupling performance for each plate and coating combination.

Table 7.1 lists the calculated DP for foam coatings on 3mm plate at specific frequencies to facilitate a comparison of elastomer performance. The 3mm of V710 provided more decoupling at all 3 frequencies than 3mm of C-1002 and 12mm of VA80. From the numbers, 23mm of VA80 provided roughly the same performance as 3mm of V710. This result was also observed by overlaying the corresponding graphs (Appendix F) and comparing the values normalized to input power.

Table 7.1: Experimental Coating Performance (3mm plate)³⁰

Foam Type	ID	Plate Thickness (mm)	Foam Thickness (mm)	DP 120 Hz	DP 520 Hz	DP 864 Hz
V710	l	3.0	3	1.4	2.6	13
VA80	n	3.0	12	0.9	2.3	2.8
VA80	q	3.0	23	1.1	1.9	12
C-1002	m	3.0	3	0.7	1.2	1.7

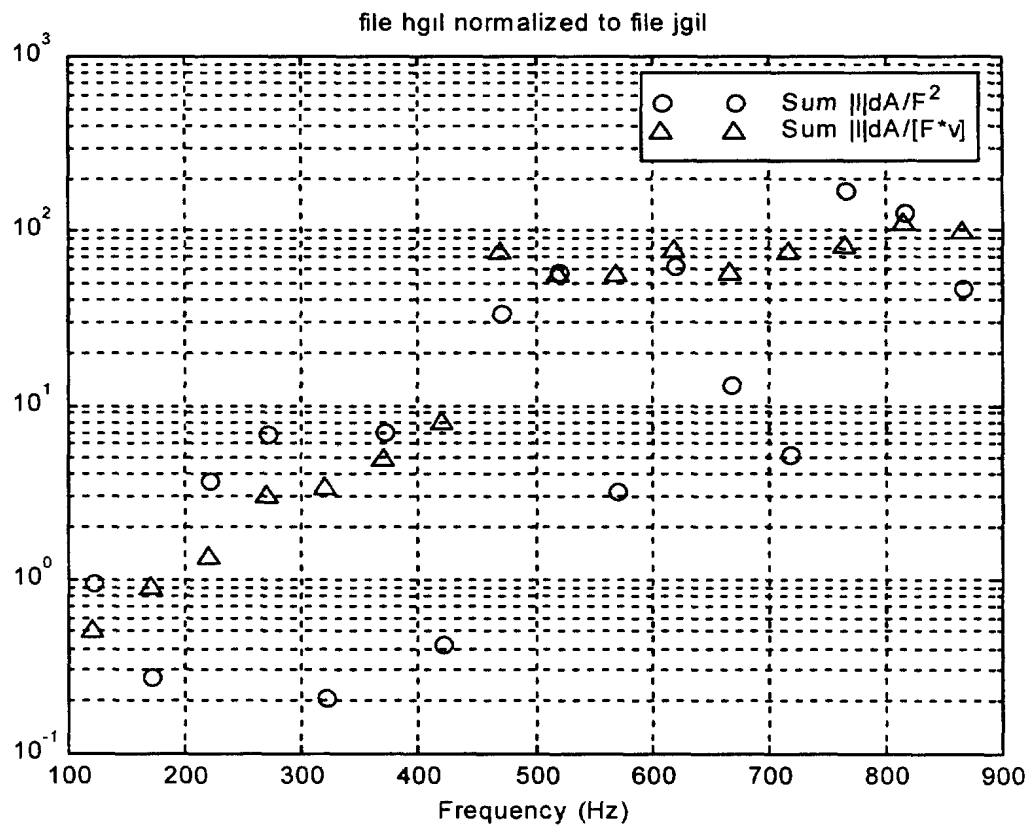


Figure 7.1: Experimental decoupling performance for a 23mm coating of SC4116 on a 9.5mm steel plate.

Table 7.2 lists the calculated DP for 9.5mm plate at specific frequencies. Only two tests were done at this plate thickness, with different foam thicknesses. Consequently, a comparison could not be made of relative coating performance for this plate thickness.

³⁰ Normalization to input power

Table 7.2: Experimental Coating Performance (9.5mm plate)³¹

Foam Type	ID	Plate Thickness (mm)	Foam Thickness (mm)	DP 120 Hz	DP 520 Hz	DP 864 Hz
SC4116	j	9.5	25	0.5	56	98
VA80	p	9.5	12	0.9	1.7	5

7.2 Observed Decoupling Performance -Tank and Barge Configurations

The combination of 25mm of SC4116 on 9.5mm thick steel plate measured in this program was also measured in the previous experimental program, but with very different plate boundary conditions and a very different scale of water volume. Instead of clamping the plate to a rigid surface such as the concrete enclosure, vibration mounts were used to suspend the plate at its four corners from a stiff frame. The coated plate had been suspended at the air water interface with the coated side in contact with the water. The acoustic intensity measurements had been performed in a similar manner to this study, but the experiment took place on a barge anchored in a bay, which provided an available water volume that was much larger than the tank volume used in this program.

The decoupling performance observed in the tank was compared with that observed from the barge to investigate whether the experimental configuration (plate boundary conditions and water volume) played a substantial role in determining the observed decoupling performance. Figure 7.2 illustrates the decoupling performance calculated from the data collected on the the barge and should be compared with Figure 7.1 (the observed decoupling performance in the tank). Both figures exhibit the same range of values. In both cases it is the decoupling performance normalized to mechanical input power that provides the smoother more continuous curve.

³¹ Normalization to input power

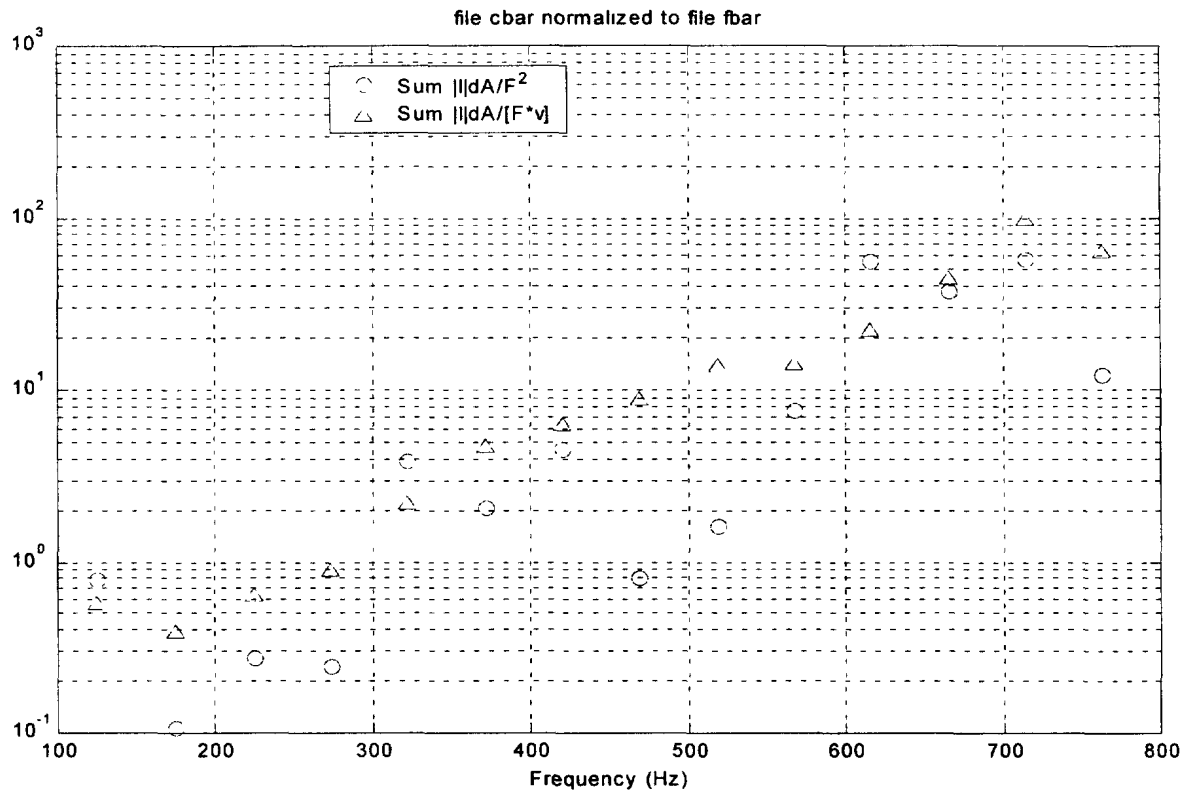


Figure 7.2: Experimental decoupling performance for a 23mm coating of SC4116 on a 9.5mm steel plate suspended with vibration supports.

The two decoupling performances are compared on the same graph in Figure 7.3 using the normalization to mechanical input power. The two performances were quite similar, appearing to be linear when plotted on a semi-logarithmic scale. The barge data lay below the tank data in the 200 Hz region where the effect of sprung mass resonance would be expected to depress decoupling performance for a plate suspended with vibration mounts at its four corners (see section 4.1). The tank data exceeded the barge data in the 500 to 600 Hz region where the effect of a standing wave in the finite volume of the tank would be expected to elevate decoupling performance (see section 4.2). These observations suggest that had the boundary conditions been similar in both tests, the only difference in observed decoupling performance would have occurred as a result of standing waves in the tank, in a localized frequency region. These observations similarly suggest that when the frequency region of standing waves is excluded from consideration, the observed decoupling performance from tank measurements could be expected to be very similar to that obtained in open water.

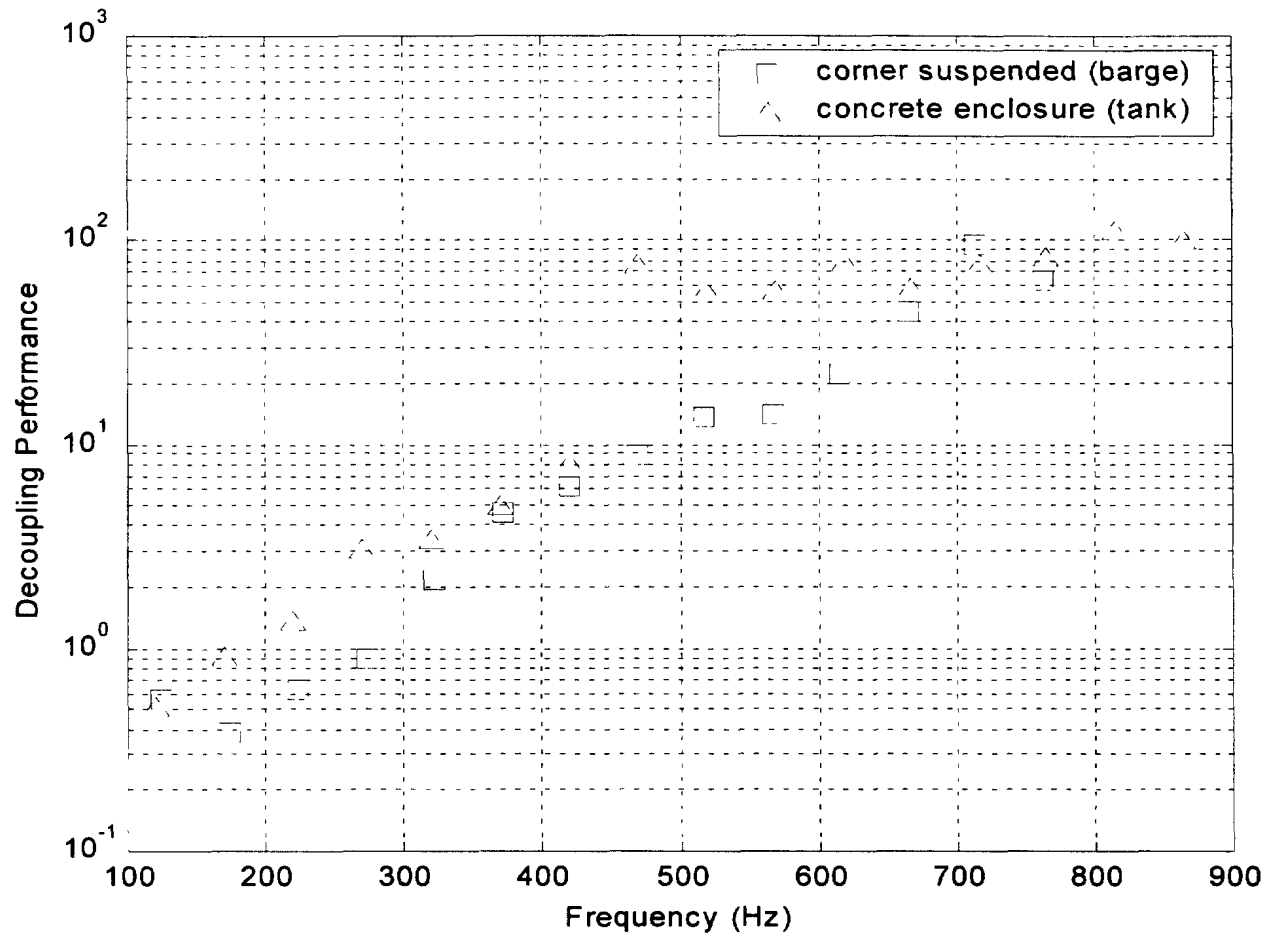


Figure 7.3: Comparison of decoupling performance for a 23mm coating of SC4116 on a 9.5mm steel plate – Barge configuration vs Tank configuration.

7.3 Example of a Partially Coated Plate

The plates used in this study were physically larger in area than those used in the previous study to accommodate the supporting surface running in a 51mm wide strip below the peripheral edge of the plates. Initially there was an interest in reducing the exposed area of the plates in this study down to that of the plates in the previous study. In between the measurements on the bare 9.5mm plate and on the fully coated 9.5mm plate (with 25mm of SC-4116), measurements were made on the 9.5mm plate in a partially coated condition. Strips of SC-4116 were glued to cover the upper plate surface along its edge extending inwards 75mm. This partial coating left a bare square area in the centre of the plate measuring 600 mm x 600 mm, reducing the exposed plate area down to 65% of its original size. The experimental decoupling performance of the partially coated plate is provided in Figure 7.4 on the same scale as the performance observed for the fully coated plate (Figure 7.1).

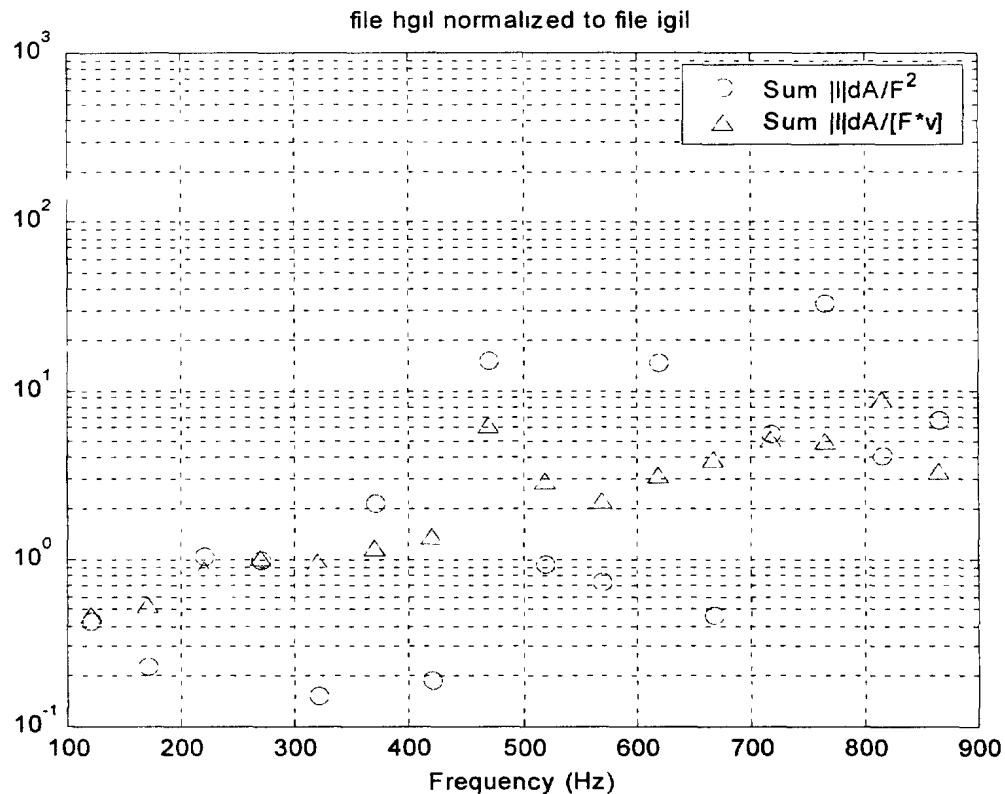


Figure 7.4: Experimental decoupling performance for a partially coated 9.5mm steel plate with 23mm SC4116.

The data shows that as the frequency increased the partial coating did noticeably reduce the radiated field. At first glance this might appear to be unexpected since the coating mostly covered the section where the bolt pattern clamped the plate to the square steel frame embedded in the concrete enclosure. However, the coating also extended 25mm beyond the underlying edge of the steel frame. Presumably this region of the plate, although bolted nearby, was vibrating with sufficient amplitude for the coating to provide some decoupling.

7.4 Example of Reversing the Coating to the Air Side

The foam coatings were presumed to function as decoupling media, rather than as damping materials. They were assumed to provide the compliance, such that to some degree, the plate displacement would not be transferred across the foam. However it was not clear whether these foams also introduced substantial damping as they deformed.

To explore this question, measurements were made with the coated side of a 3mm plate facing inwards into the concrete enclosure. This orientation placed the bare side of the plate in contact with the water, and the coated side facing the air in the cavity of the enclosure³². The test used the 3mm plate coated with 3mm of V-710. Graphs of the experimental decoupling performance for the coating facing outwards (plate L) and inwards (plate S) are provided in appendix F. When the coating faced outwards, the decoupling performance increased from approximately 1.5 at 100 Hz to about 15 at 900 Hz. By comparison, when the foam faced inwards, the decoupling performance scattered about unity across the same frequency band. The comparison confirmed that the main effect of the foam was that of a decoupler.

This same type of test was also conducted with the 3mm plate coated with C-1002 damping material to examine whether this material was compliant enough to provide any decoupling. Graphs of the experimental decoupling performance for the coating facing outwards (plate M) and inwards (plate R) are provided in appendix F. When the coating faced outwards, the decoupling performance increased from approximately 1 at 100 Hz to about 2 at 900 Hz. When the material faced inwards, the decoupling performance hovered between 1 and 2 across the same frequency band. The material was at best a very weak decoupler.

7.5 Comparison of Experimental and Modelled Performance

The experimental values of decoupling performance³³ were compared with the modelled performance. It was observed that the experimental performance did not exhibit the troughs indicative of sprung mass resonance discussed in section 4.1. This feature is illustrated in Figure 7.5 which compares the experimental and observed decoupling performance for 3mm of V710 foam on a 3mm plate. As can be seen, the sprung mass resonance effect creates a trough from 100 to 500 Hz, while the experimental data seems to follow a smooth line that joins unity at 0 Hz to the tangent to the curve at 600 Hz. Appendix G contains graphs of experimental and predicted performance for all the plate and coating combinations tested. The same trend was observed in these figures as well. In hindsight, the sprung mass resonance was a condition that the experimental apparatus precluded. This effect would have required the free edge condition of a floating setup such as House (1991) used, and the clamped plate edges effectively eliminated this possibility.

For the 3mm plate tests, the experimental data exhibited a sudden decrease in amplitude with increasing frequency somewhere between 500 and 600 Hz, and then continued to again rise with increasing frequency. For example in Figure 7.5, just past 500 Hz the experimental data exhibited a drop in amplitude. Then beyond 500 Hz the experimental amplitudes seem to rise again with frequency, loosely paralleling the theoretical curve.

³² The shaker was attached to the plate, not the surface of the coating

³³ Calculated from the absolute value of the measured intensity integrated over the mapping plane

Figure 7.5 has the lowest sprung mass frequency of the three cases involving 3mm plate. Above 600 Hz the calculated DP was about a factor of 2 to 6 down from the modelled DP. The other two cases with 3mm plate appear to show closer agreement between the model and the calculated DP above 600 Hz but it is believed that this was only because those cases had higher sprung mass centre frequencies that tended to depress the modelled DP curve above 600 Hz.

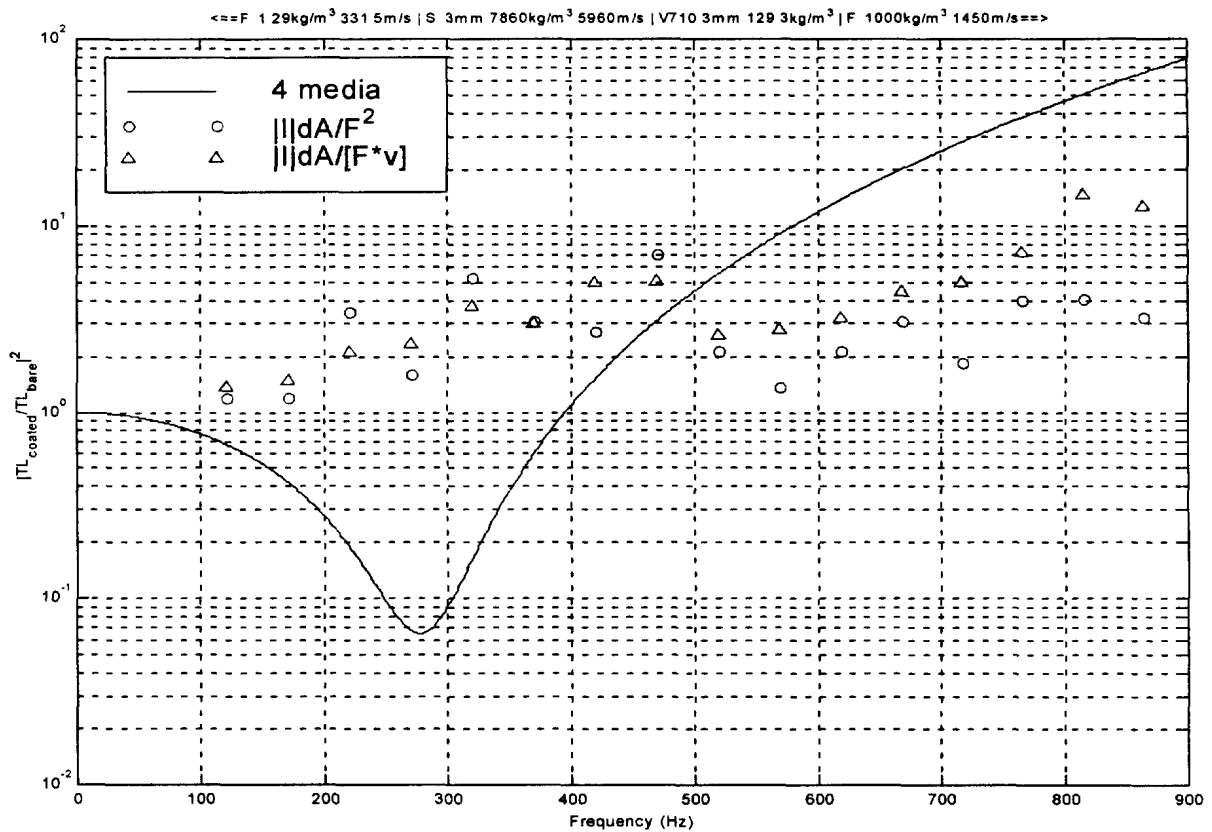


Figure 7.5: Experimental and modelled decoupling performance for 3mm of V710 on 3mm plate.

The results with 9.5mm plate tests seemed to follow trends similar to those of the 3mm plate tests. Figure 7.6 shows the experimental and observed decoupling performance for 12mm of VA80 foam on a 9.5mm plate.

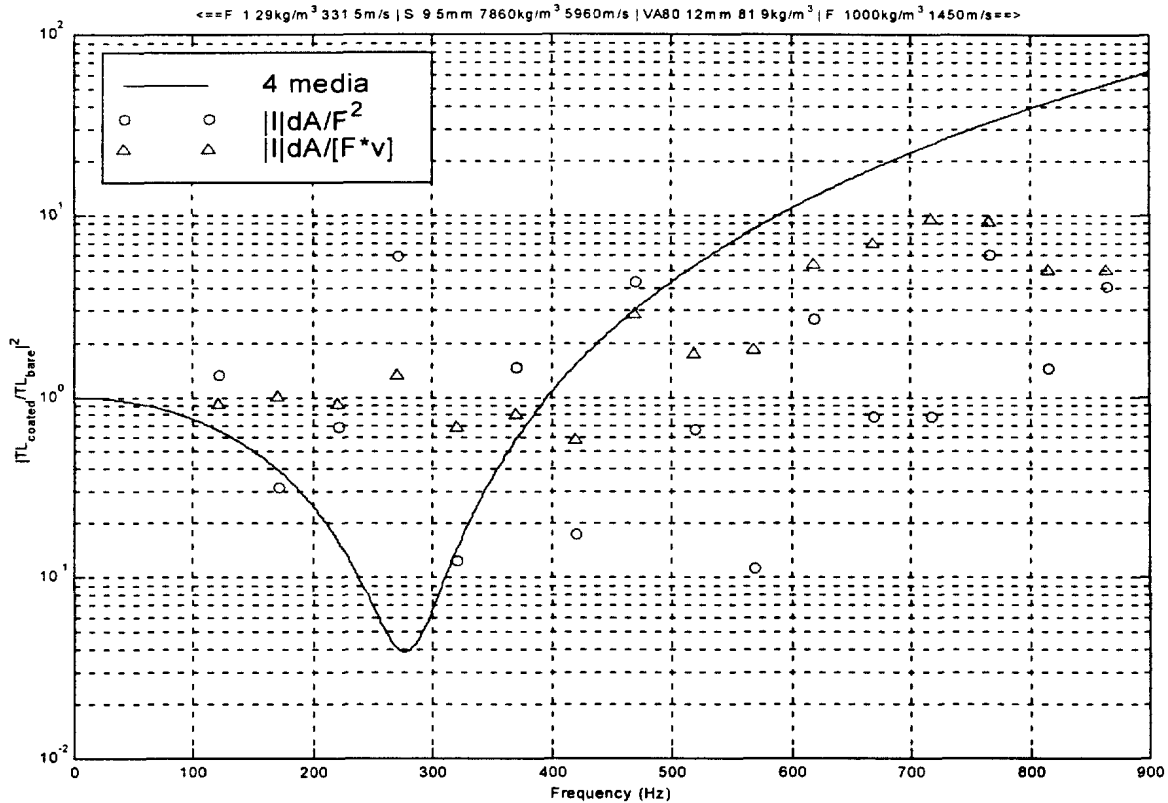


Figure 7.6: Experimental and modelled decoupling performance for 12mm of VA80 on 9.5mm plate.

From Figure 7.6, the experimental performance did not exhibit the trough indicative of sprung mass resonance. Well above the centre frequency of sprung mass resonance the calculated DP was about a factor of 2 to 10 down from the modelled DP. The same comments also applied to the only other coated 9.5mm plate example (25mm of SC4116).

From the comparison of modelled and experimental DP it became apparent that the model and experimental setup were not well matched, foremost because the model supported the possibility of sprung mass while the experimental setup precluded it. This was unfortunate because the sprung mass response dominated a large region of frequency in most of the cases examined. Outside the frequency region where sprung mass dominated response, the calculation of DP with absolute intensity underestimated the theoretical DP by a factor of 2 to 10. There were several potential sources of error that could have resulted in underestimation. The error may have been due to the use of absolute intensity; absolute intensity was a compromise made in order to obtain a quantitative estimate of DP. It was possible that the source of the discrepancy resided with the difference in scale between the finite dimensions of the plate and infinite plate dimensions assumed by the model. The source of the discrepancy may have been related

to differences in propagating waves; the model used plane waves while the real plate supported flexural waves.

Another source for the discrepancy between experimental and modelled DP may have been caused by a difference in measurement temperatures. The foam properties had been measured at temperatures of ~ 20 degrees C while the water temperature in the tank had been between 11 and 15 degrees C during intensity measurements. The colder water would have tended to raise the magnitude of the dilatational modulus (L). Whether any of the foams had suffered a substantial increase in their modulus in the colder water relative to the values measured in air remained unresolved. However, an increase in modulus (L) would generally have reduced their experimental DP. Figure 7.7 illustrates the modelled DP for the 3mm V710 coating on a 3mm plate, assuming a 50% increase in the magnitude of L . Above the frequency of the sprung mass region, the increase in $|L|$ moved the modelled DP closer to the experimental DP (compare with Figure 7.5).

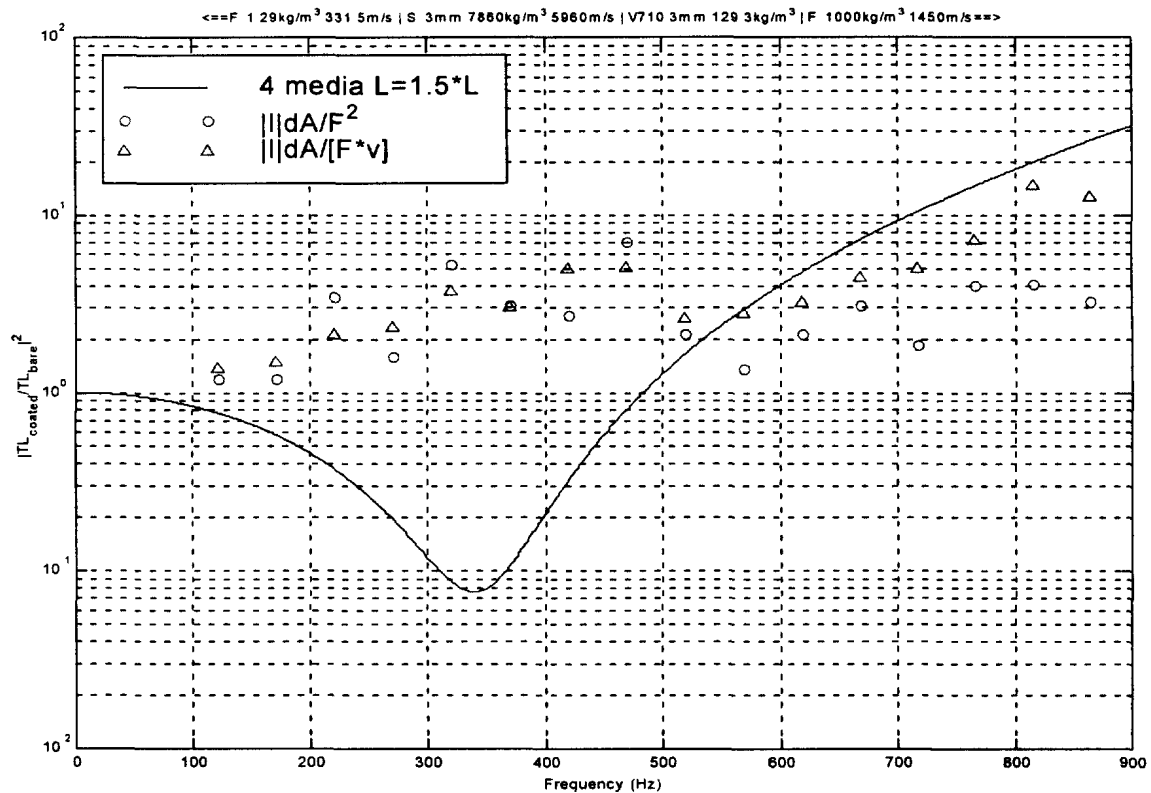


Figure 7.7: The effect of a 50% increase in the dilatational modulus.

8.0 DISCUSSION

This study investigated ways and means of quantifying the sound suppression performance of foam elastomer coatings for use on ship's hulls³⁴. The program started by implementing a model that calculated the decoupling performance of a foam elastomer coating attached to a steel plate. The program then developed a method to measure the frequency dependent dilatational modulus of foam elastomers in the 100-1000 Hz frequency range. Measurements on foam samples with this method produced the material property information required by the model for theoretical decoupling performance predictions. In parallel, the experimental setup from the previous program was changed to provide more consistent plate mounting conditions in a more controlled supporting structure. Subsequently, the acoustic field radiated from several different foam coated plates was measured with the experimental setup. Lastly, a comparison was made between what the model predicted and what was experimentally observed.

There were two criteria by which the experimental method for obtaining the foam samples' dilatational modulus was judged. The method was examined for its ability to obtain a dilatational modulus that was relatively independent of the thickness of the foam sample. The method was also judged by the modulus value it produced at the frequency where the foam sample could be approximated as a simple spring, where a second independent calculation of the effective modulus could be obtained. For the most part the results were insensitive to material thickness between 100 and 900 Hz, provided the sample thickness to diameter ratio was kept small ($\sim 1:25$). There was also reasonable agreement at the frequency where the foam sample could be approximated as a simple spring. These two agreements provided confidence in the method of measurement. This part of the experimental program was considered to have been successful.

The model utilized the material properties of the foam, steel and adjacent fluids. It was a simple model in the sense that it was based on plane waves. The plate and coating had specified thicknesses, but they were assumed infinite in length and width. Predictions were made for the various plates and coatings between 100 and 900 Hz where there was confidence that the foam material property information fed to the model was reasonably accurate. This part of the program also functioned well. However, as will be discussed, the results were specific to the assumed boundary conditions.

The structural setup for testing the elastomers in the tank worked quite well as a vibration test setup. The multi-point clamping of the plates with torqued bolts provided a clamping condition that remained constant with time. This approach eliminated problems that had occurred in the previous study with fatiguing supporting vibration mounts. There had been concern that the concrete/plate assembly could leak without indication during vibration tests. However, the interior of the concrete test structure was pressurized to the hydro static head acting on the plate plus an extra half psi. This pressurization served two purposes. It identified the position of initial minute leaks with bubble trails which were

³⁴ Many of the techniques applied in this study were suggested or continued from the previous study covering the same topic

then sealed; the structure was found to be water tight thereafter. The pressurization also balanced off the bowing effect on the plate of the net hydrostatic force. It was found that the measured frequency response of a coated plate was the same at the beginning and end of measurements which provided confidence in the stability of the setup. Lastly, with the coating facing upwards from the bottom of the tank, it was possible to visually confirm that air bubbles were not attached to the coating, a question that was difficult to address with previous setups where the coating faced down towards the tank bottom. As an experimental setup, this arrangement worked quite well, although as will be discussed, the boundary conditions of the plate differed from the model.

When the experimental and modelled results were compared, the physical differences between the boundary conditions of the model and the boundary conditions of the test structure were highlighted. It became apparent that the model and the experimental apparatus were not well matched. In the model, the infinite extents of the plate and coating meant that the plate was theoretically not restrained except for the action of the foam coating on one side and the light fluid (air) on the other side. This situation allowed the plate and foam to have a sprung mass response where the foam and plate looked like simple spring pushing a dead mass. By comparison, the coated test plate was bolted to the concrete supporting enclosure. Experimentally the plate edges were clamped. This restraint inhibited the condition of sprung mass resonance. The plate could not freely move as a dead mass sprung on the foam coating. It became apparent during the comparison of experimental and theoretical decoupling performance just how much the sprung mass effect dominated the modelled decoupling performance of the coated plate at lower frequencies. In every case the modelled performance had a large dip over a broad frequency range centred on the sprung mass frequency, while the experimental decoupling performance passed smoothly over the same frequency region.

It had been planned to develop the methods for assessing coating performance in a small test facility where the environment could be controlled. Consequently, the experimental measurements took place in an acoustically small tank. The parameter used to quantify the sound field was time averaged acoustic intensity. This measurement was employed because of its ability to average out the reverberent energy flow (associated with a small tank) to obtain the net flow of energy. It was assumed that intensity measurements integrated across a plane a few centimeters from the coated plate's surface would be the net power radiated by the coated plate. Positive net flow would be expected at all frequencies.

In the previous study, the net acoustic power flow measured near the coating surface was both positive and negative. The negative net flow had been attributed to extraneous contaminating acoustic fields, perhaps from vibrations of the supporting structure. The experimental arrangement in this program was designed to mitigate support structure vibrations with the introduction of a concrete support box. However negative acoustic power flow was still observed in some frequency regions. Physically then, the measured net power crossing the plane above the coating could not be treated as the net power radiated by the coated plate. While the reasons for this behaviour were investigated with additional measurements, the issue was never resolved. The same approach was then

employed as in the previous program. The absolute power flow crossing the measurement plane was taken to be a measure of the acoustic power circulating in the near field. Decoupling performance was estimated from the apparent reduction of the absolute power flow crossing the measurement plane above the surface of the coated plate as opposed to the net flow.

Normally, the assessment of the utility of decoupling performance calculated with absolute power flow might be guided by the level of agreement between experimental and modelled performance. However, this aspect was difficult to assess because the model allowed for a sprung mass response that the experimental setup did not have. Much of the difference between the decoupling performance calculated from experiment, and the modelled decoupling performance, was because of difference in sprung mass response. Above the region of sprung mass resonance, the decoupling performance calculated from experiment typically underestimated the plane wave theoretical estimate while roughly paralleling the theoretical curve. With the 9.5mm plate, the estimated experimental performance above sprung mass resonance was about a factor of 2 to 10 below the curve of modelled performance. With the 3mm plate the estimated experimental performance above sprung mass resonance was about a factor of 2 to 6 below the curve of modelled performance.

Experimentally, a direct connection to net radiated power in the tank could not be established with intensity measurements. This is an area for concern. Exploring the reasons for this situation within the existing setup would be a worthwhile exercise that would support any future work in a small tank. The results of that exercise would presumably determine whether intensity measurements are the appropriate acoustic measurement for this application.

Theoretically, the model allowed a sprung mass behaviour that dominated the lower frequency region. This effect was found to be too overwhelming. The decoupling response was effectively controlled over a broad frequency region by the thicknesses and properties of the plate and coating at just one frequency. It did not appear that a sprung mass response was an asset theoretically, for a general comparison of the noise reduction capability of different coatings. A model whose boundary conditions precluded a large sprung mass response would be an improvement over the existing model, and would be more indicative of the experimental apparatus. If alternatively, the user finds the sprung mass effect of benefit, then the clamping of the experimental plate edges by the support structure would need to be removed. One means of accomplishing this condition would be to float the plate and coating on the water surface, or suspend a self contained setup at mid depth.

Some directions can be pursued without additional measurements. The data sets collected to date contain spatial grids of the pressures in a plane close to the submerged coating surface. It might be informative to recalculate the decoupling performance with this data and compare the result to the decoupling performance calculated from absolute power.

REFERENCES

- Burns, J., Dubbelday, P.S. and Ting, R.Y. "Dynamic Bulk Modulus of Various Elastomers"
Journal of Polymer Science: Part B: Polymer Physics, Vol. 28, 1187-1205, (1990).
- Cannon, C.M., Nashif, A.D. and Jones, D.I.G. "Damping Measurements on Soft Viscoelastic Materials Using a Tuned Damper Technique"
Shock and Vibration Bulletin, 38, 151-163, (1968).
- DREA, Private Communication, April 29, 1998
- Edwards, J.L. and Hicks, D.R. "Useful Range of a Mechanical Impedance Technique for Measurement of Dynamic Properties of Materials"
J. Acoust. Soc. Am. 52(3) Part 2, 1053-1056, (1972).
- Edwards, J.L. and Hicks, D.R. "A Mechanical Impedance Technique for the Measurement of the Dynamic Properties of Materials"
Proc 1971 AFSC Sci. Eng. Symp. Dayton, Ohio, Vol. III (1971).
- Jones, D.I.G. "Temperature-Frequency Dependence of Dynamic Properties of Damping Materials"
Journal of Sound and Vibration, 33(4), 451-470, (1974).
- Jones, D.I.G. and Parin, M.L. "Technique for Measuring Damping Properties of Thin Viscoelastic Layers"
Journal of Sound and Vibration, 24(2), 201-210, (1972).
- Klein, K. and Hamm, C.A., "Measurements of Sound Intensity as a Tool for Comparing Relative Merit of Noise Reduction Coatings"
DREA Contract Report 97/442 (1997).
- House, J.R.C. "Considerations for Underwater Decoupling Treatments"
Proc. Institute of Acoustics 13 Part 3, 166-173, (1991).
- Nashif, A.F. "A New Method For Determining Damping Properties of Viscoelastic Materials"
Shock and Vibration Bulletin, 36, 37-47, (1967).
- Snowden, J. C. "Vibration isolation: Use and characterization"
J. Acoust. Soc. Am. 66(5), 1245-1274, Nov. (1979).

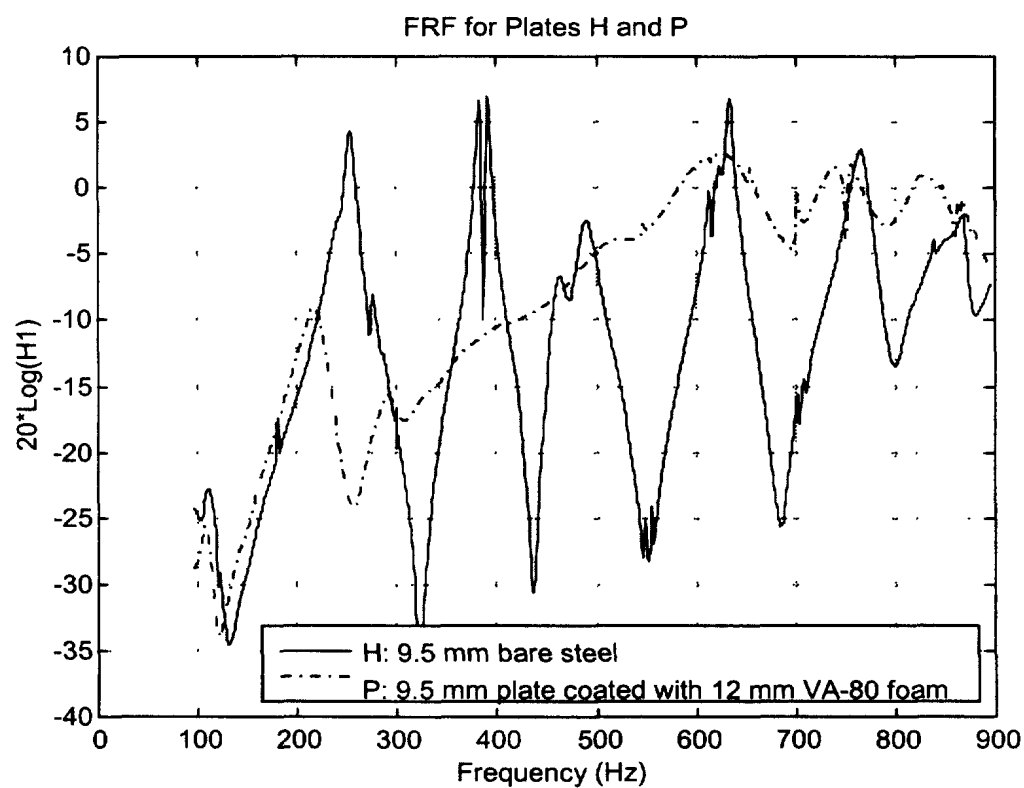
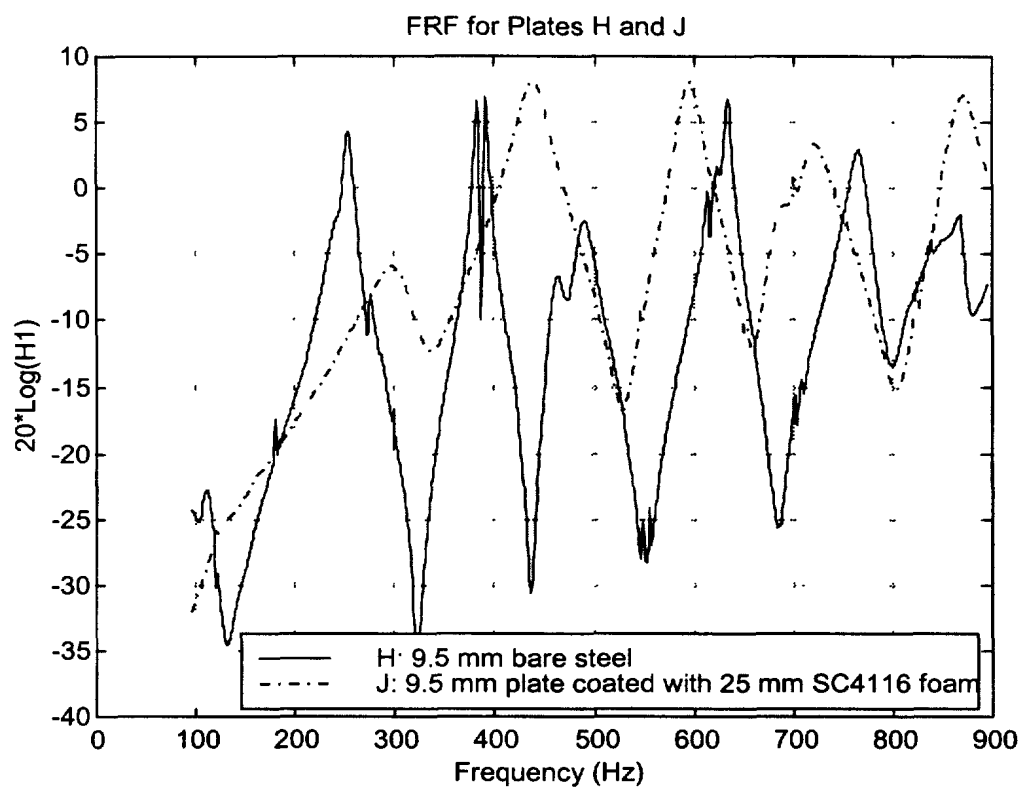
Appendix-A Elastomer Descriptions

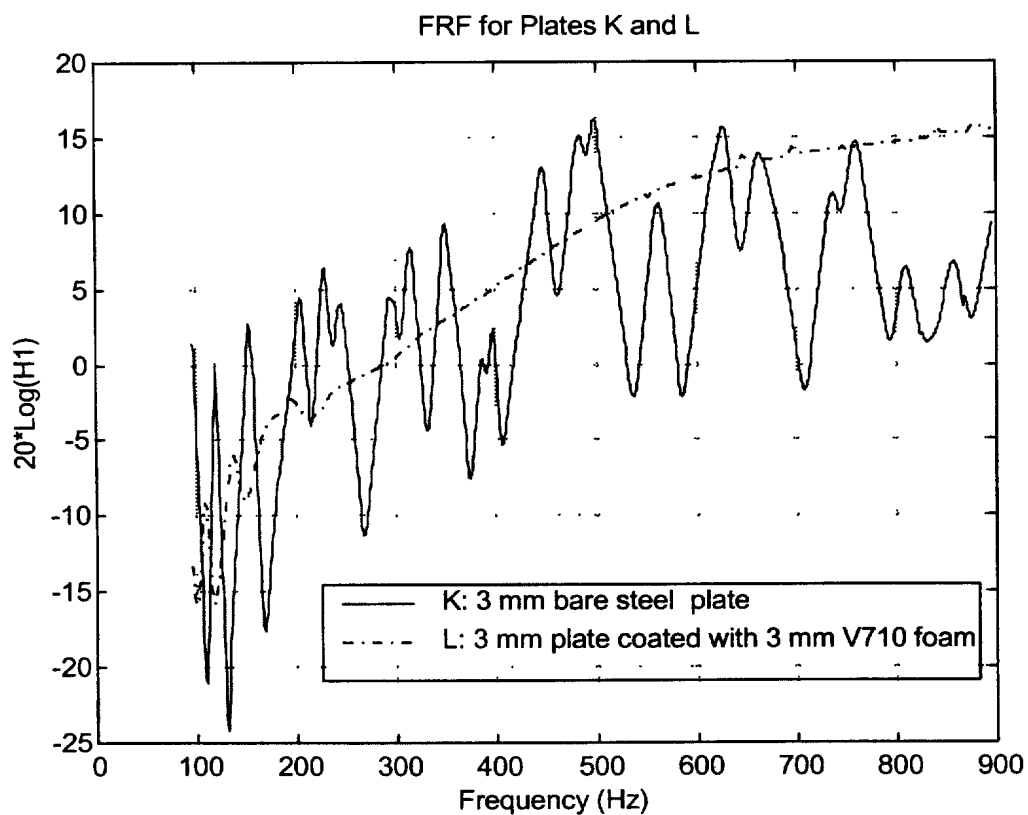
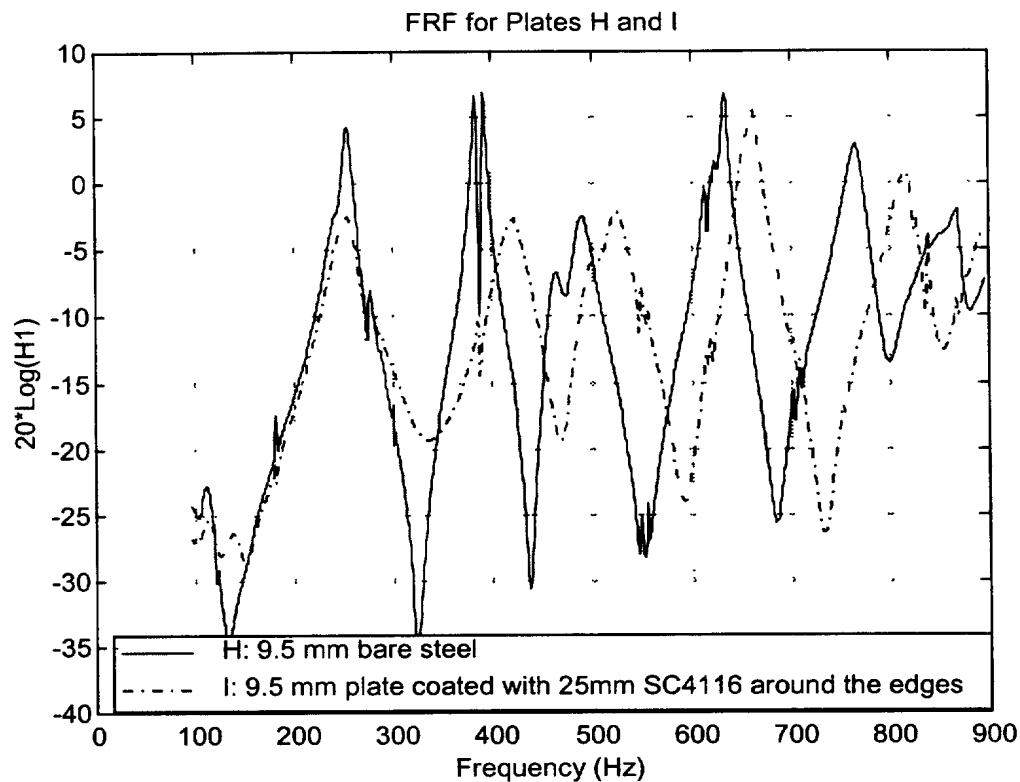
Table A.1 Elastomer and foam descriptions

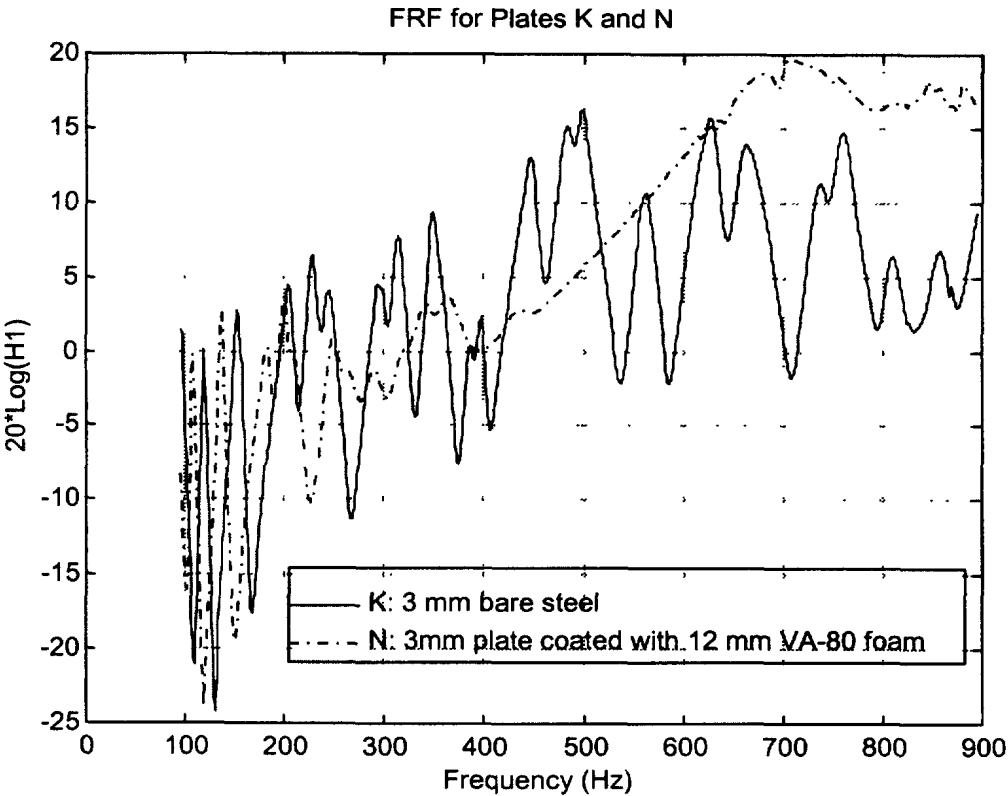
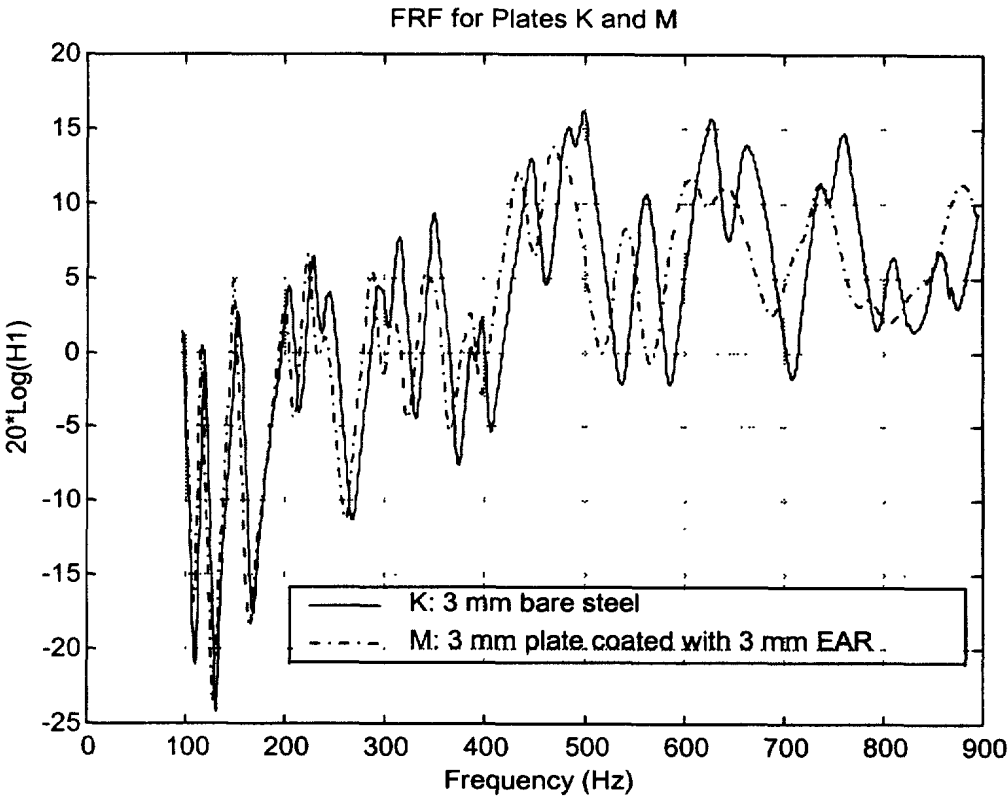
Short Name	Supplier	Description	Measured Density³⁵	Measured Hardness³⁶
SC-4116	Thomson-Gordon Ltd. 3225 Mainway Drive Burlington, Ontario L7M 1A6	Neoprene/ EPT/ SBR closed cell foam SC-41 (ASTM 1056-67)	92.9 km/m ³	49 Shore 00/ 85 Shore 000 (7.29 mm) 53 Shore 00/ 89 Shore 000 (23.74 mm)
V-710	Thomson-Gordon Ltd. 3225 Mainway Drive Burlington, Ontario L7M 1A6	PVC Foam TGV 710 AB 7 lb/ft ³	129.3 km/m ³	22 Shore 00/ 66 Shore 000 (5.92mm)
VA-80	Zotefoams Inc. 319 Airport Rd. Hackettstown, NJ 07840 USA	Ethylvinylacetate Foam Evazote VA-80	81.9 km/m ³	64 Shore 00/ 94 Shore 000 (6.75mm)
C-1002	E-A-R Specialty Composites 7911 Zionsville Road Indianapolis, IN 46268 USA	Plasticized PVC	1280 km/m ³	56 Shore A (25mm)

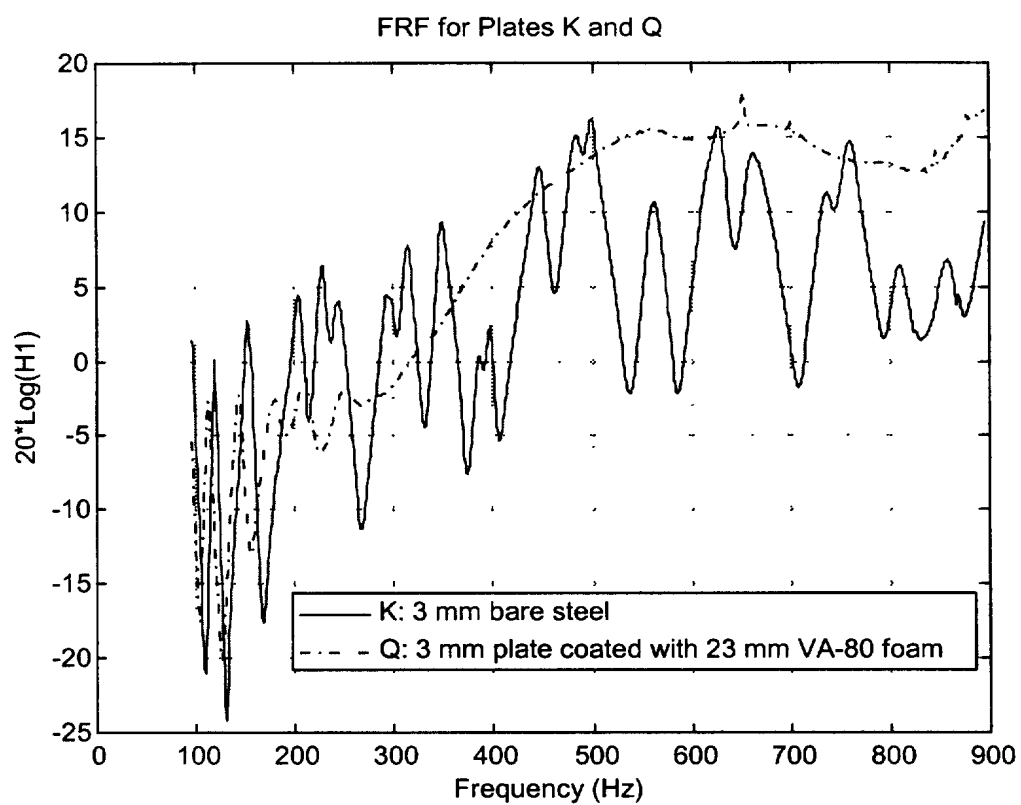
³⁵ Measured by GIL³⁶ Information supplied by DREA

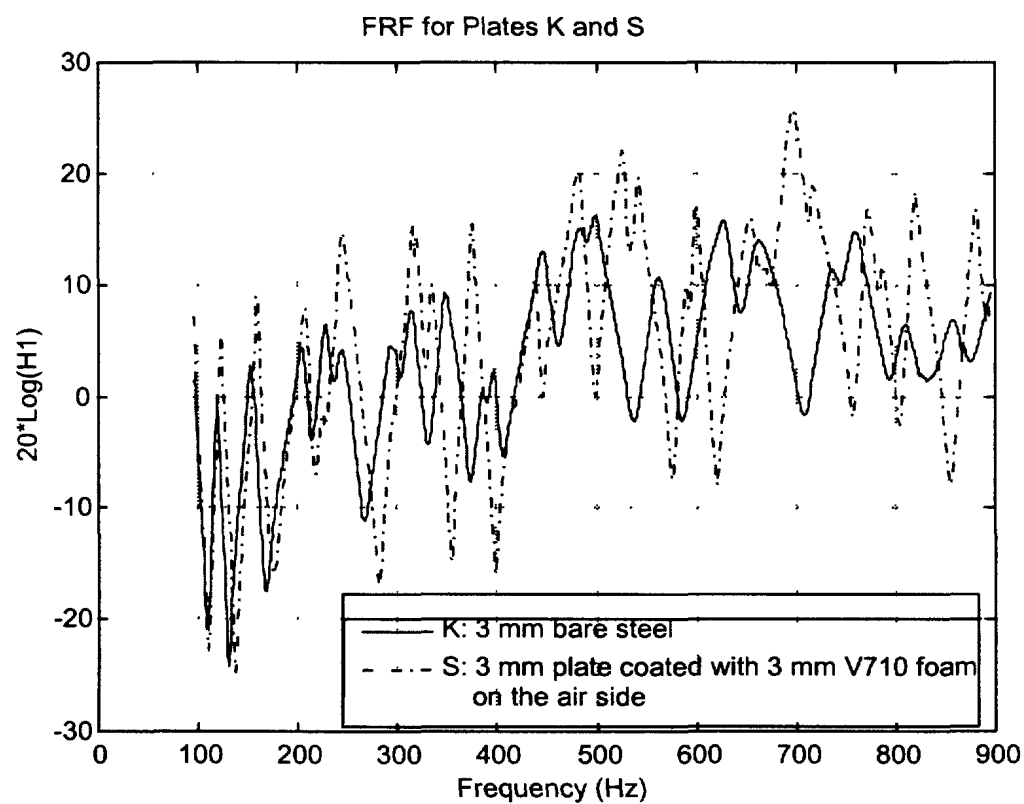
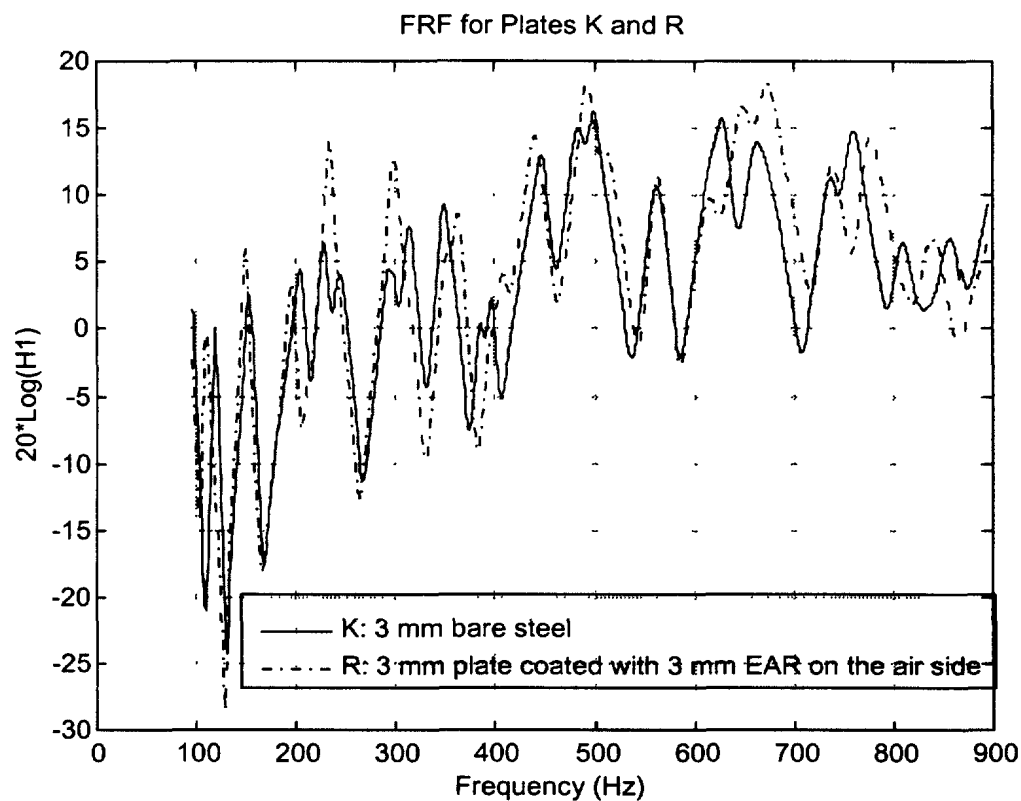
Appendix-B
Observed Frequency Response Functions











Appendix-C
Observed Input Power and Radiated Acoustic Power

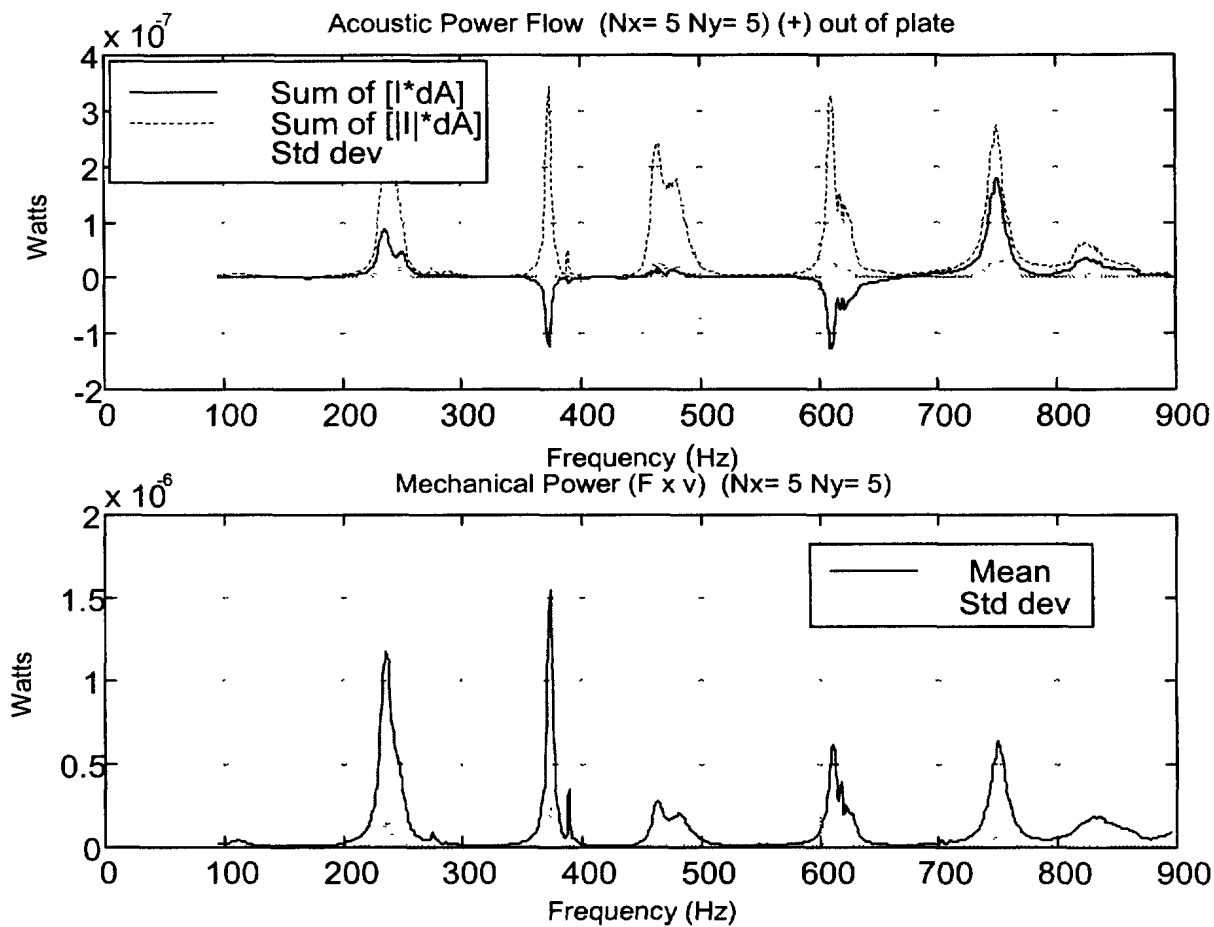


Plate H: 9.5 mm bare steel plate

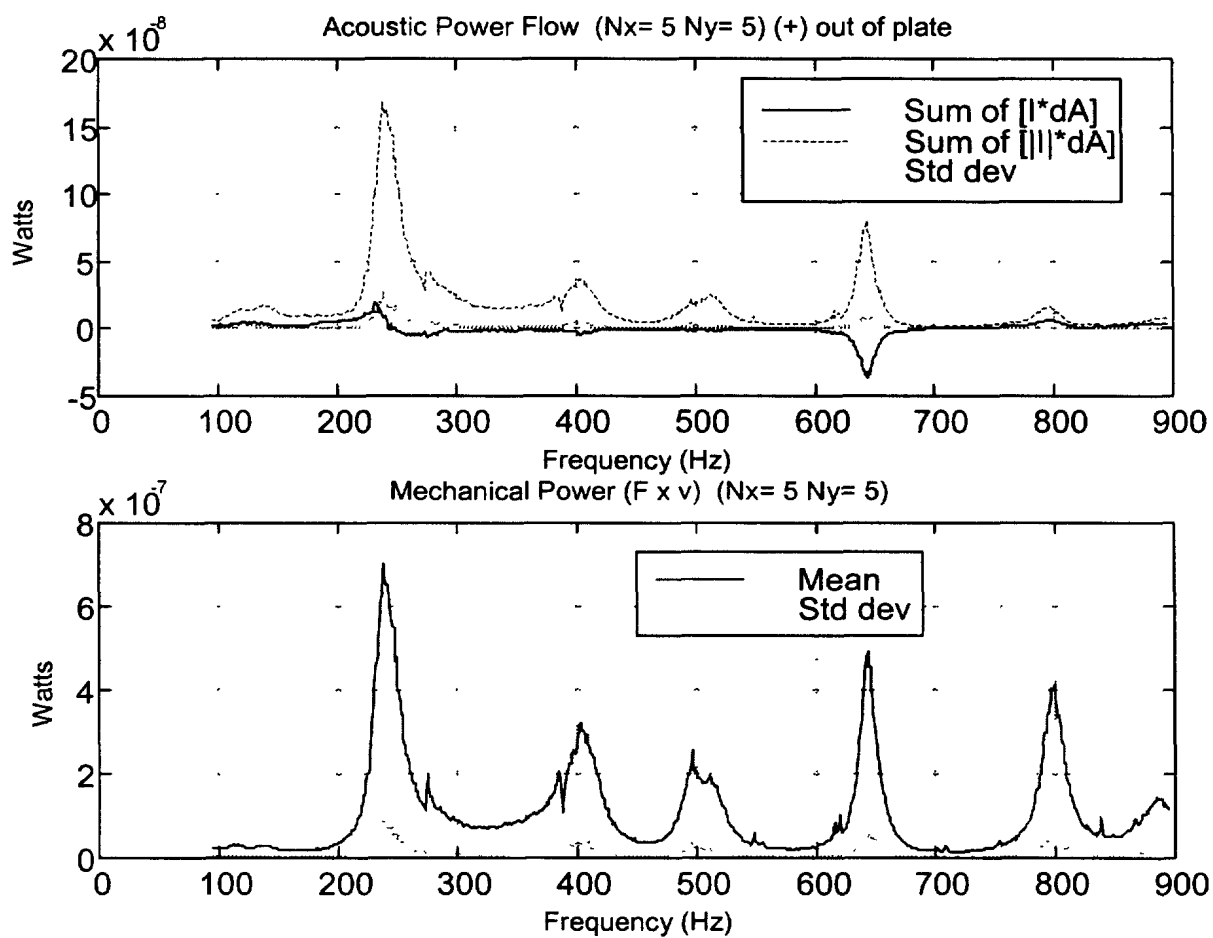


Plate I: 9.5 mm steel plate edge coated
with 25 mm SC4116 foam

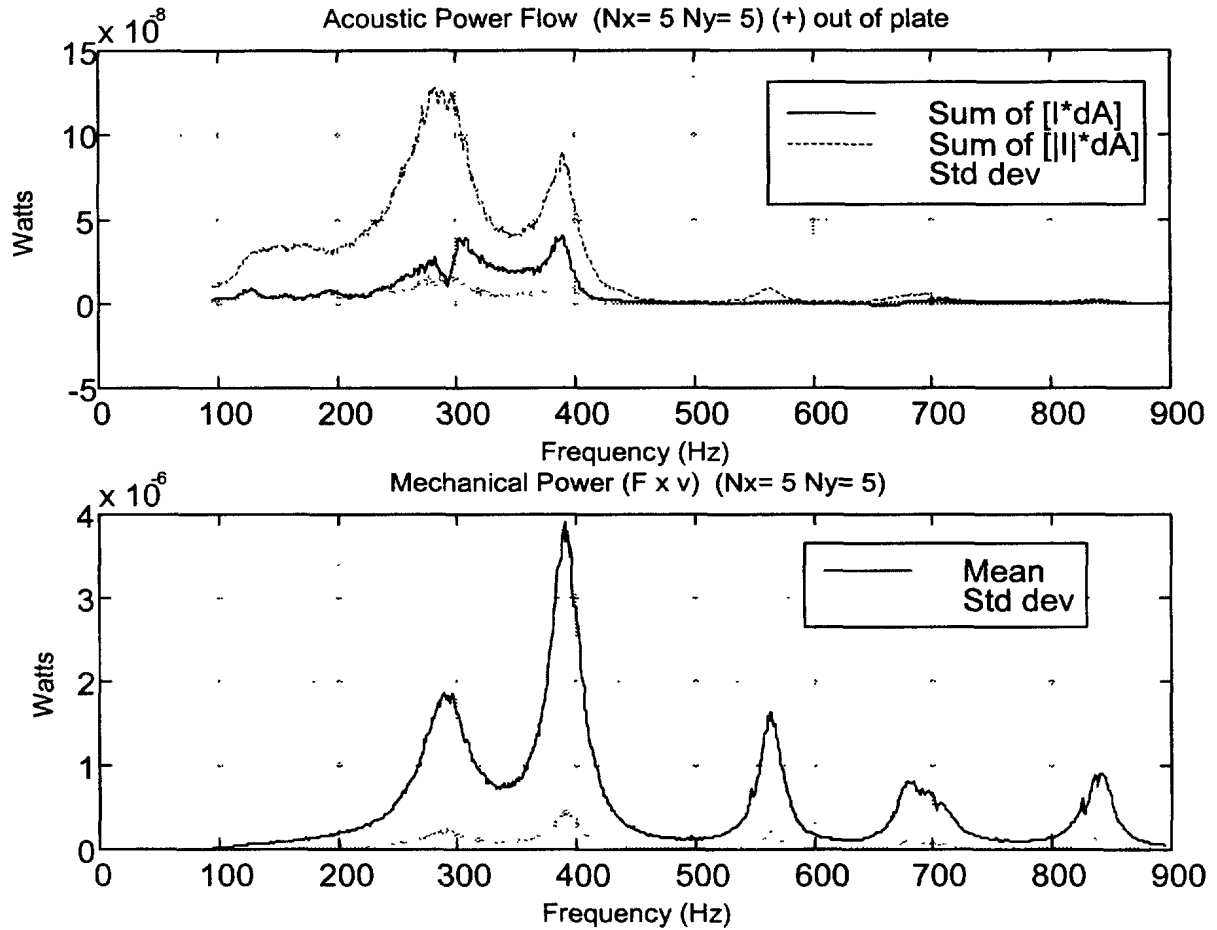


Plate J: 9.5 mm steel plate coated with 25 mm
SC4116 foam

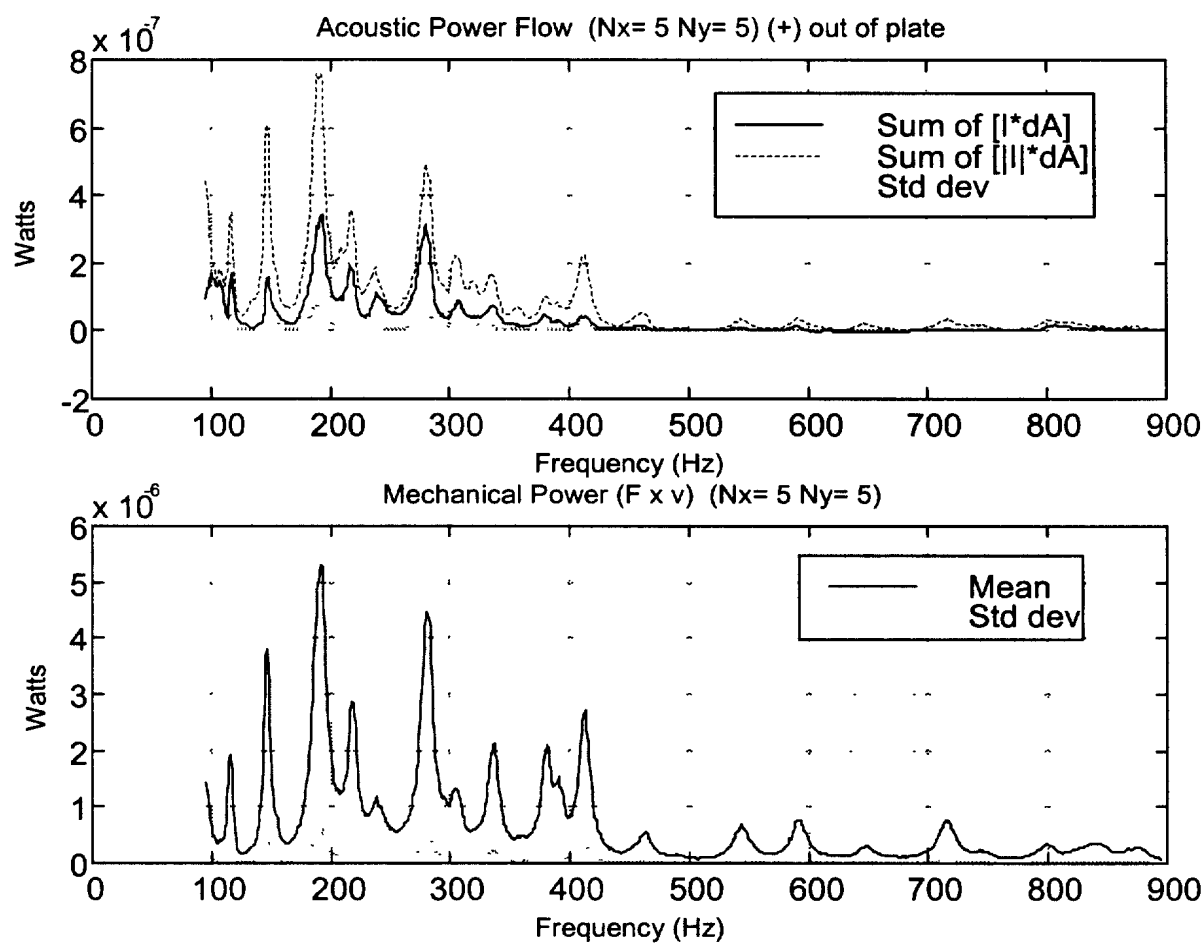


Plate K: 3 mm bare steel plate

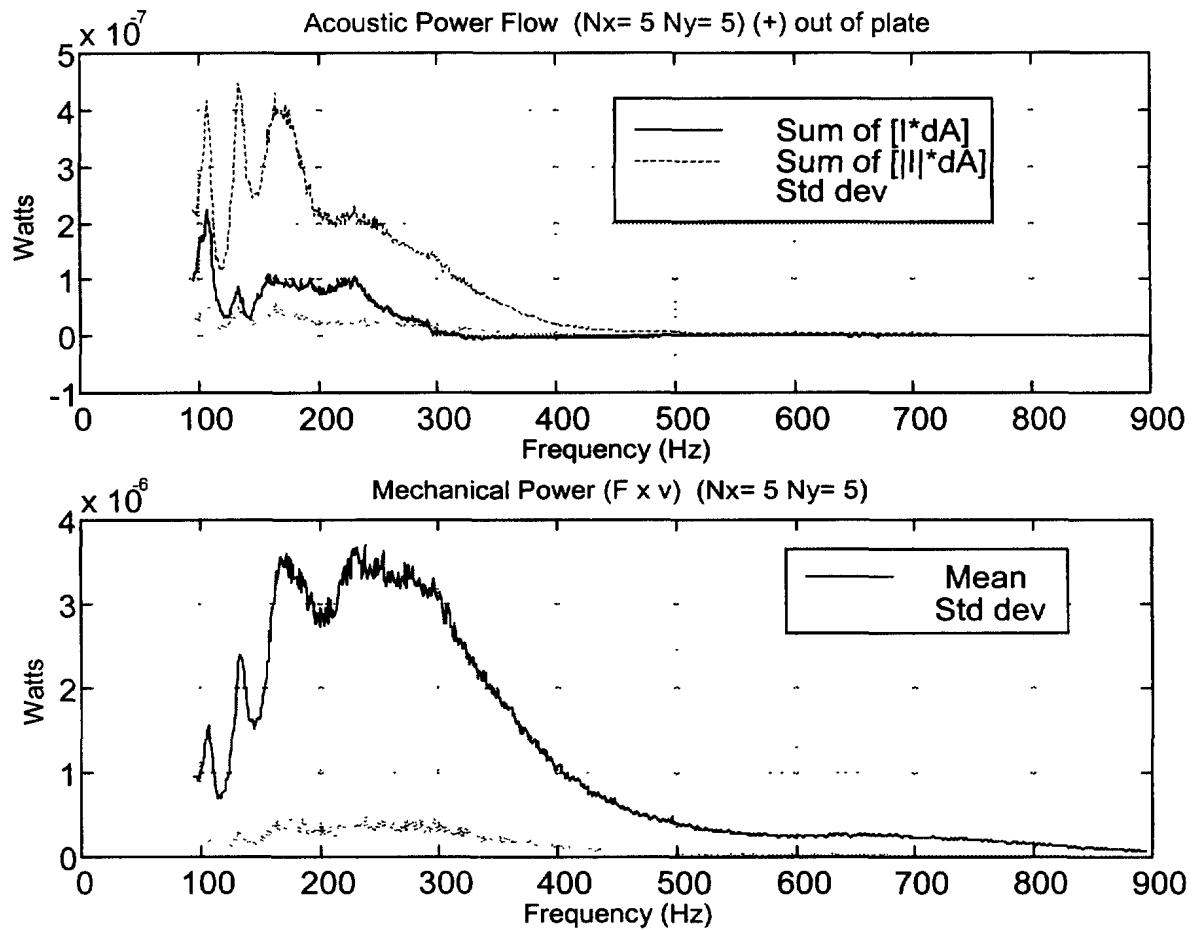


Plate L: 3 mm steel plate coated with
3 mm V710 foam

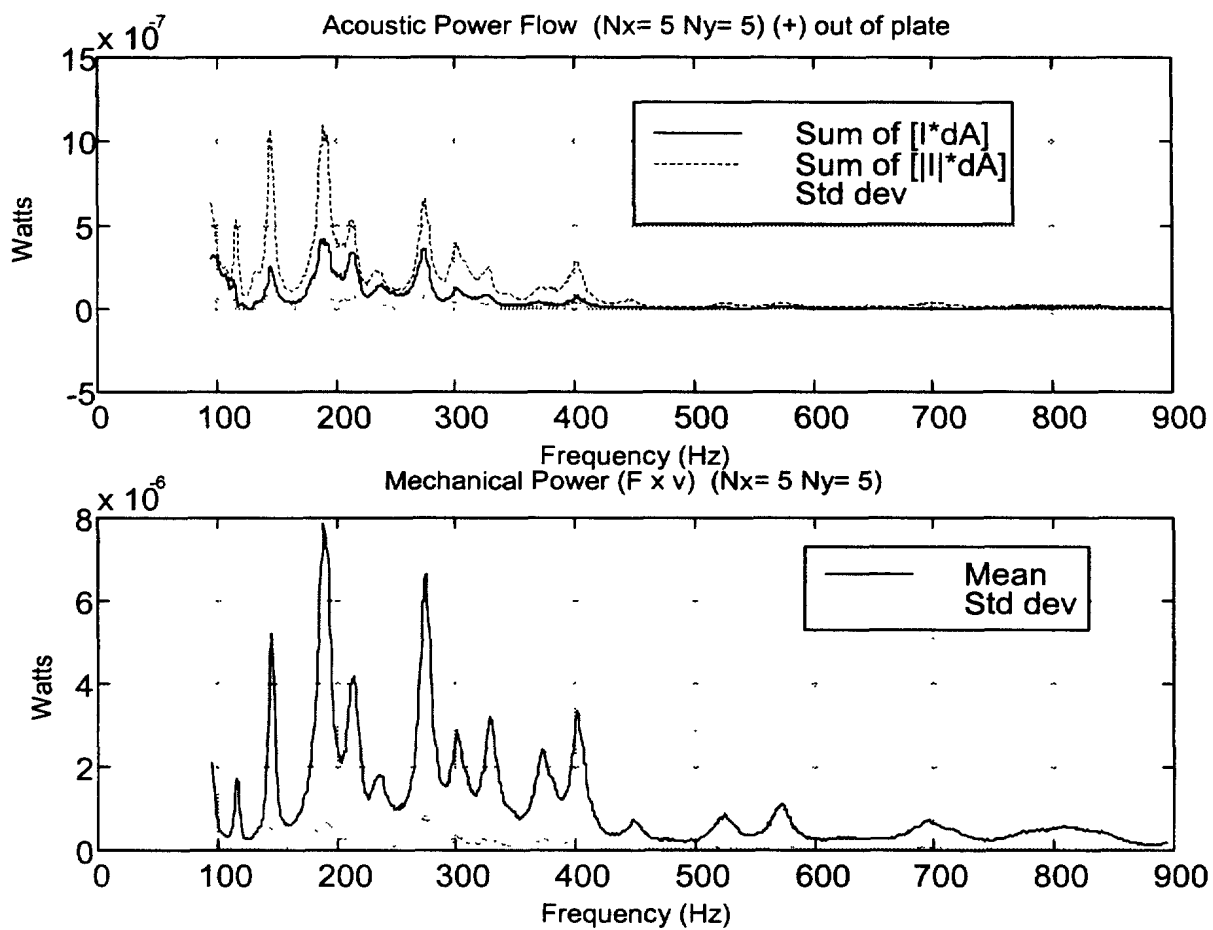


Plate M: 3 mm steel plate coated with 3 mm C-1002

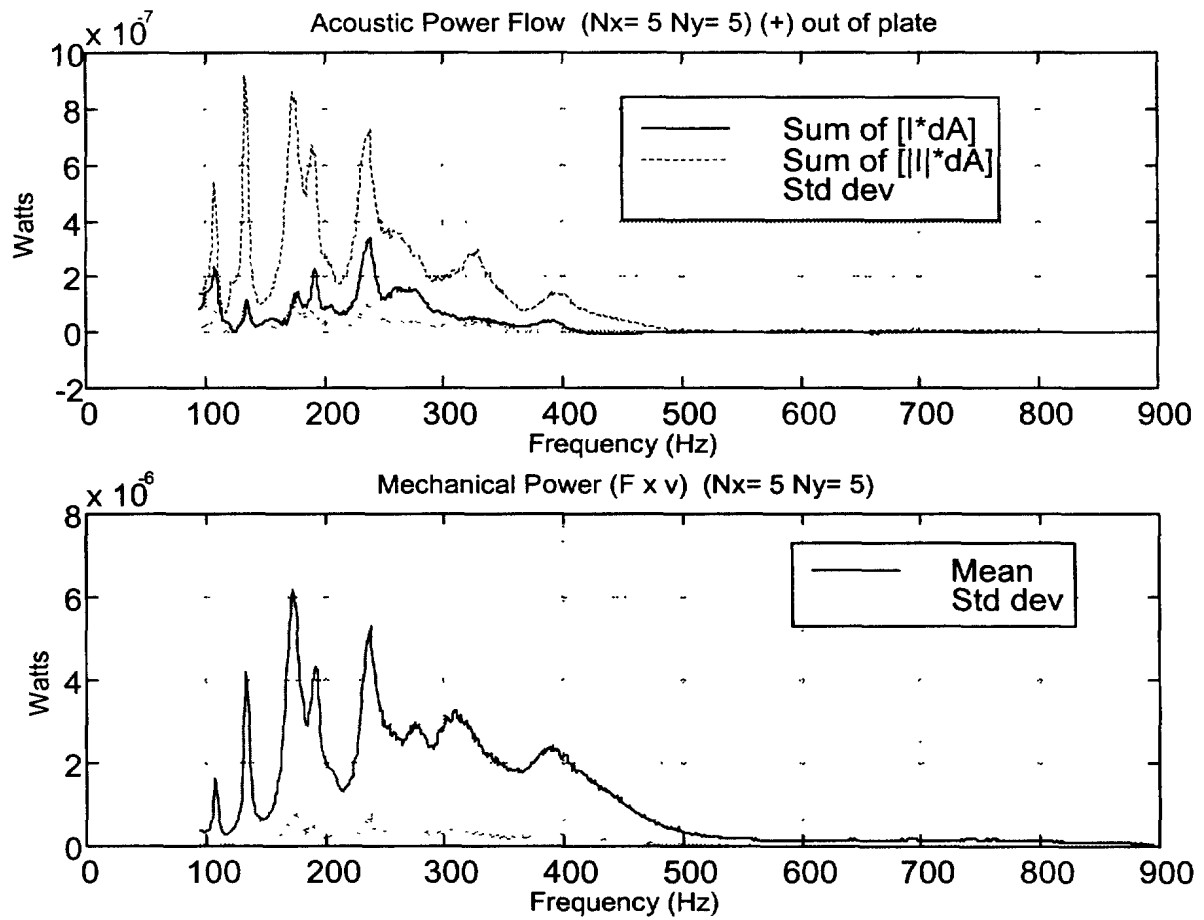


Plate N: 3 mm steel plate coated with 12 mm
VA80 foam

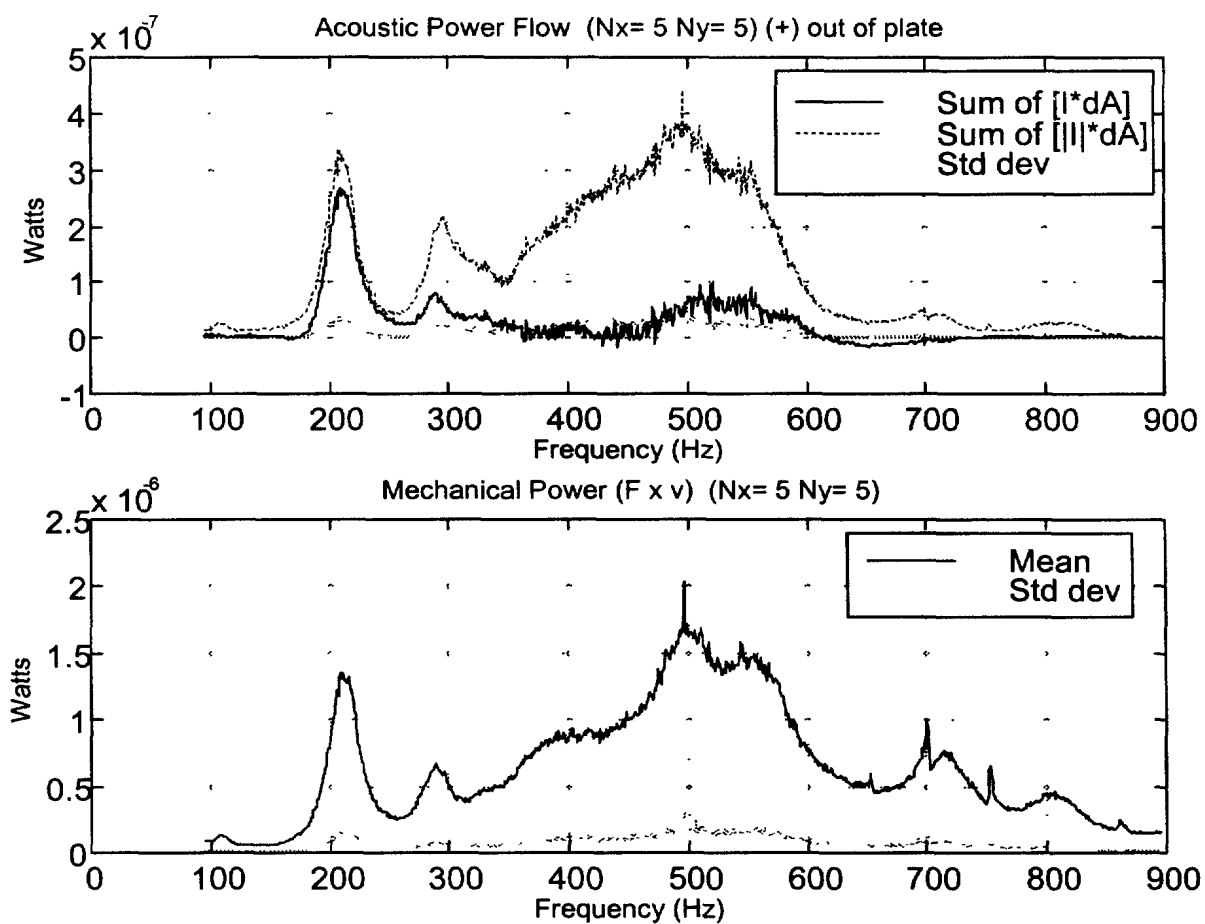


Plate P: 9.5 mm steel plate coated with 12 mm
VA80 foam

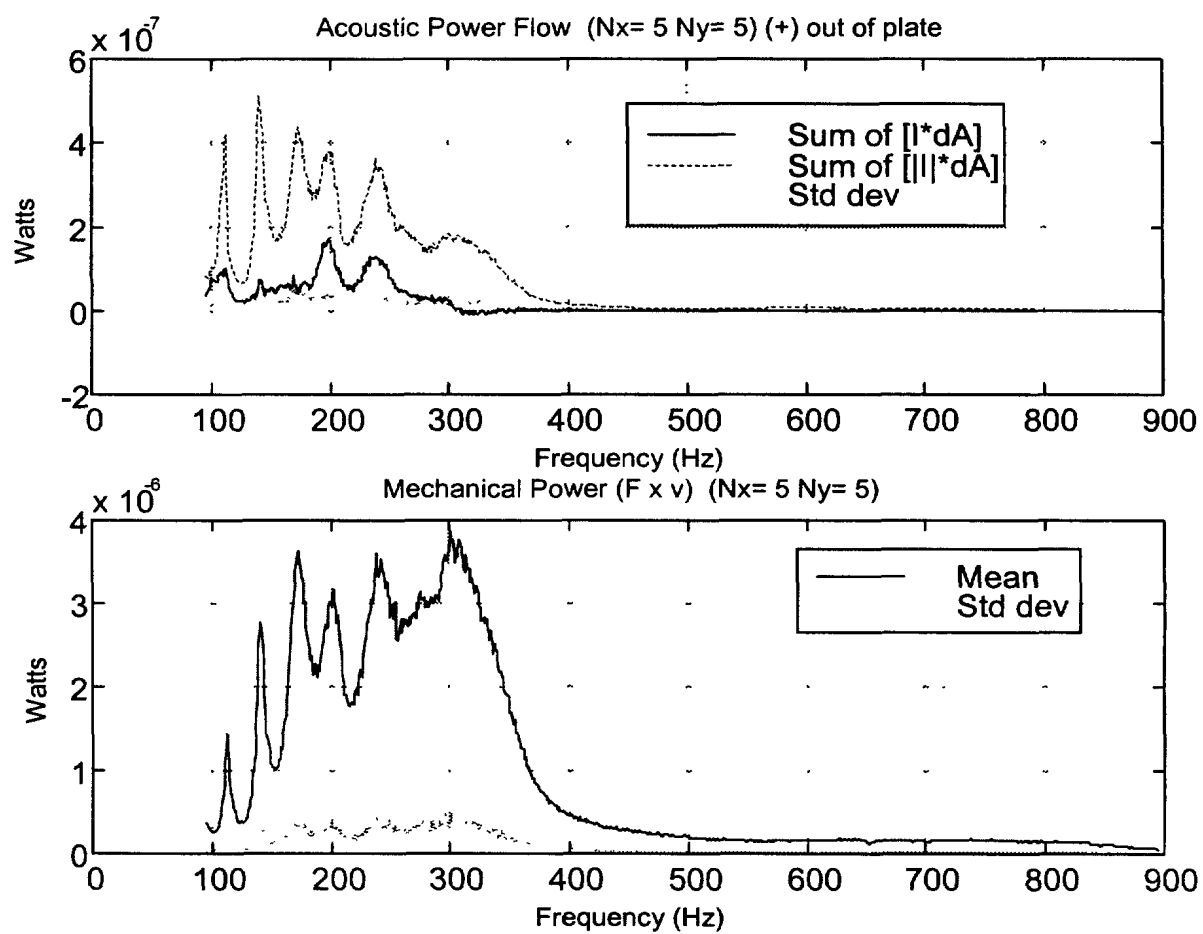


Plate Q: 3 mm steel plate coated with 23 mm
VA80 foam

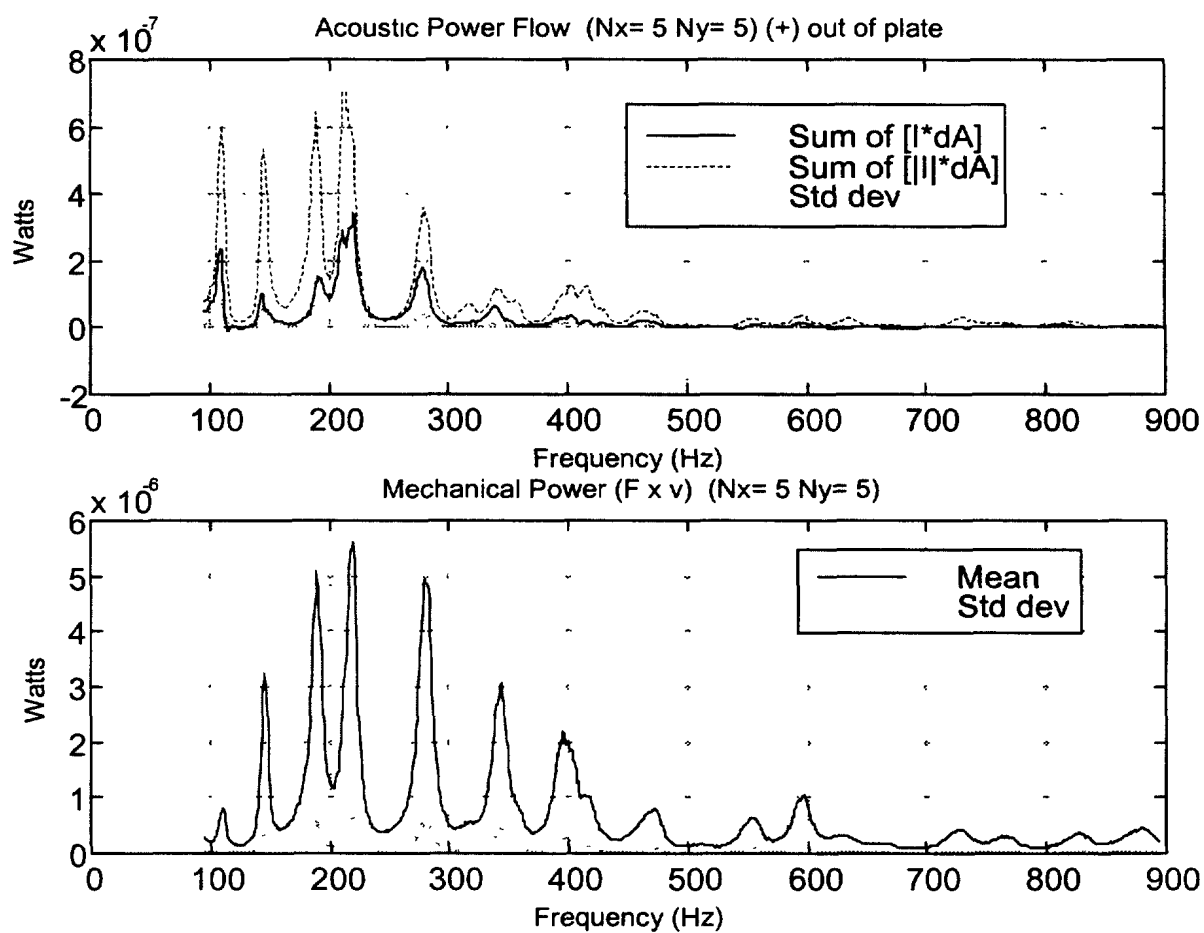


Plate R: 3 mm steel plate coated with 3 mm
C-1002 (coating on air side of plate)

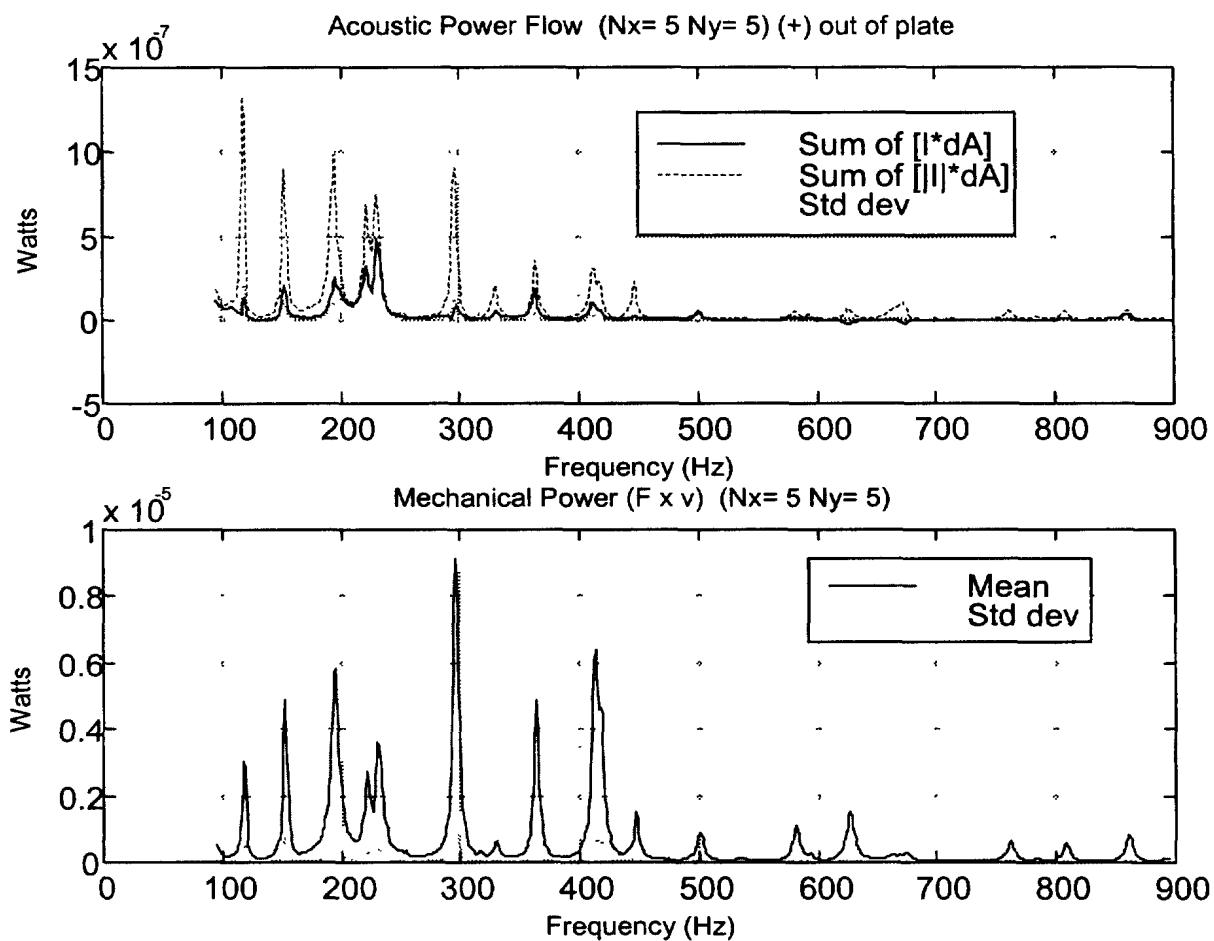


Plate S: 3 mm steel plate coated with 3 mm
V710 foam (coating on air side of
plate)

Appendix-D
Normalized Net and Absolute Radiated Power

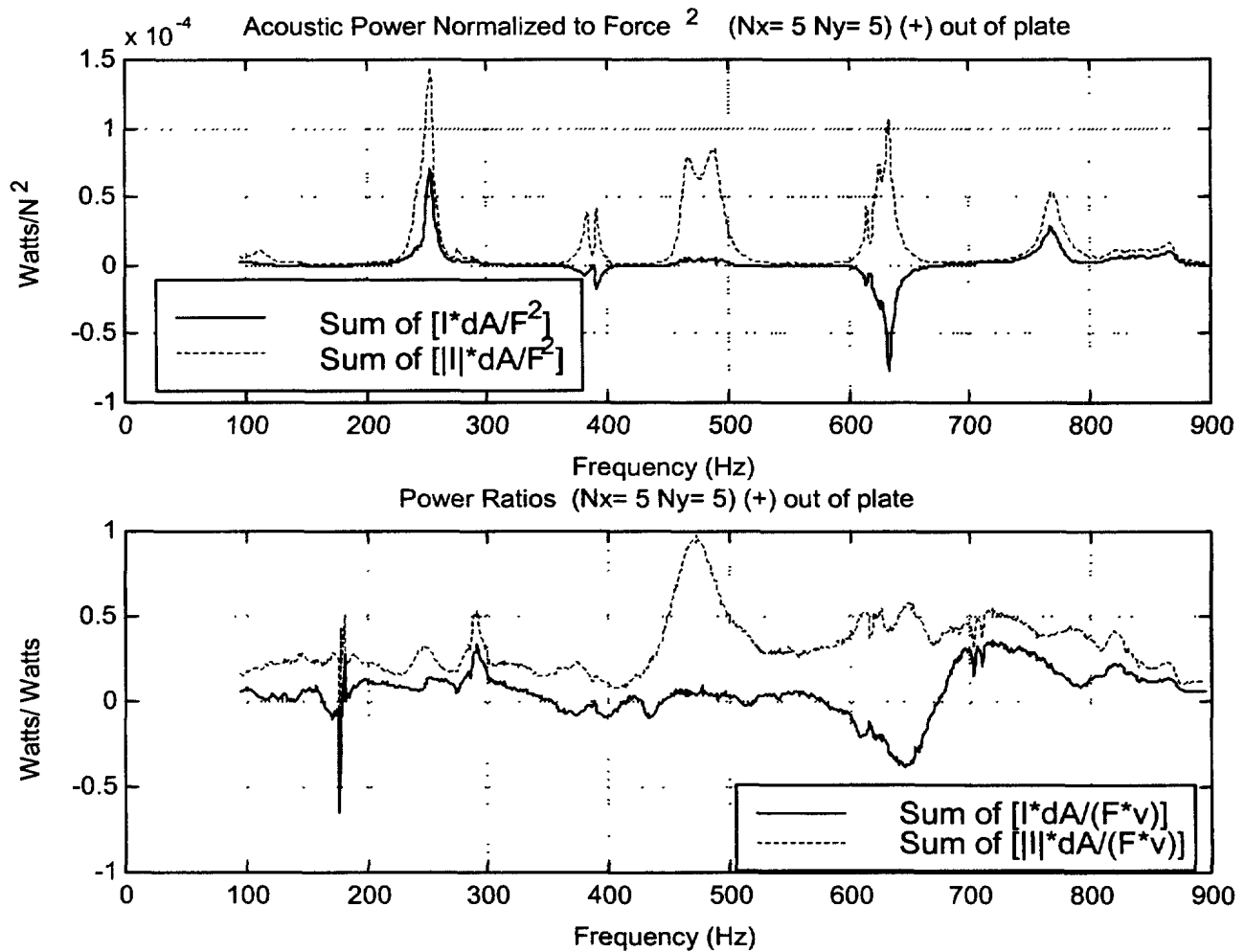


Plate H: 9.5 mm bare steel plate

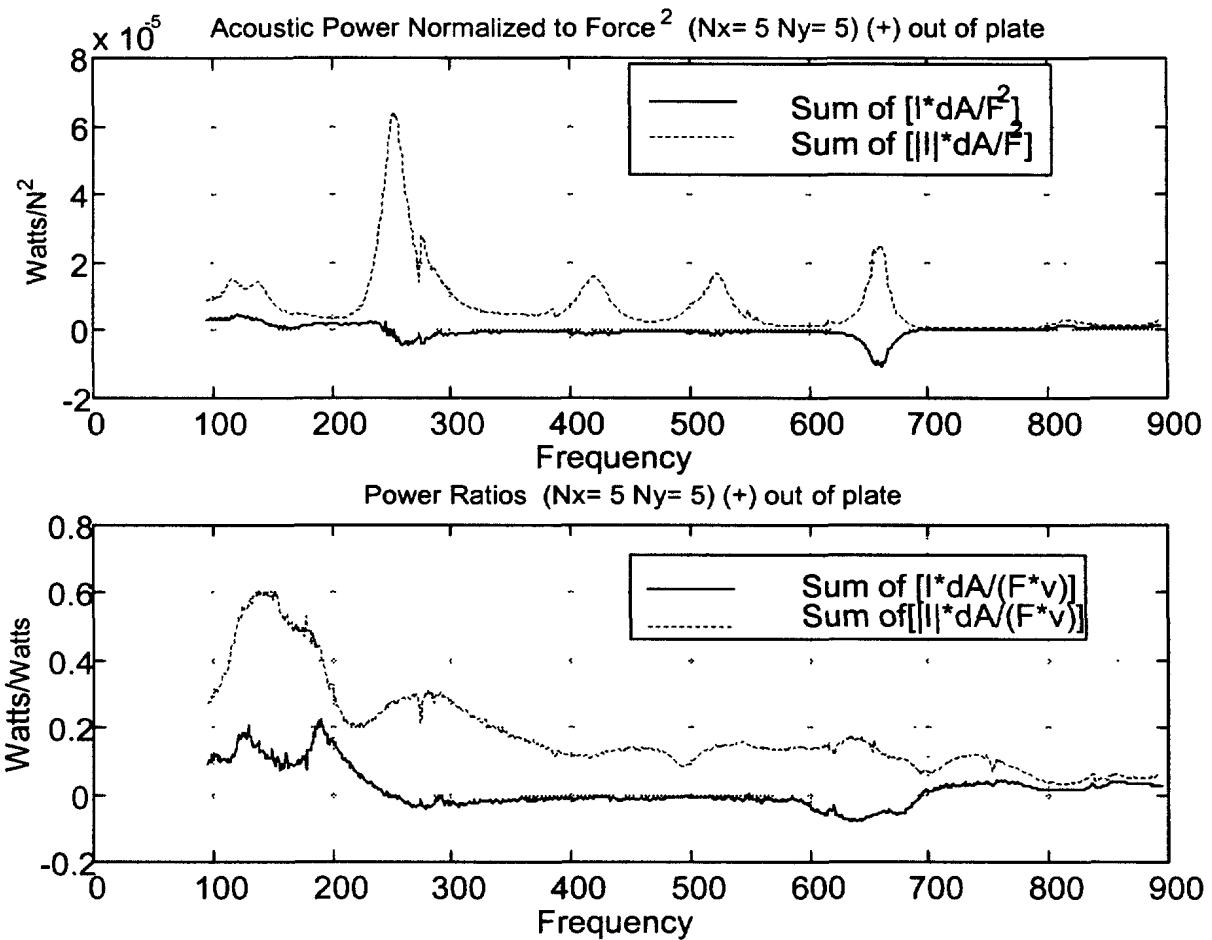


Plate I: 9.5 mm steel plate edge coated with
25 mm SC4116 foam

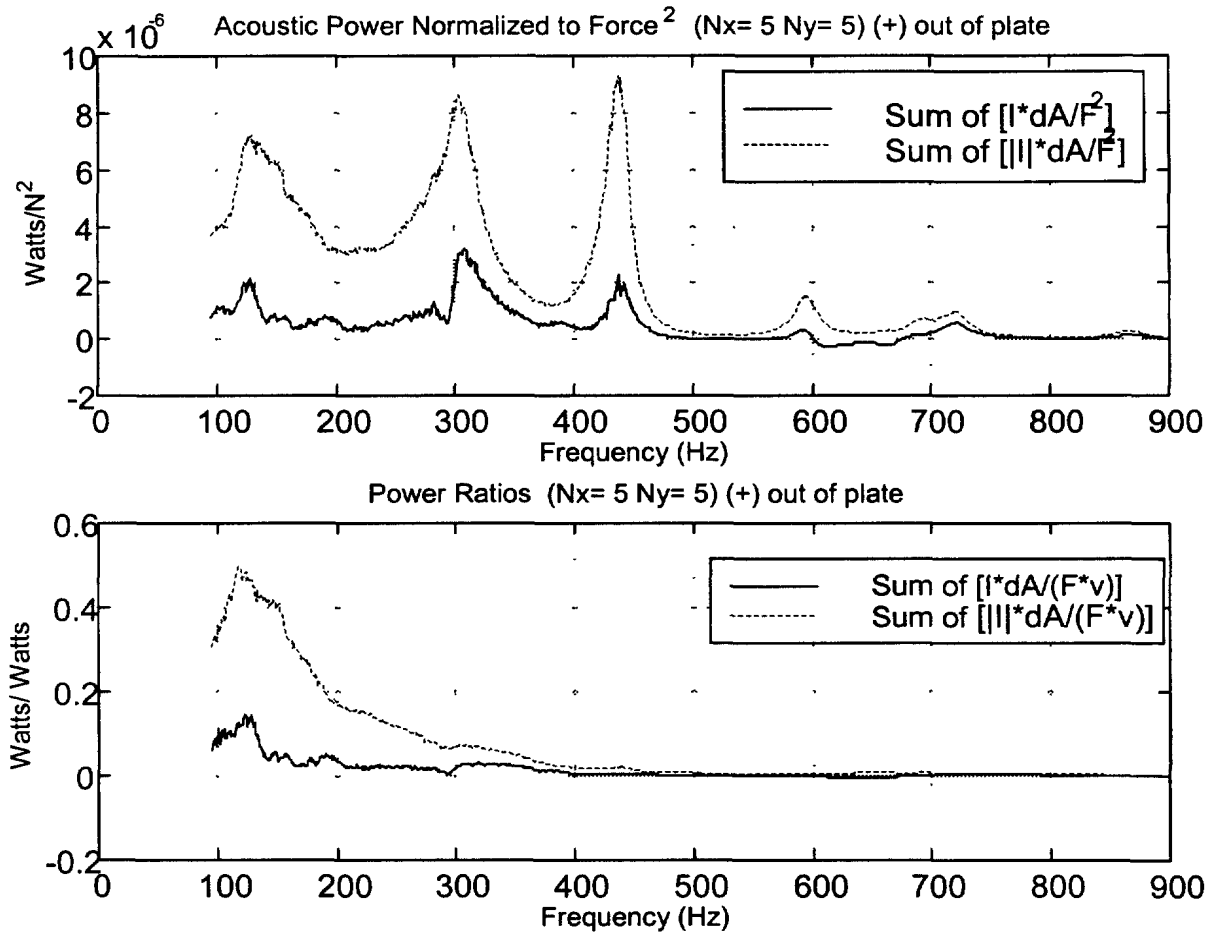


Plate J: 9.5 mm steel plate coated with 25 mm
SC4116 foam

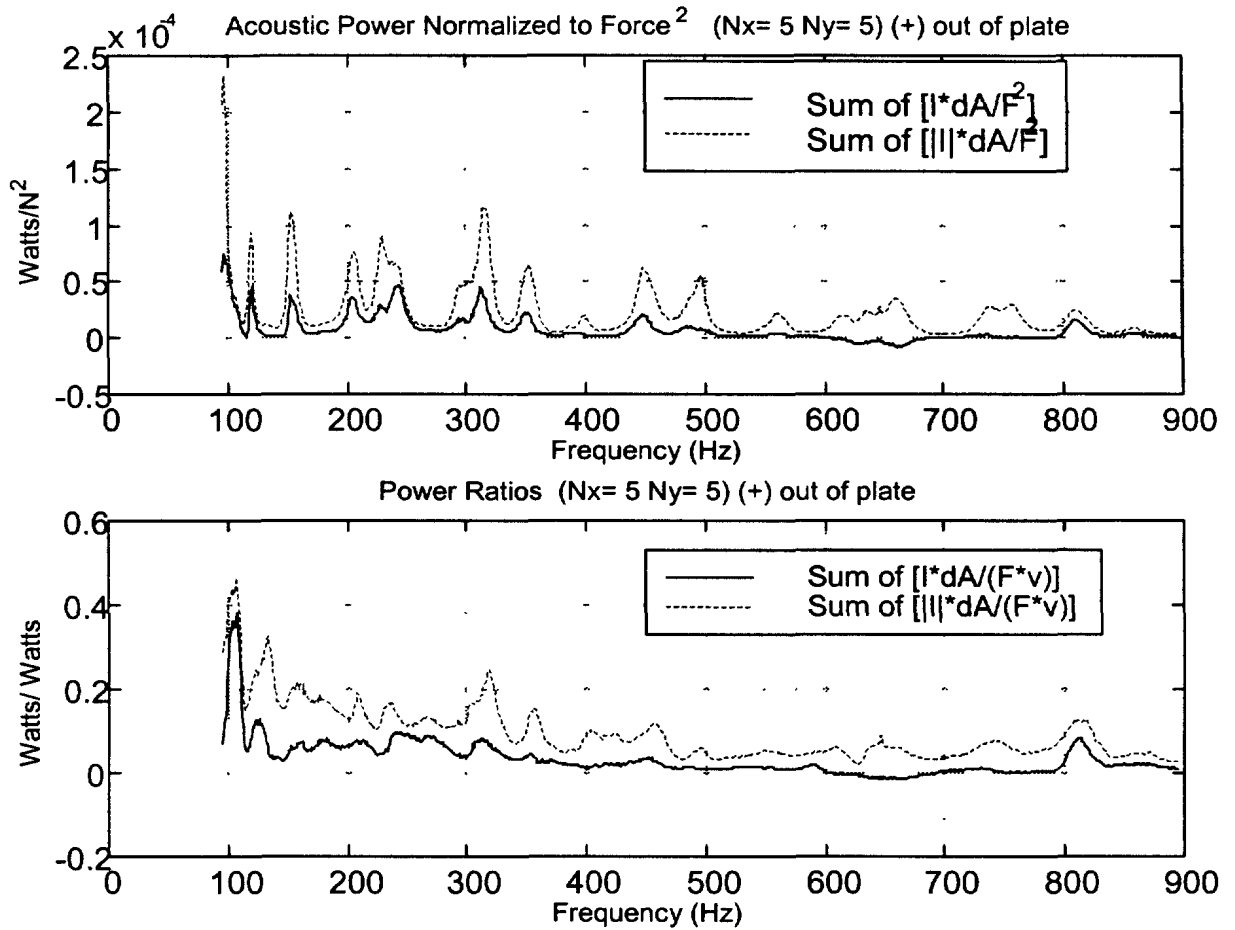


Plate K: 3 mm bare steel plate

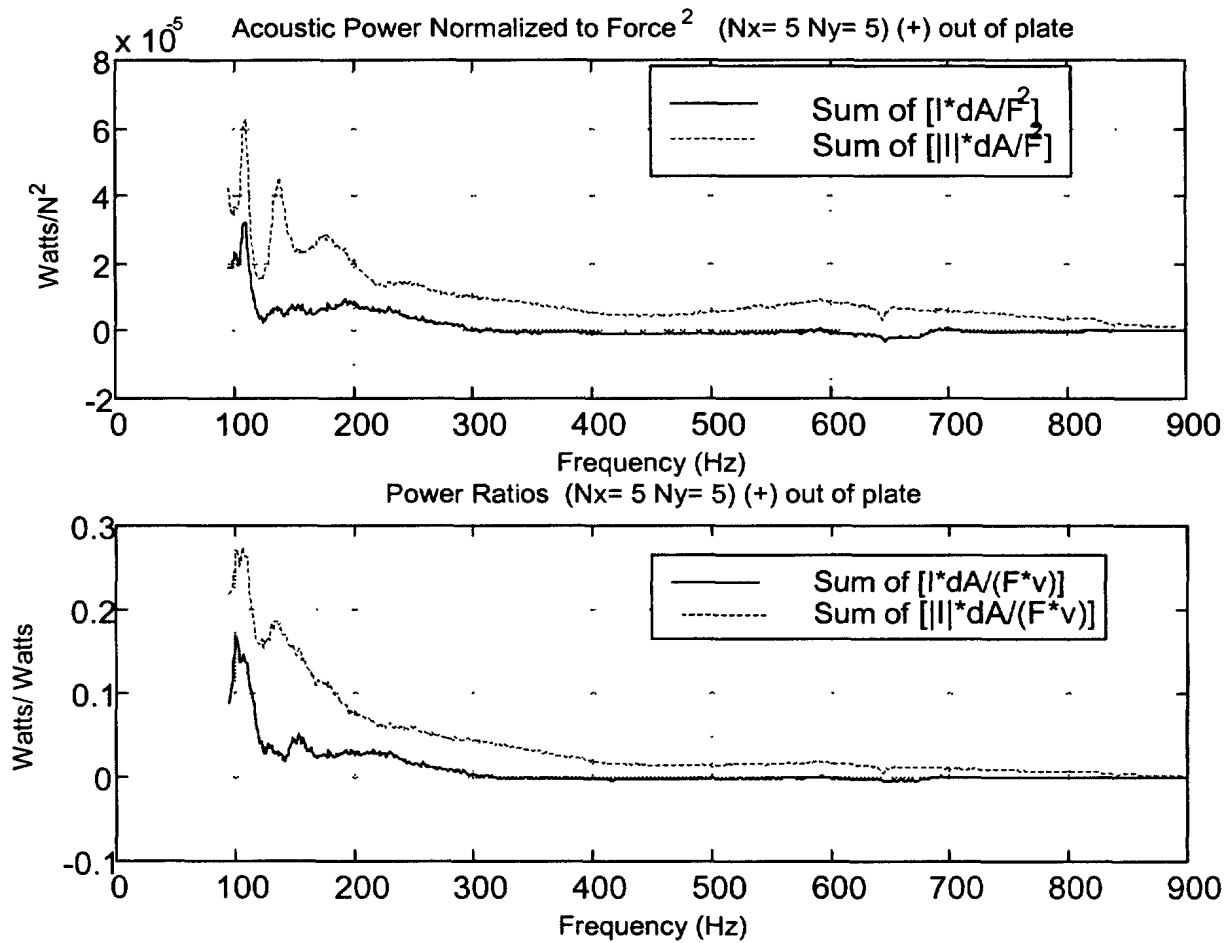


Plate L: 3 mm steel plate coated with
3 mm V710 foam

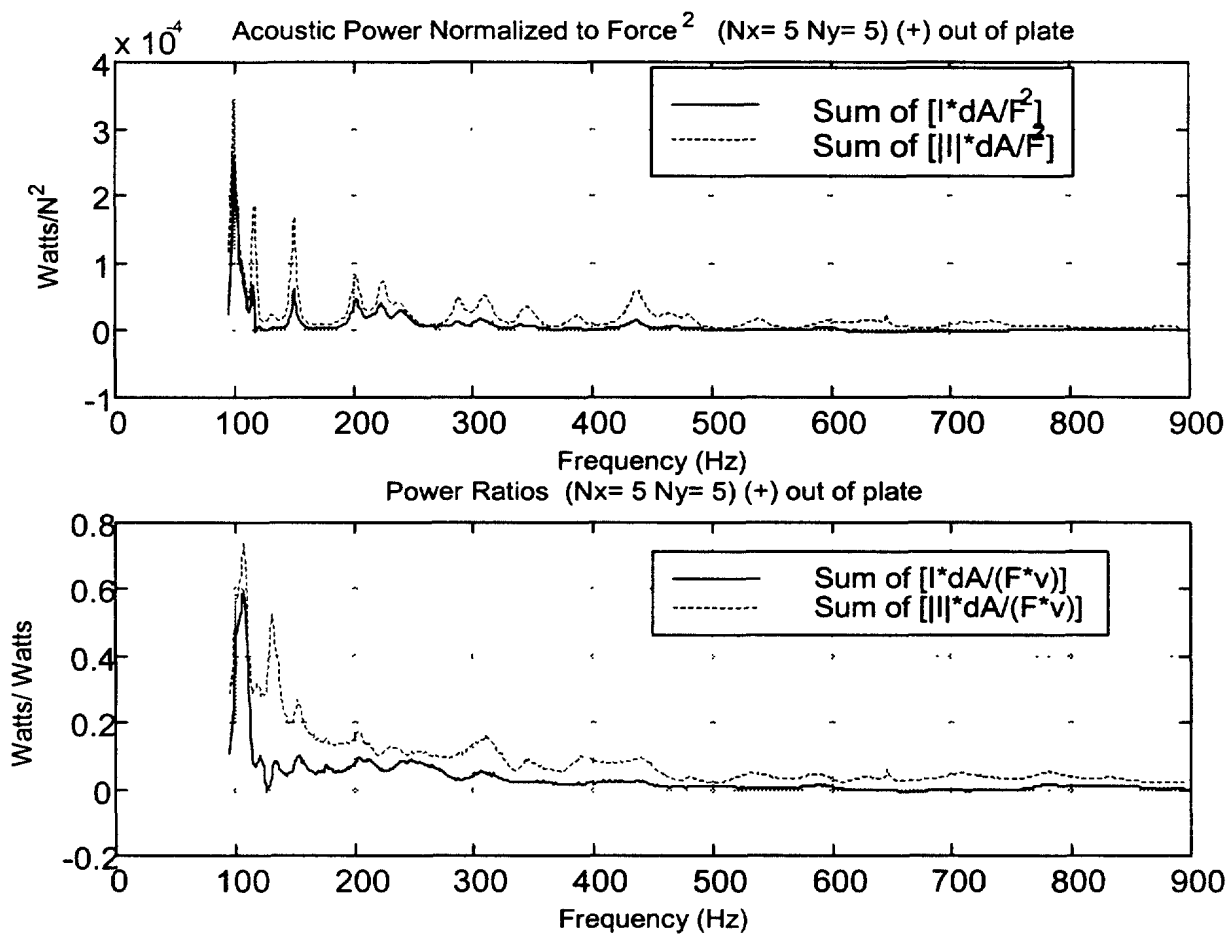


Plate M: 3 mm steel plate coated with 3 mm
C-1002

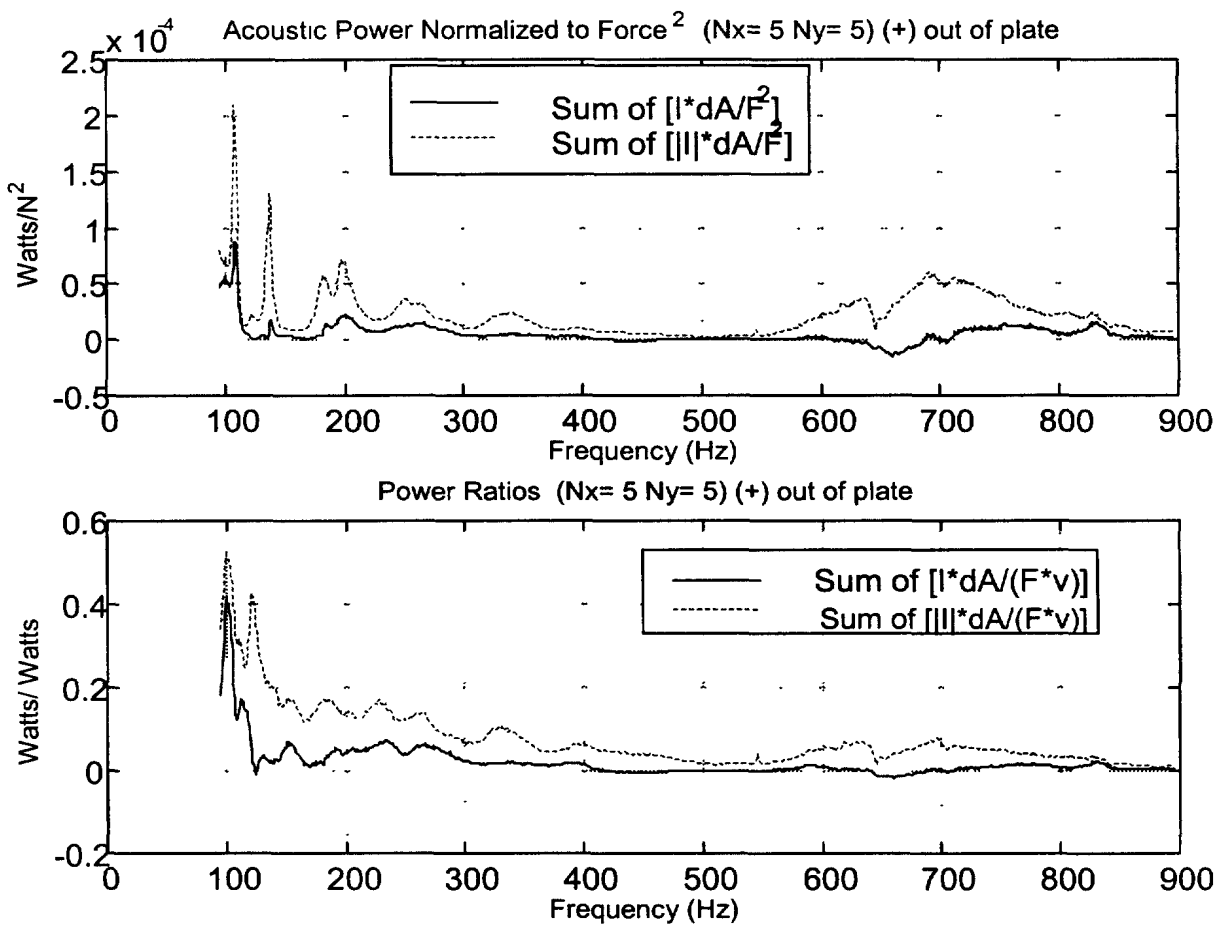


Plate N: 3 mm steel plate coated with 12 mm
VA80 foam

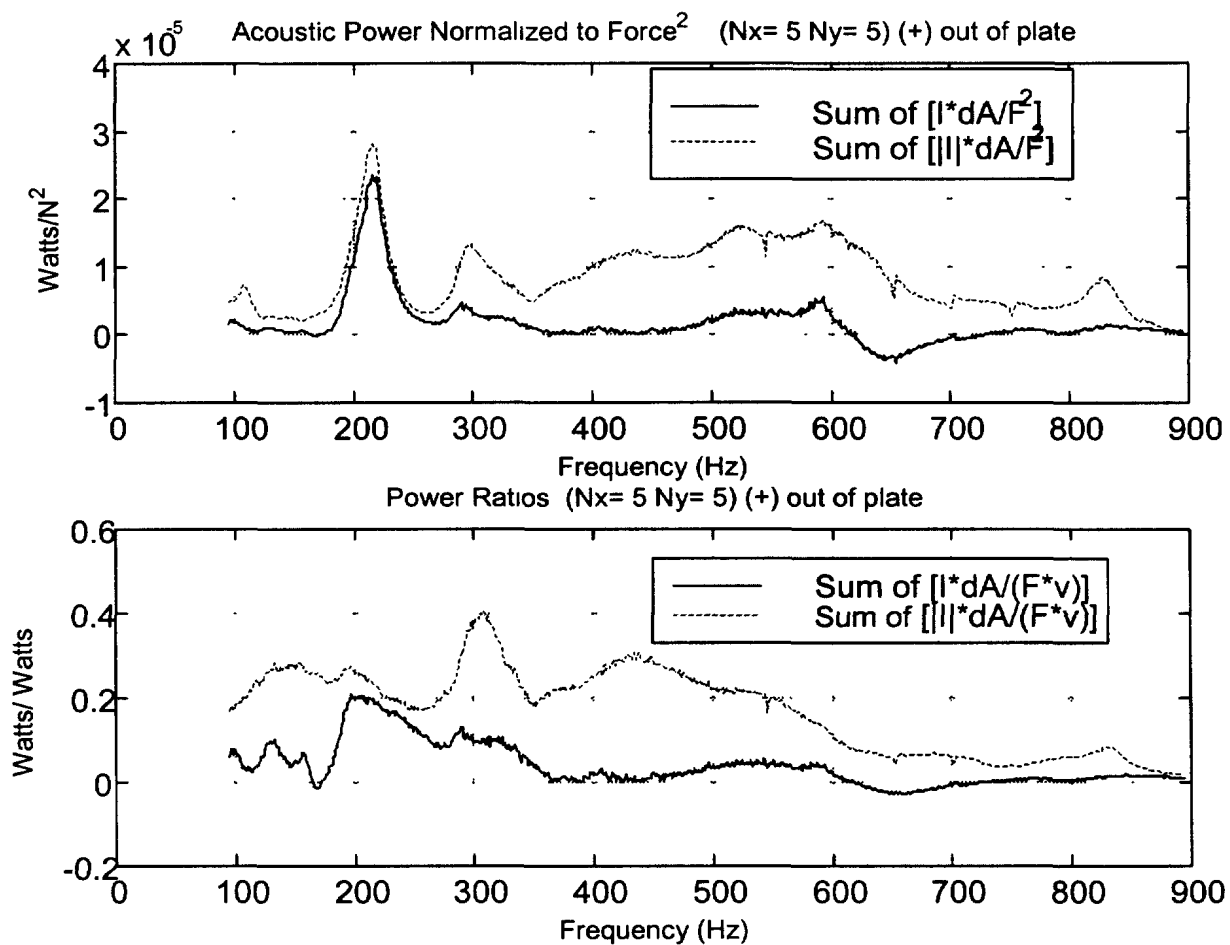


Plate P: 9.5 mm steel plate coated with 12 mm
VA80 foam

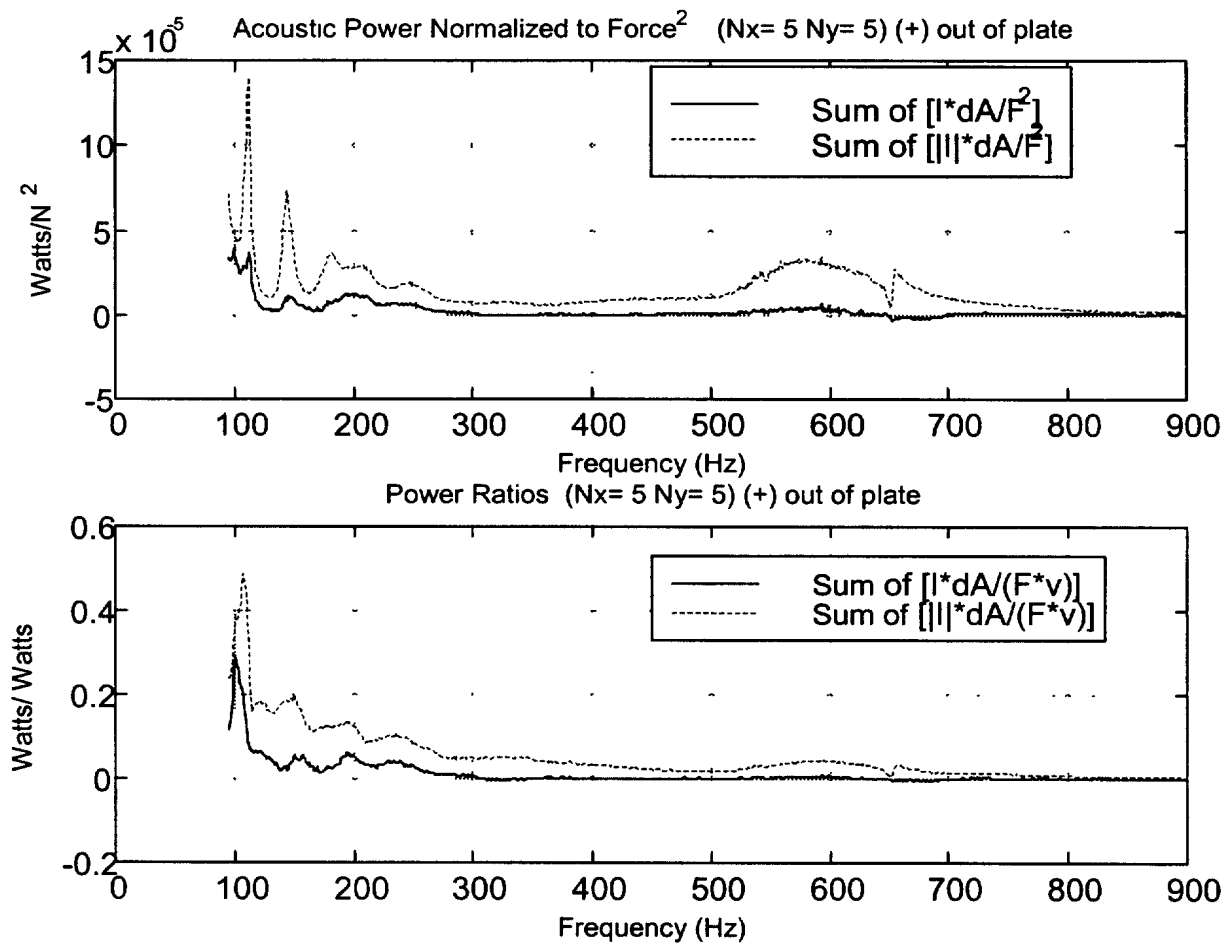


Plate Q: 3 mm steel plate coated with 23 mm
VA80 foam

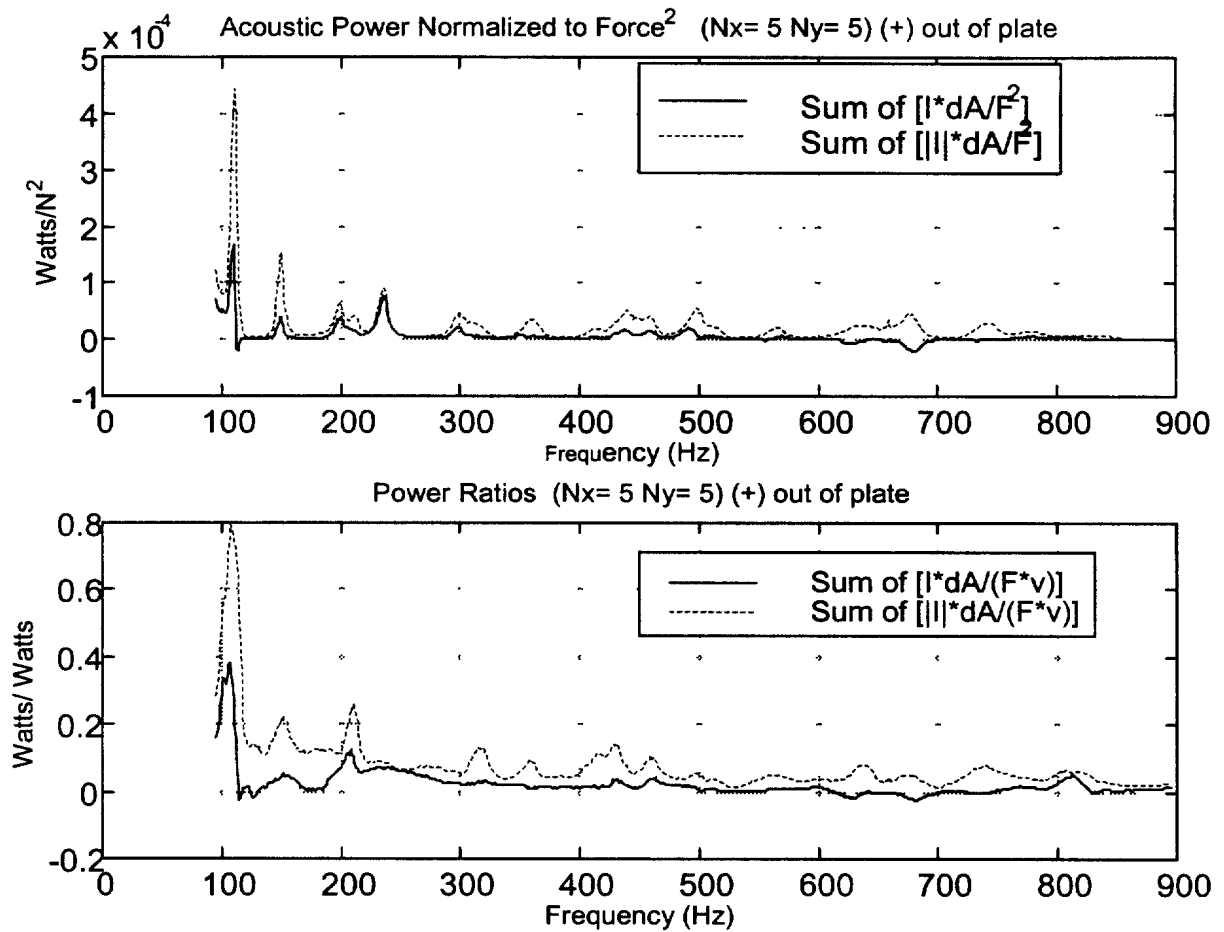


Plate R: 3 mm steel plate coated with 3 mm
C-1002 (coating on air side of plate)

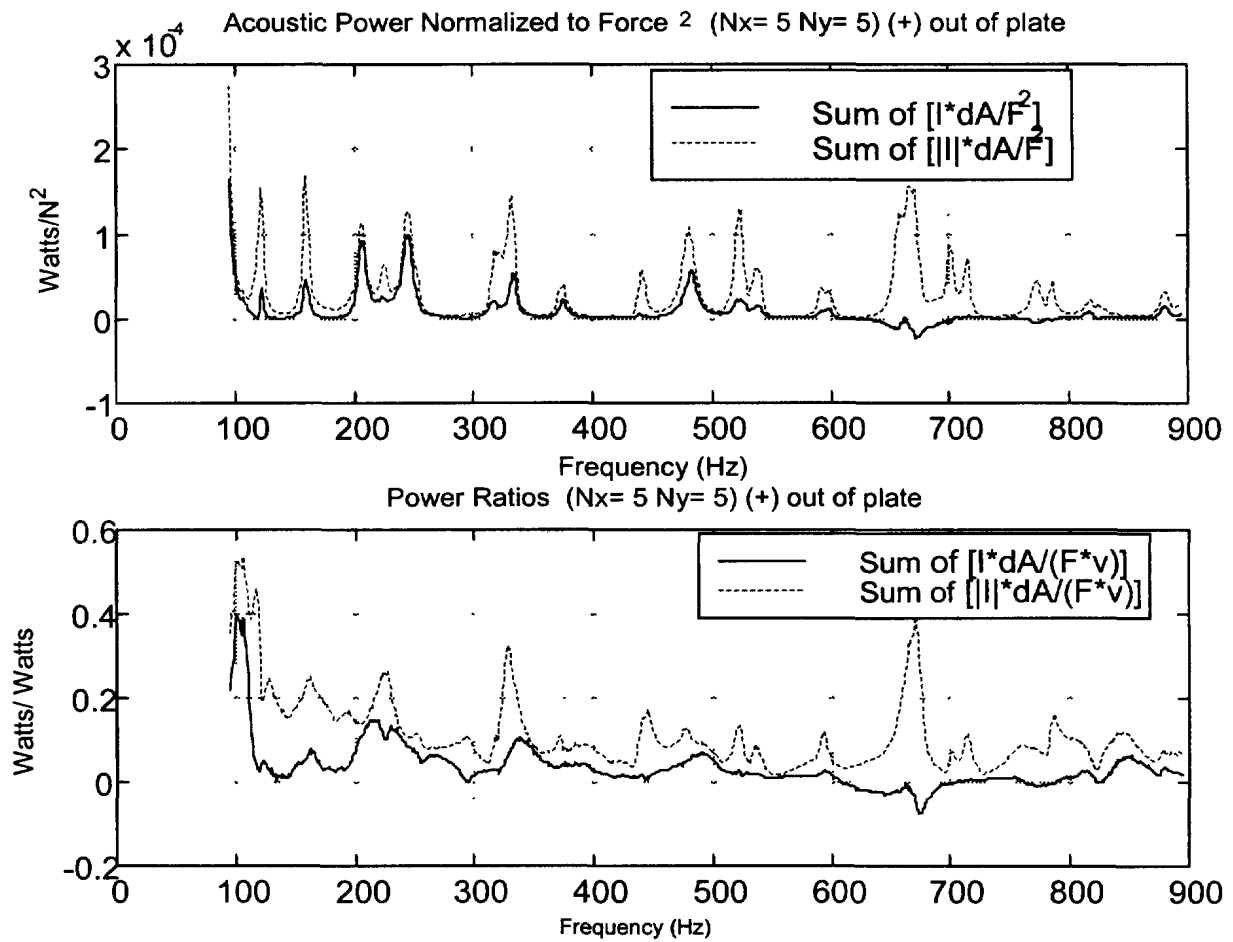


Plate S: 3 mm steel plate coated with 3 mm
V710 foam (coating on air side of
plate)

Appendix-E
Normalized Absolute Radiated Power: Uncoated vs Coated

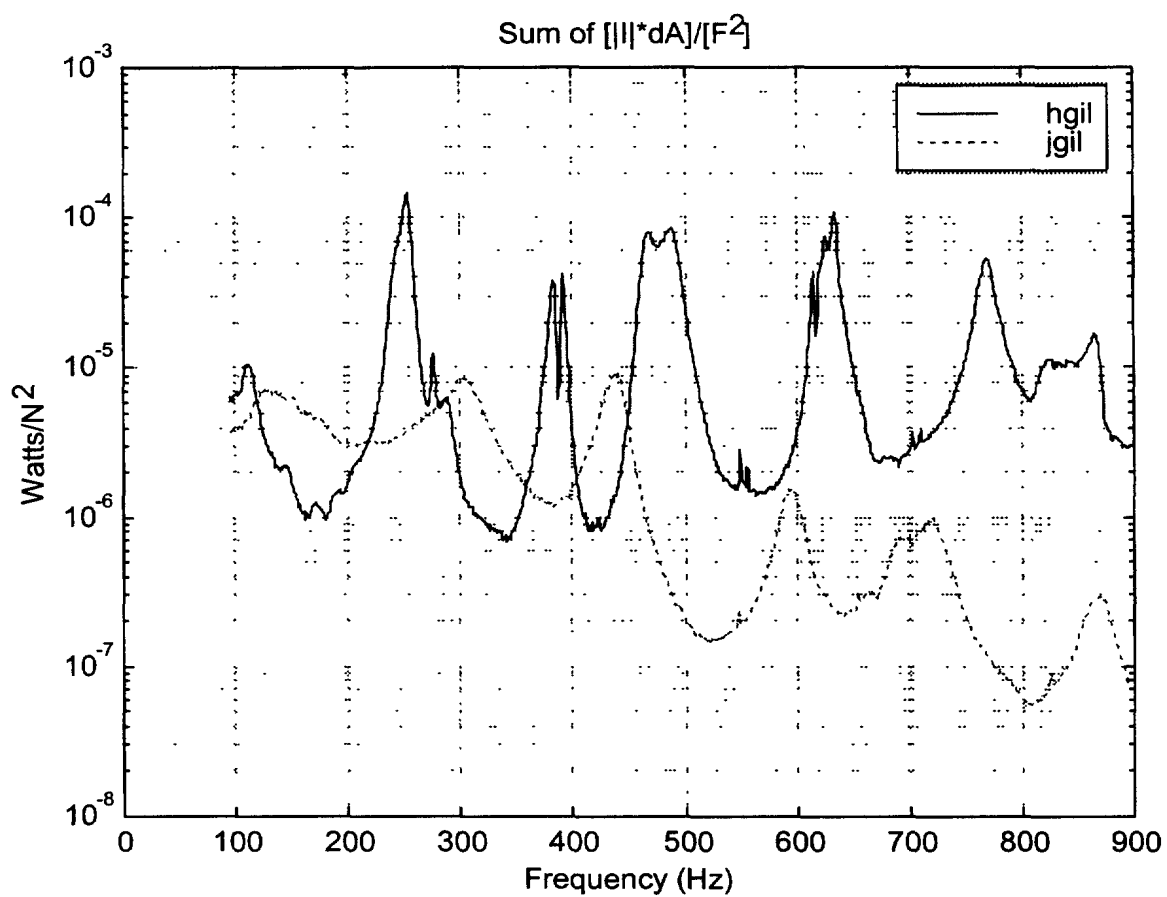


Plate H (9.5 mm bare steel) vs Plate J (9.5 mm steel with 25 mm SC4116)

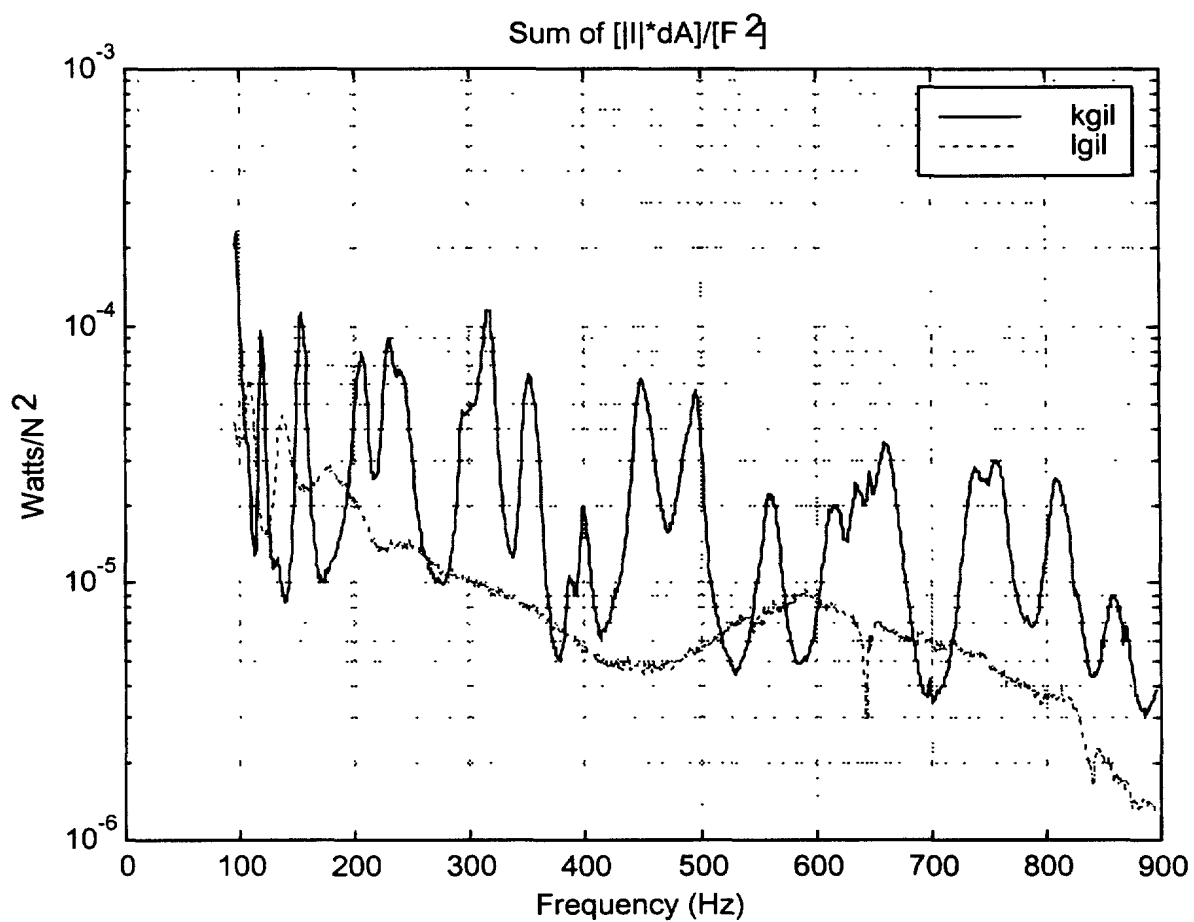


Plate K(3 mm bare steel) vs Plate L (3mm steel with 3 mm V710)

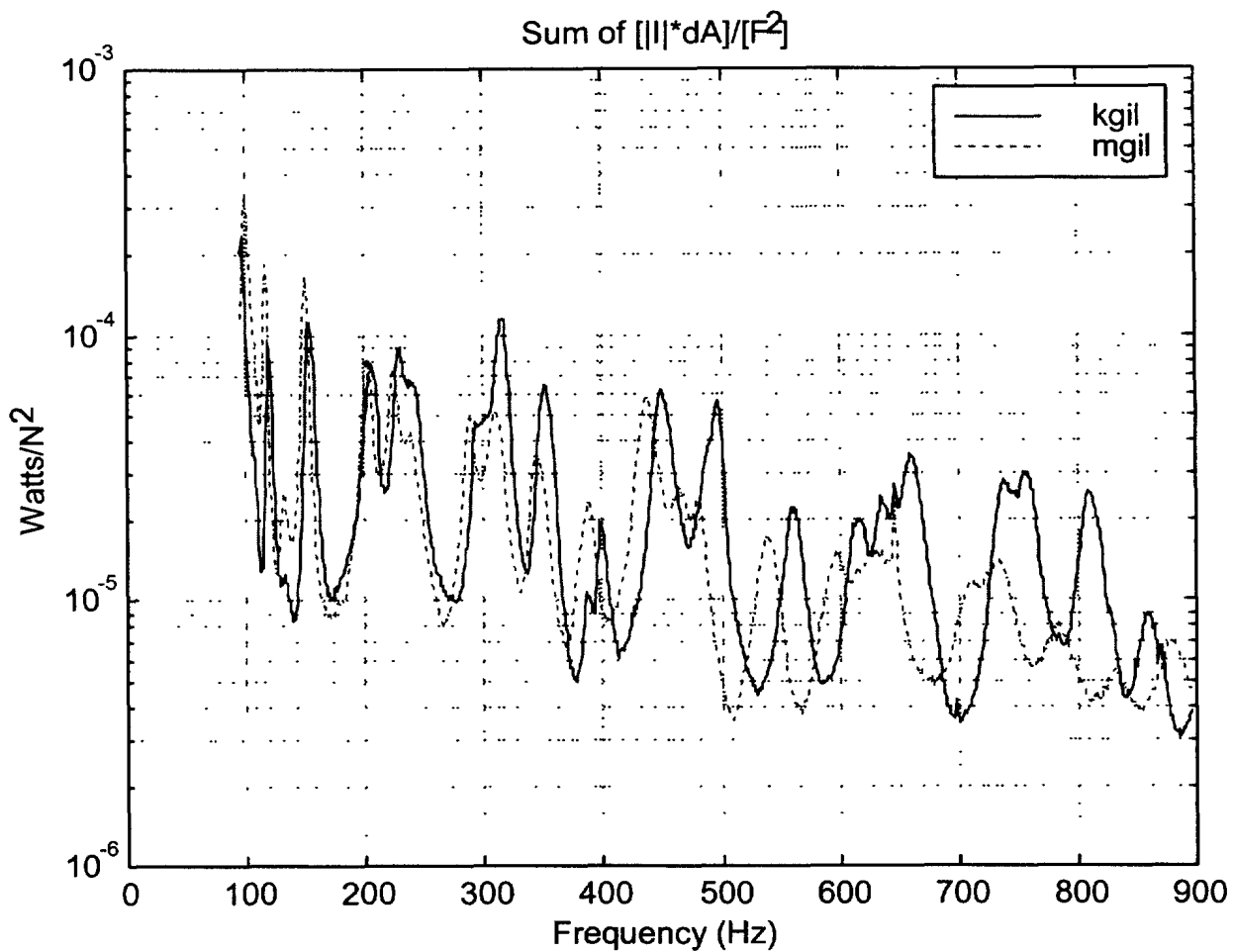


Plate K (3 mm bare steel) vs Plate M (3 mm steel with 3 mm C-1002)

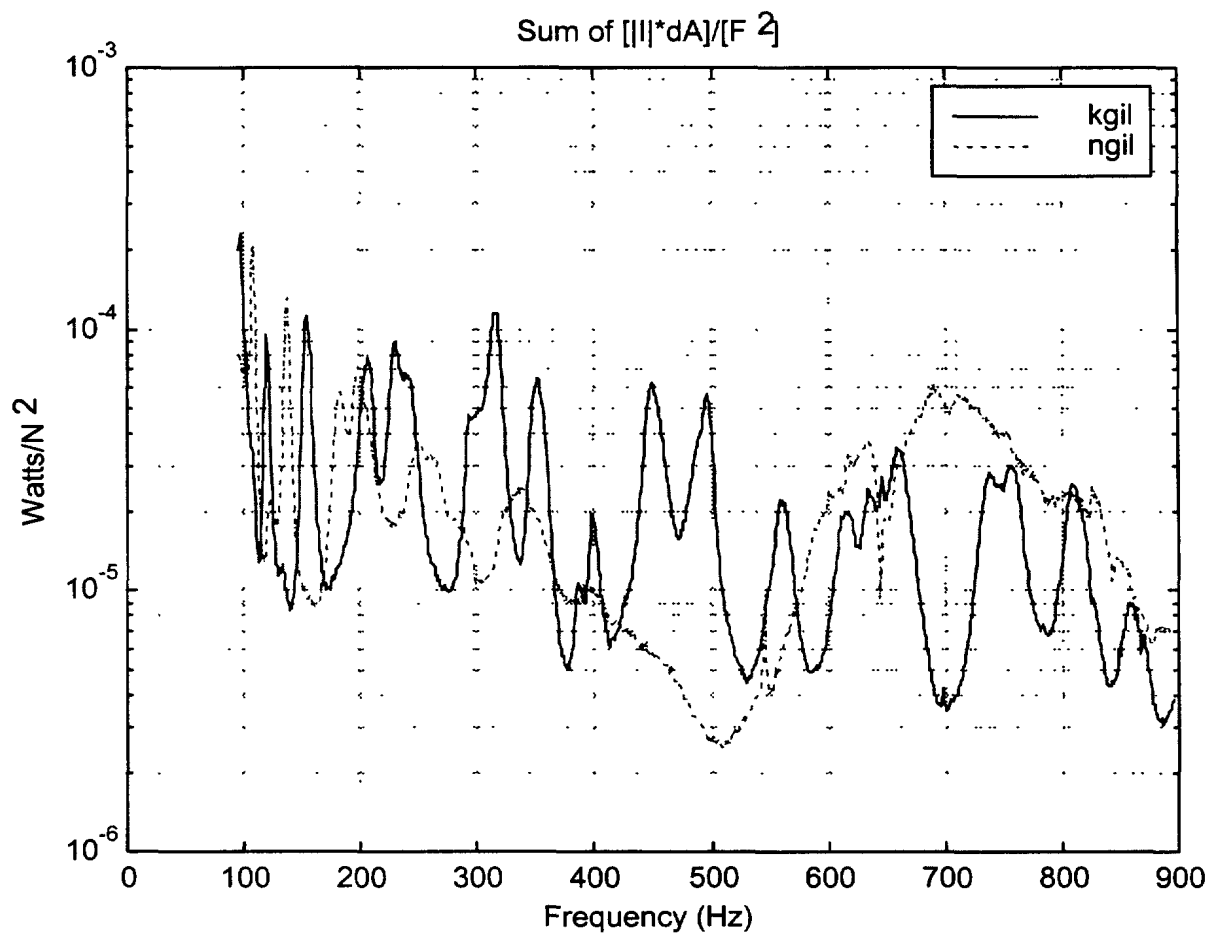


Plate K (3 mm bare steel) vs Plate N (3 mm steel with 12 mm VA80)

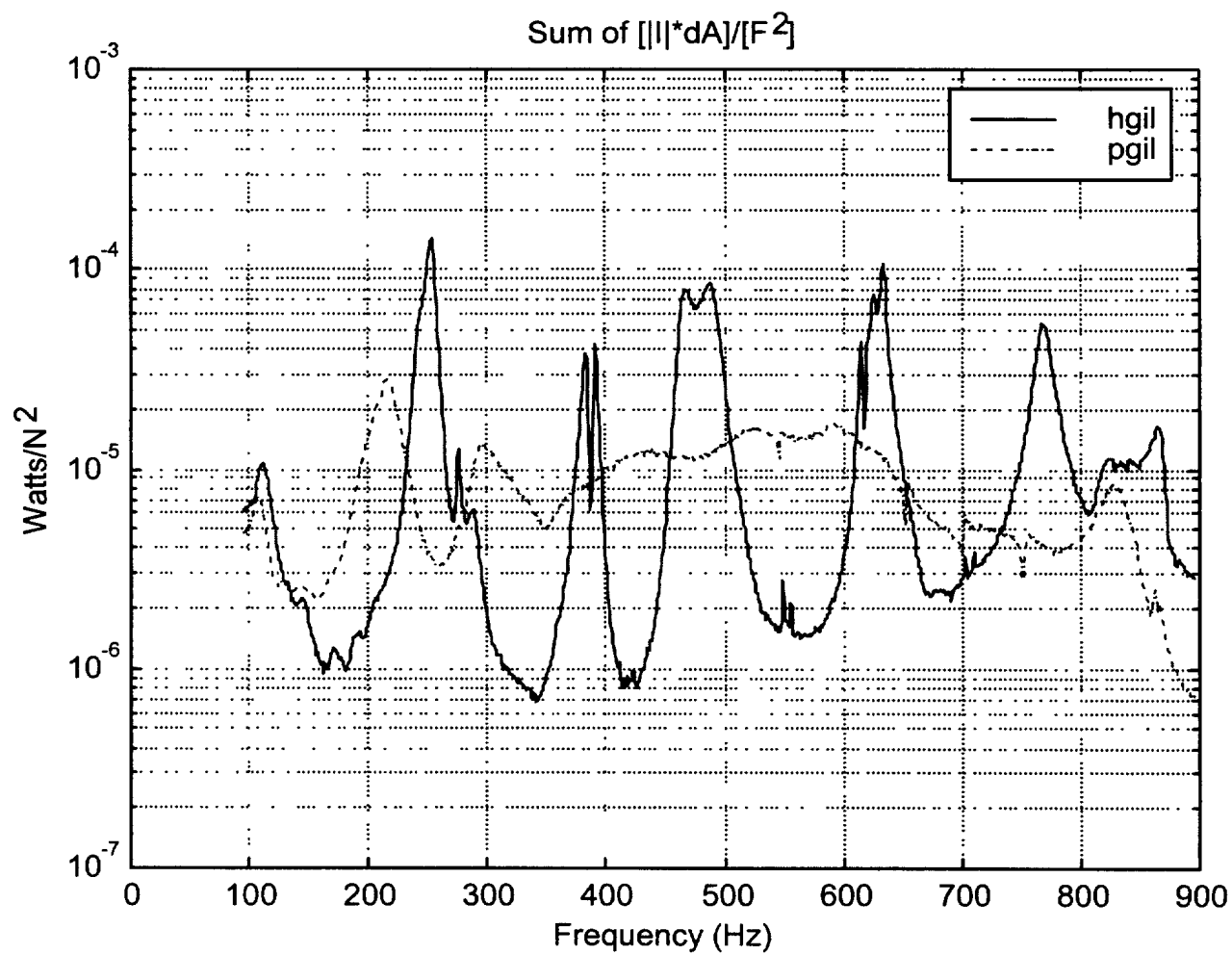


Plate H (9.5 mm bare steel) vs Plate P (9.5 mm steel 12 mm VA80)

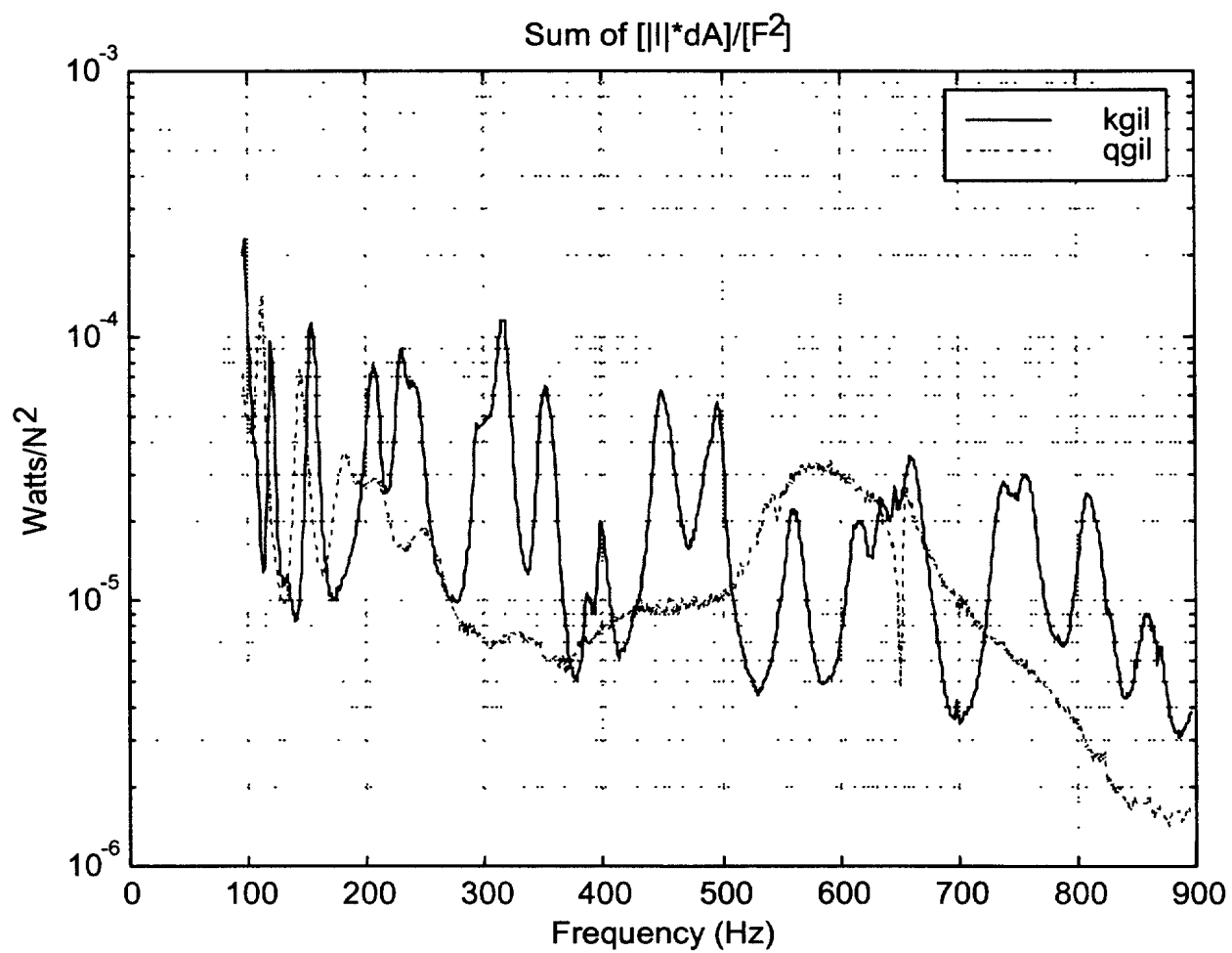


Plate K (3 mm bare steel) vs Plate Q (3 mm steel with 23 mm VA80)

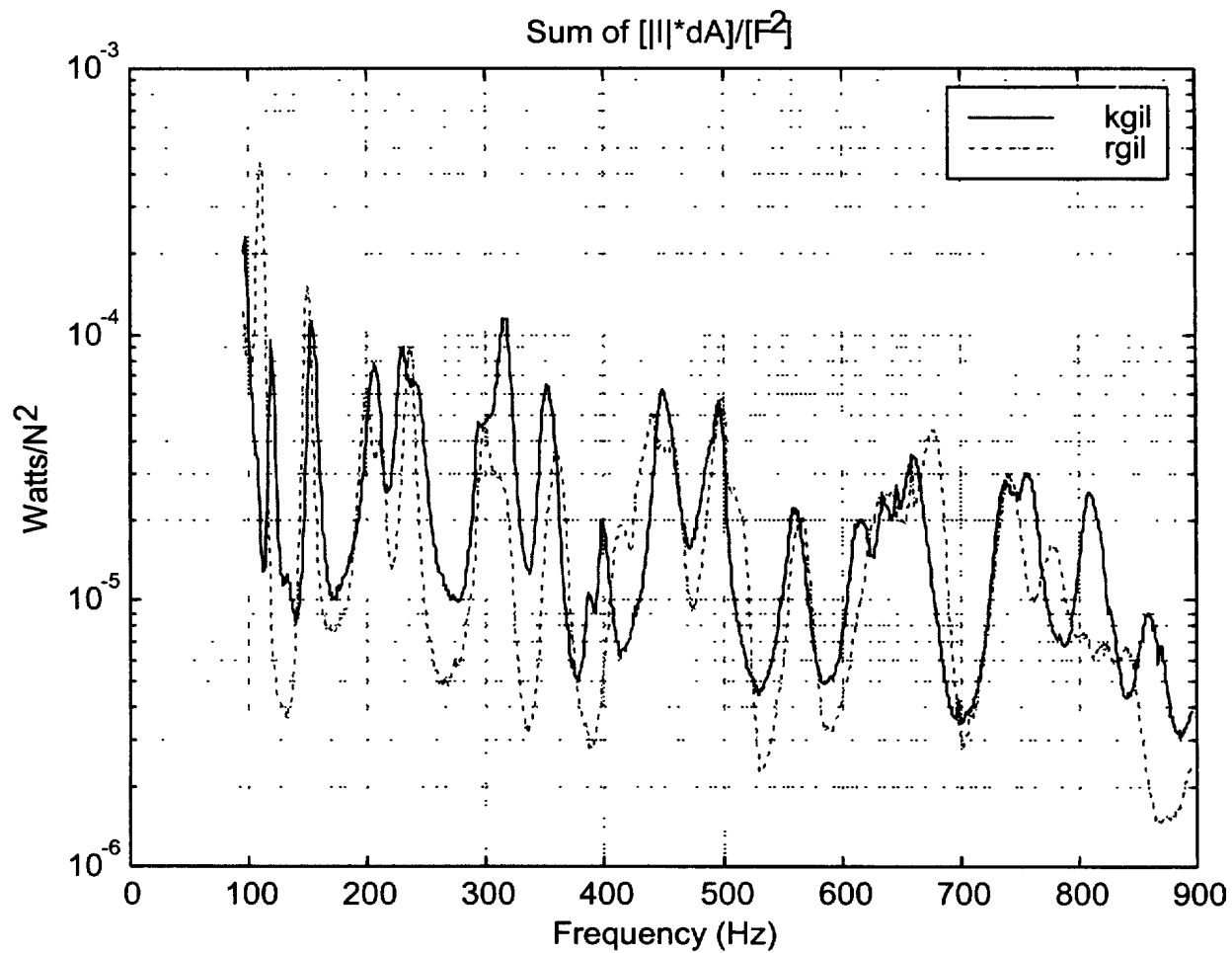


Plate K (3 mm bare steel) vs Plate R (3 mm steel with 3 mm C-1002 coating on air side of plate)

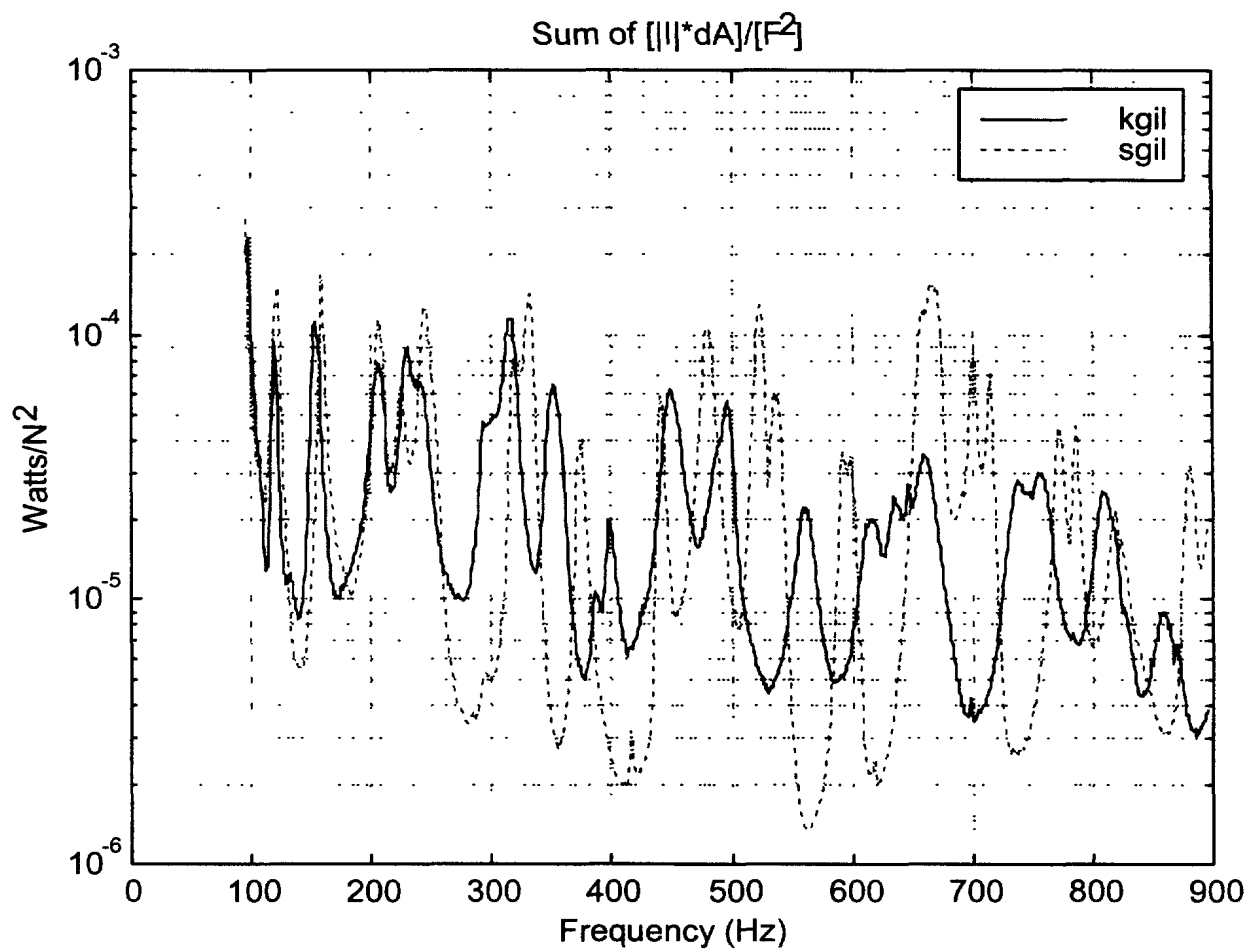


Plate K (3 mm bare steel) vs Plate S (3 mm steel with 3 mm V710 coating on air side of plate)

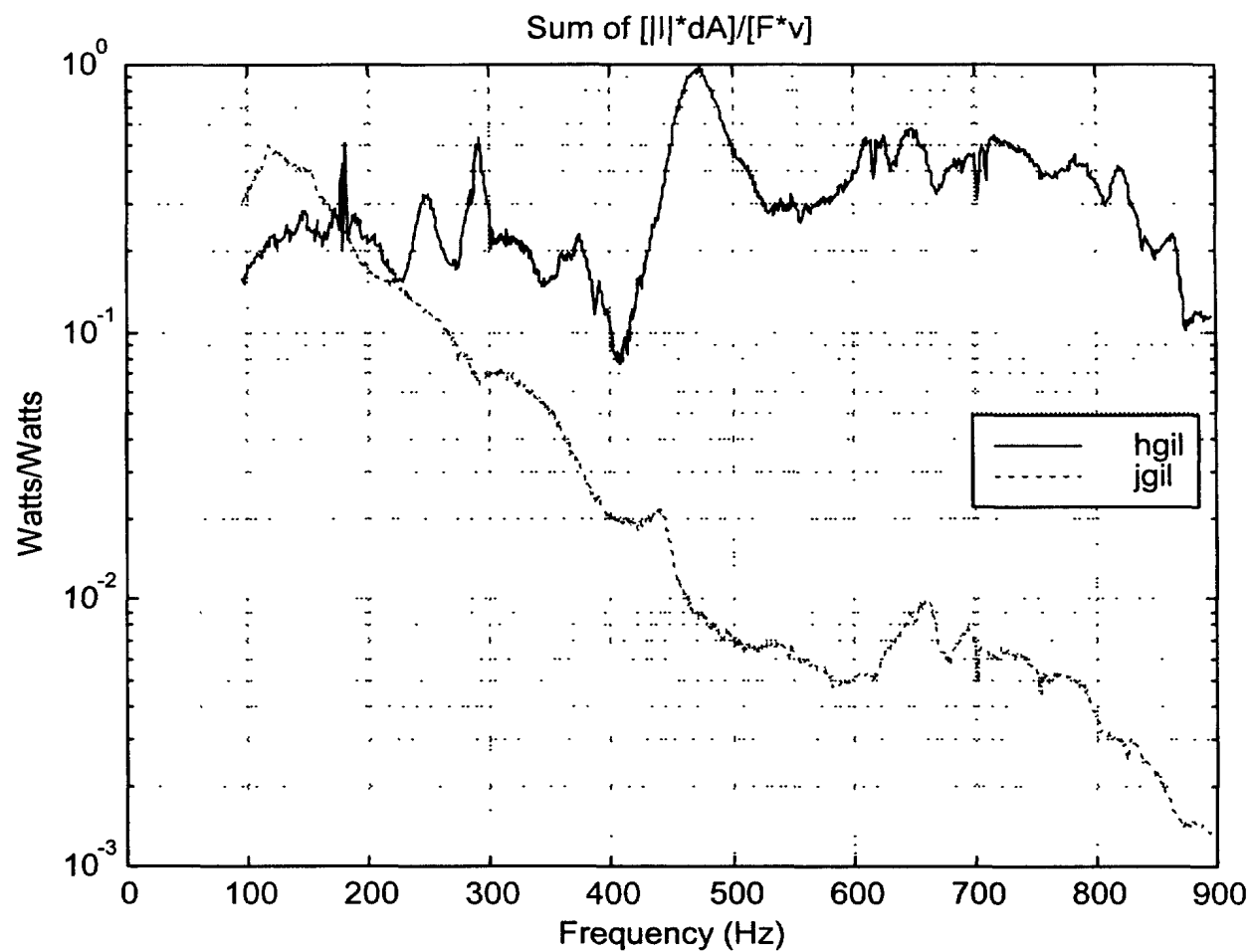


Plate H (9.5 mm bare steel) vs Plate J (9.5 mm steel with 25 mm SC4116)

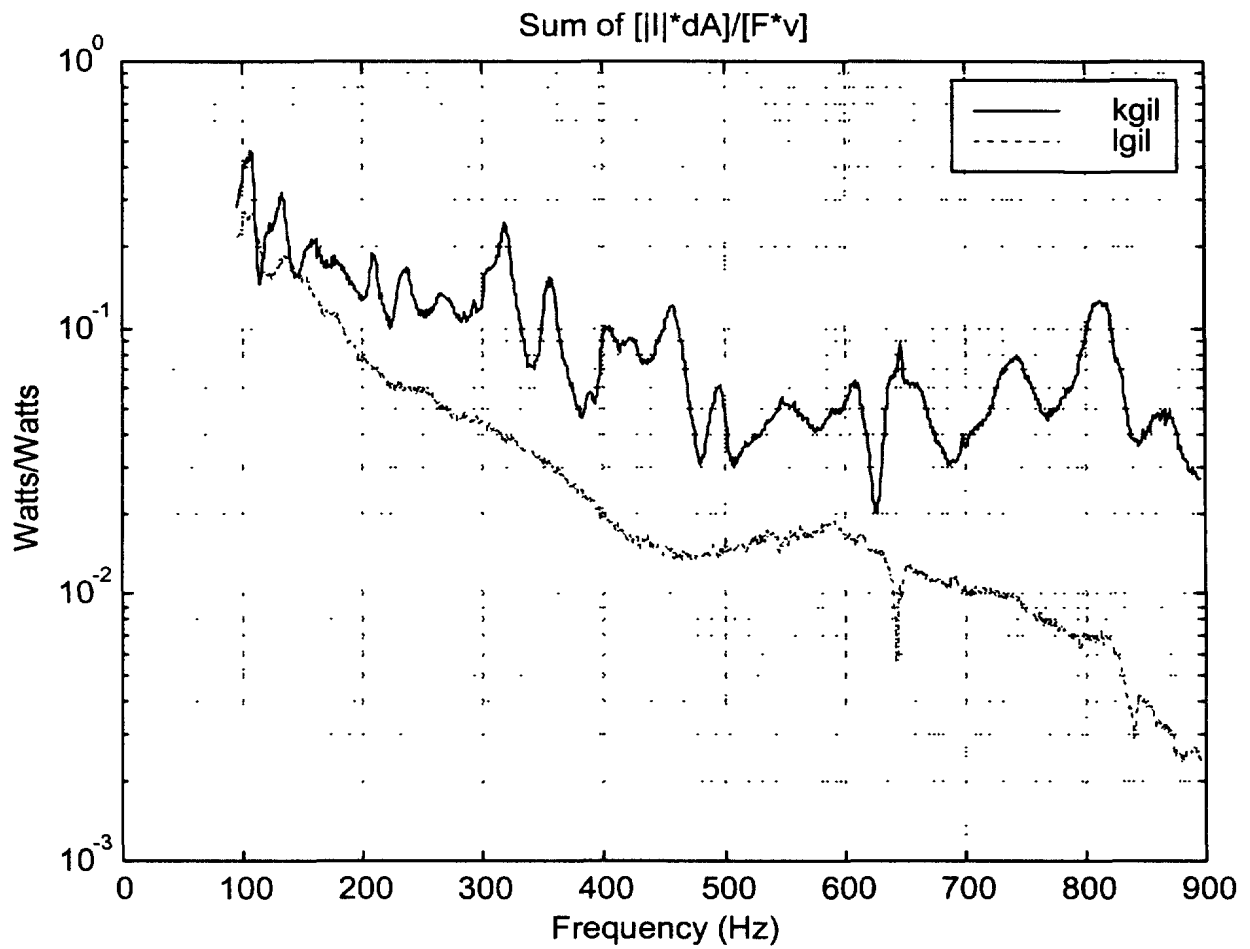


Plate K(3 mm bare steel) vs Plate L (3mm steel with 3 mm V710)

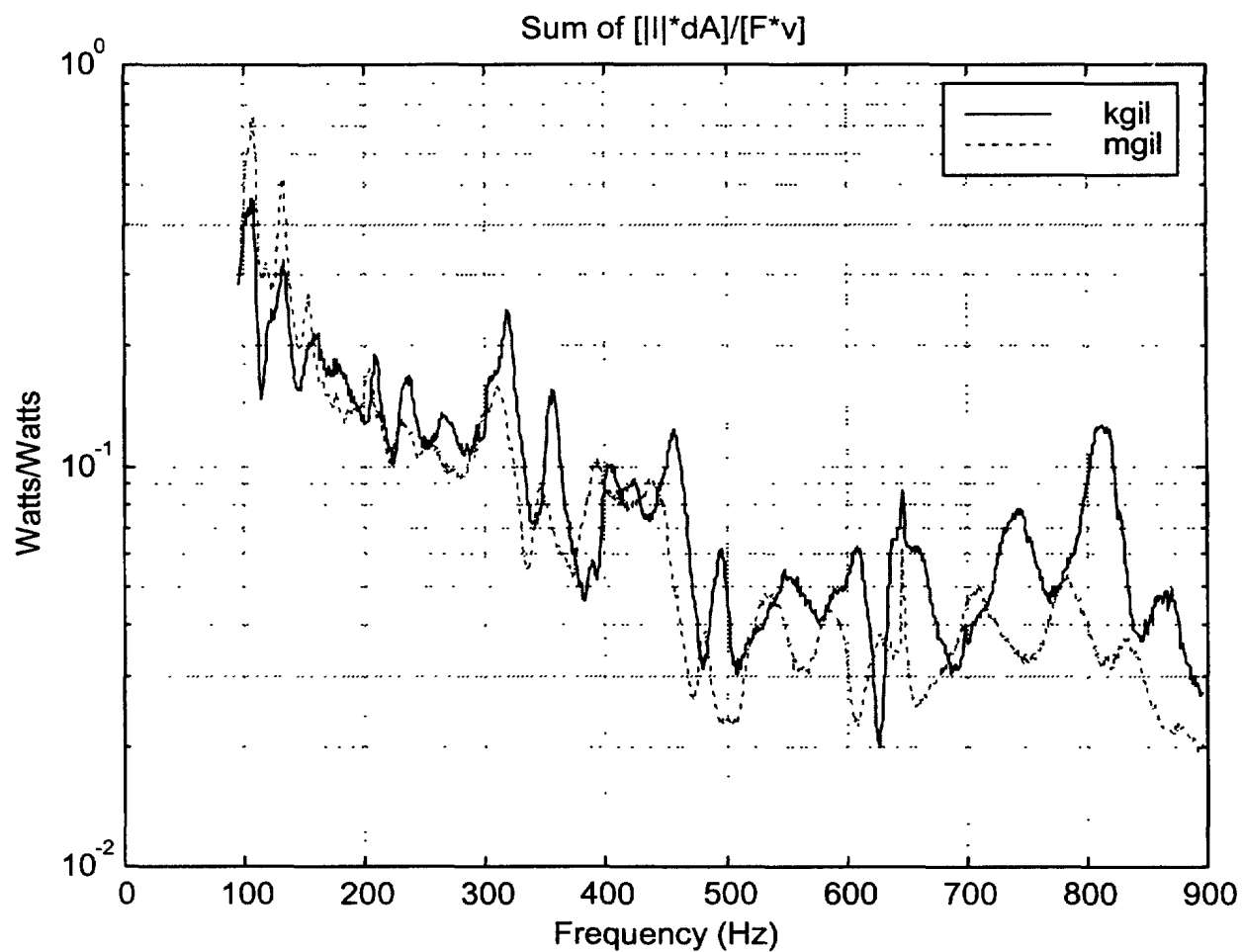


Plate K (3 mm bare steel) vs Plate M (3 mm steel with 3 mm C-1002)

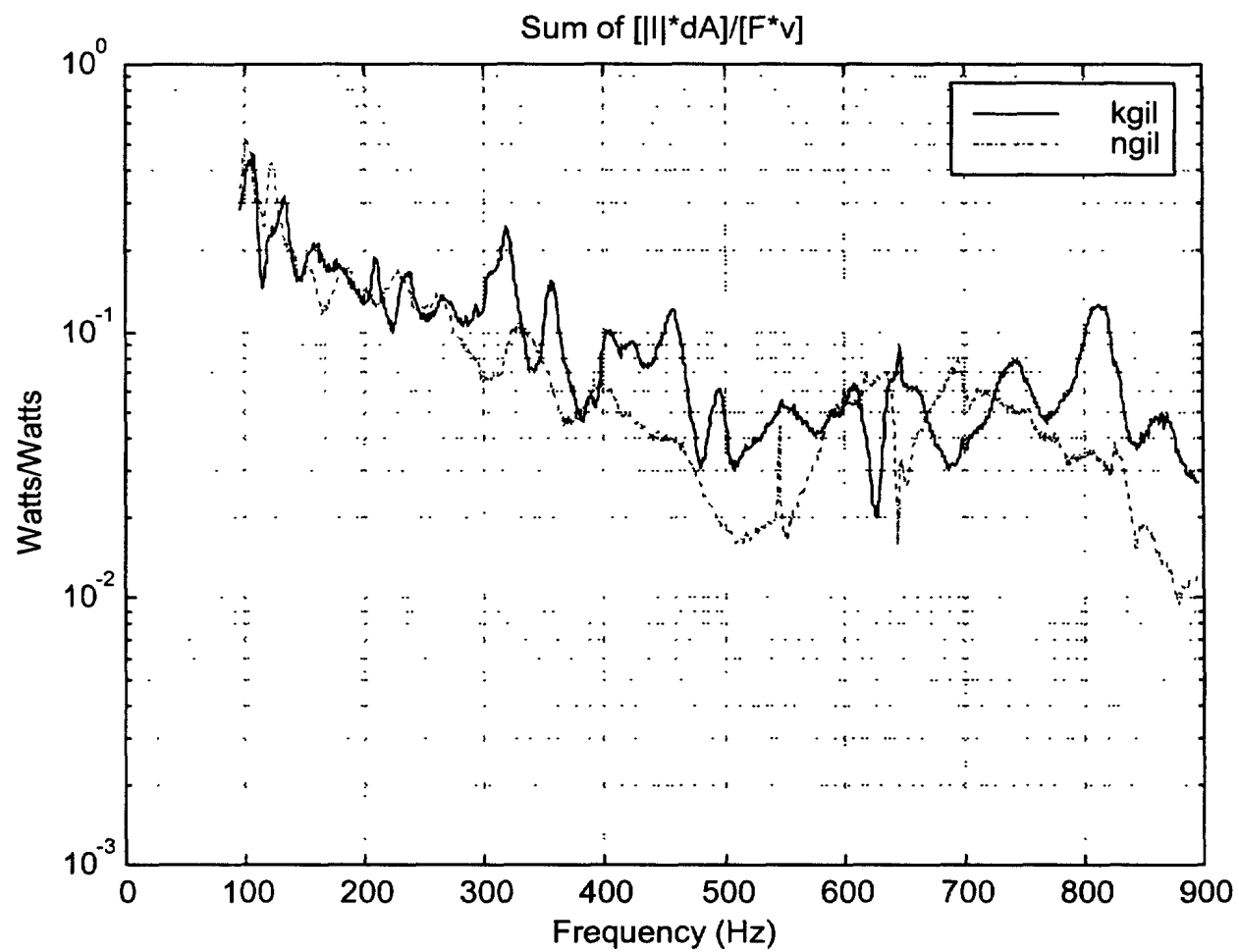


Plate K (3 mm bare steel) vs Plate N (3 mm steel with 12 mm VA80)

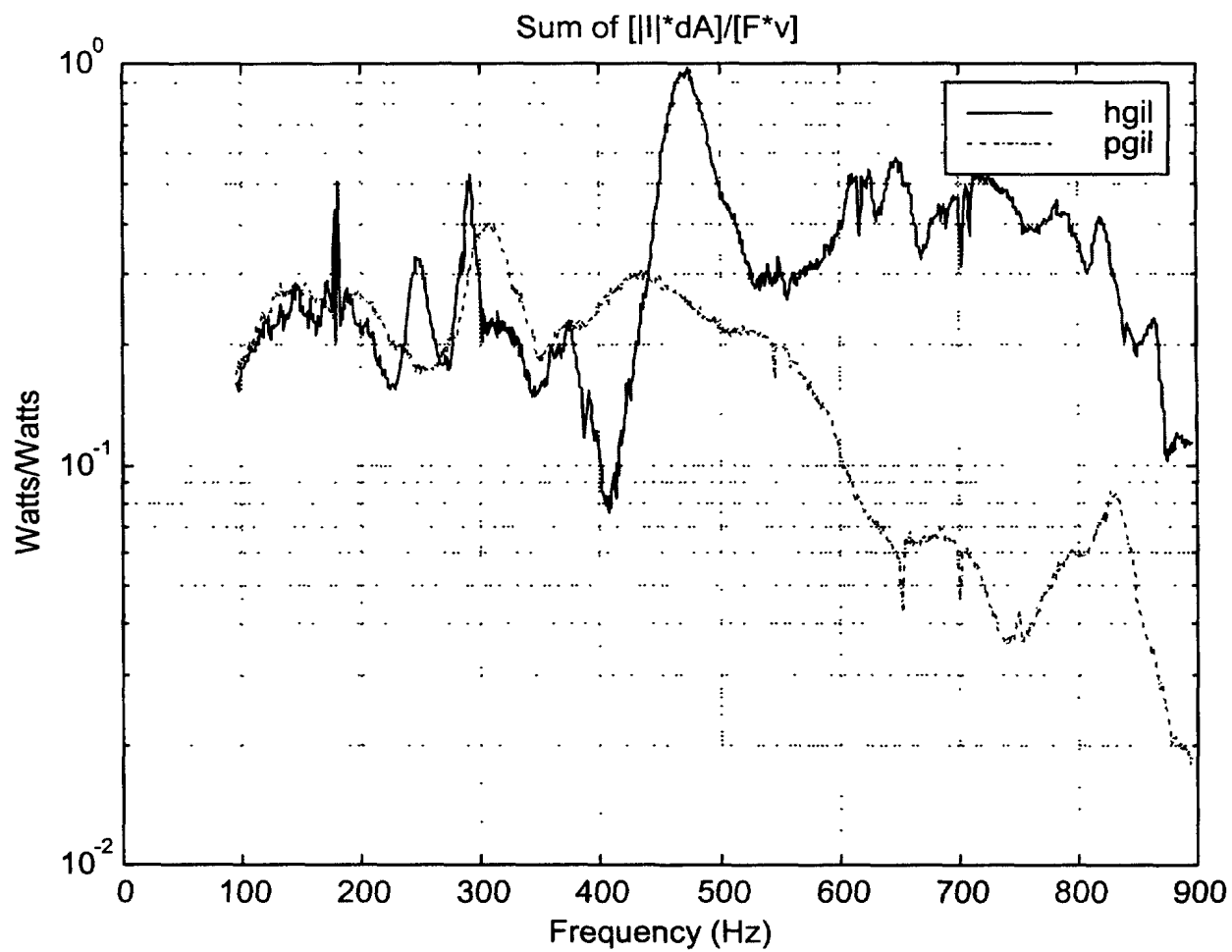


Plate H (9.5 mm bare steel) vs Plate P (9.5 mm steel with 12 mm VA80)

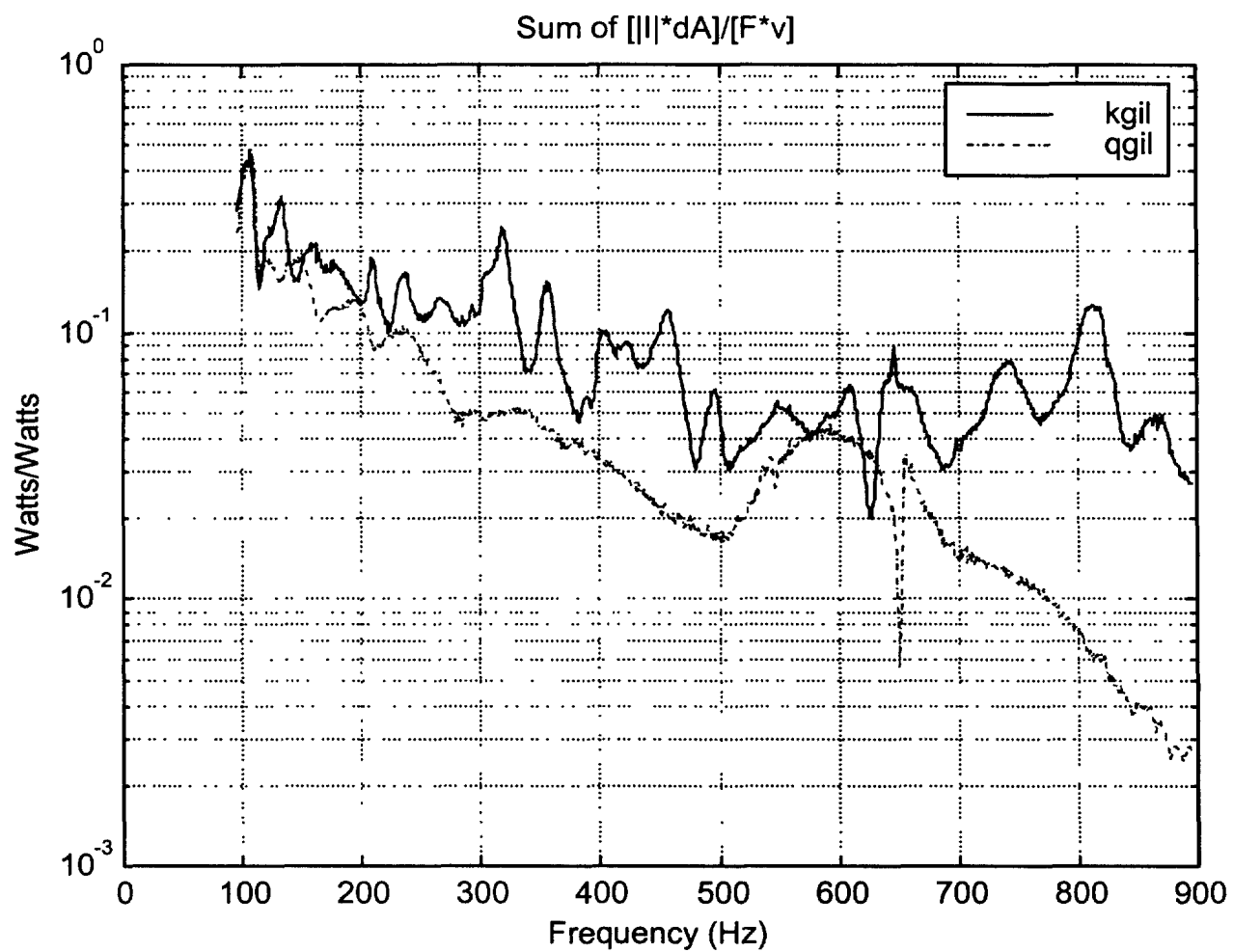


Plate K (3 mm bare steel) vs Plate Q (3 mm steel with 23 mm VA80)

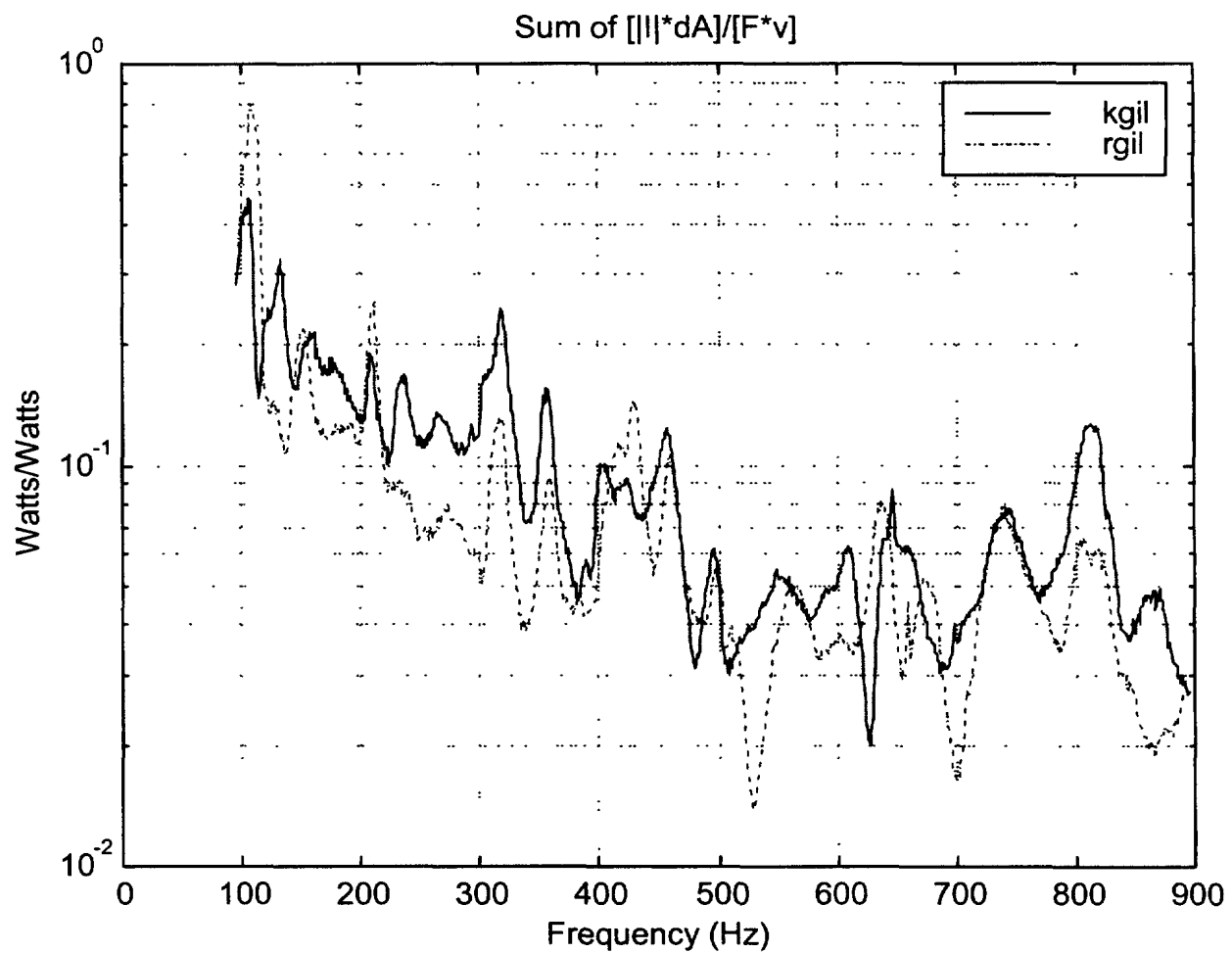


Plate K (3 mm bare steel) vs Plate R (3 mm steel with 3 mm C-1002 coating on air side of plate)

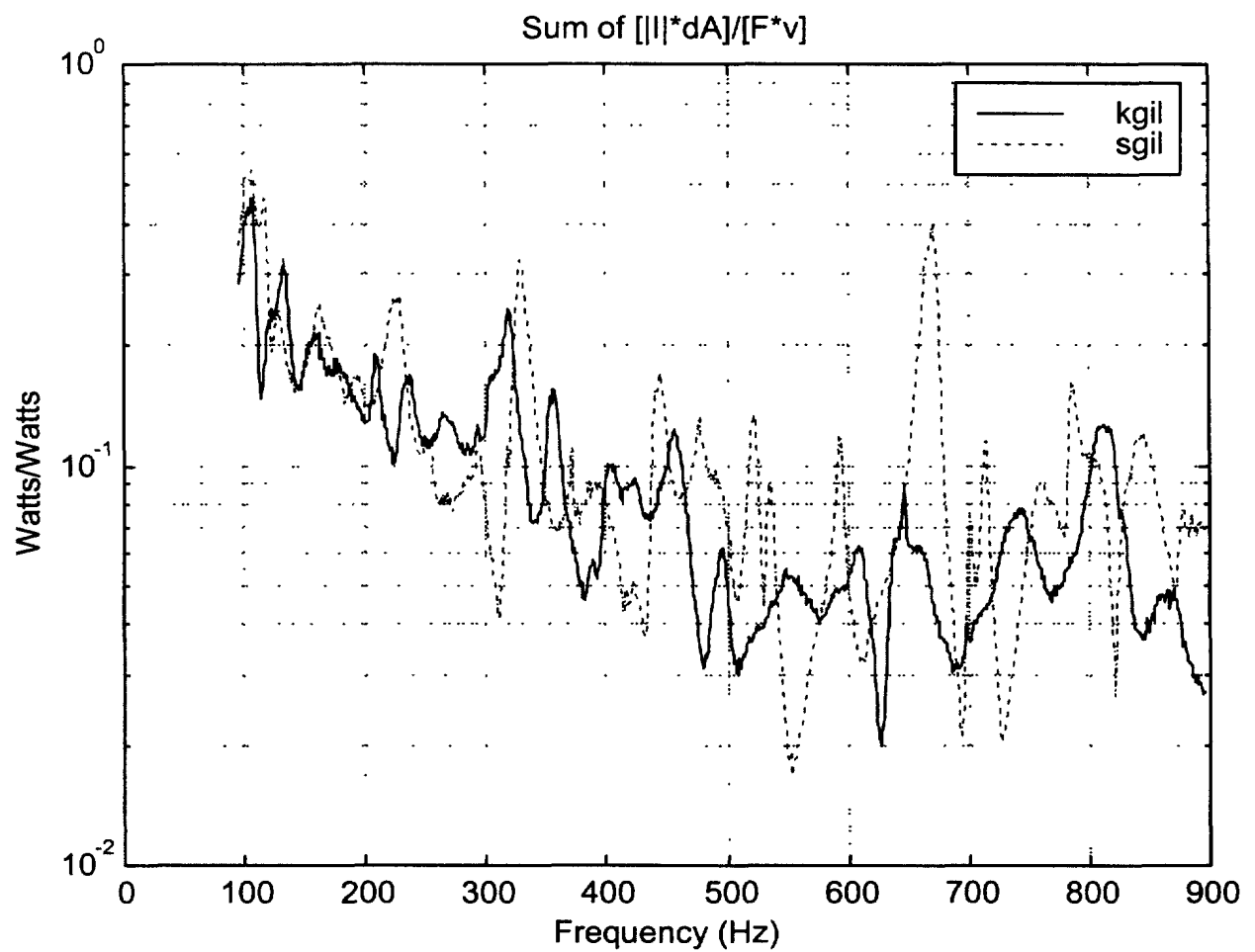


Plate K (3 mm bare steel) vs Plate S (3 mm steel with 3 mm V710 coating on air side of plate)

Appendix-F
Experimental Decoupling Performance
From Normalized Absolute Power

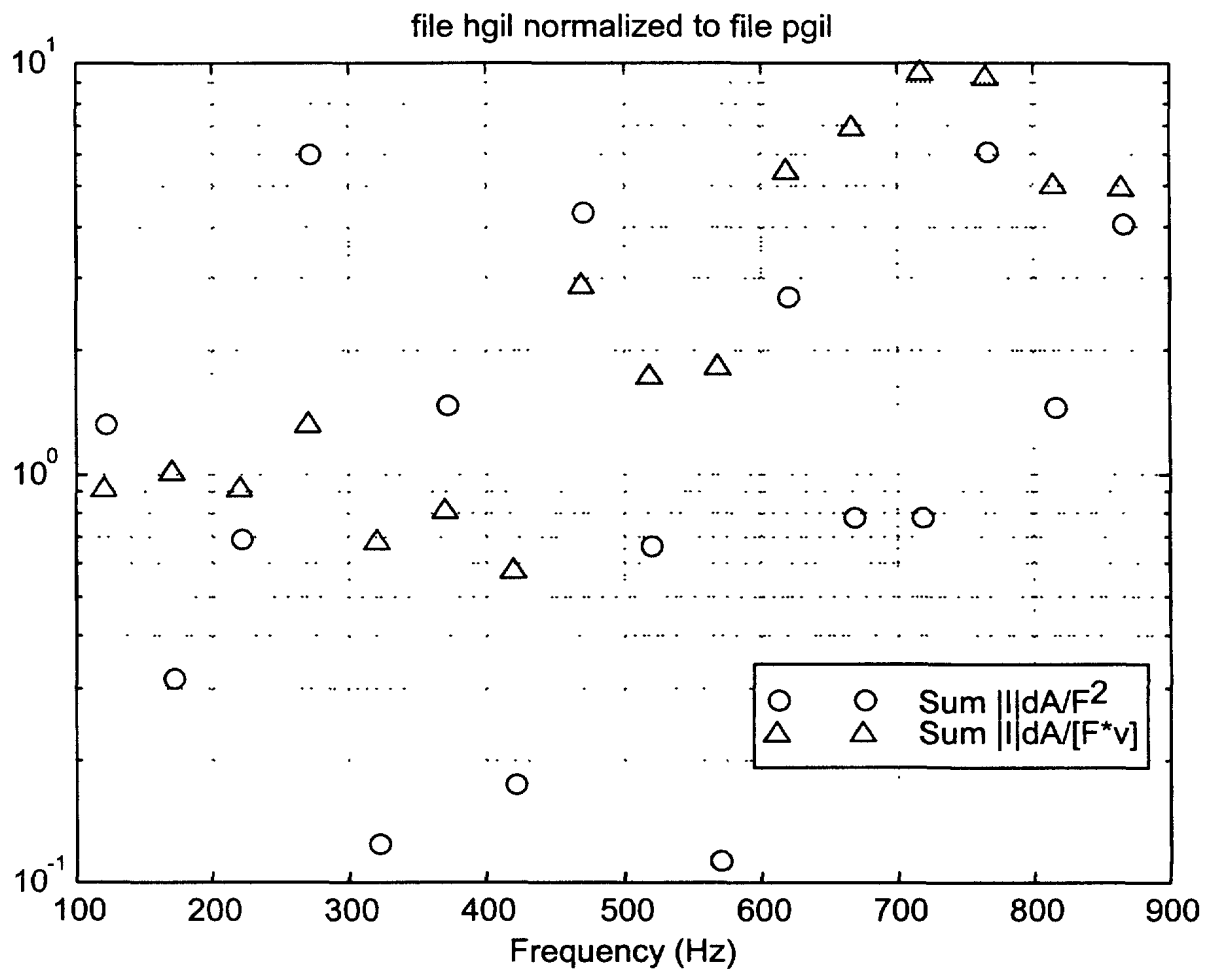


Plate H (9.5 mm bare steel) vs Plate P (9.5 mm steel 12 mm VA80)

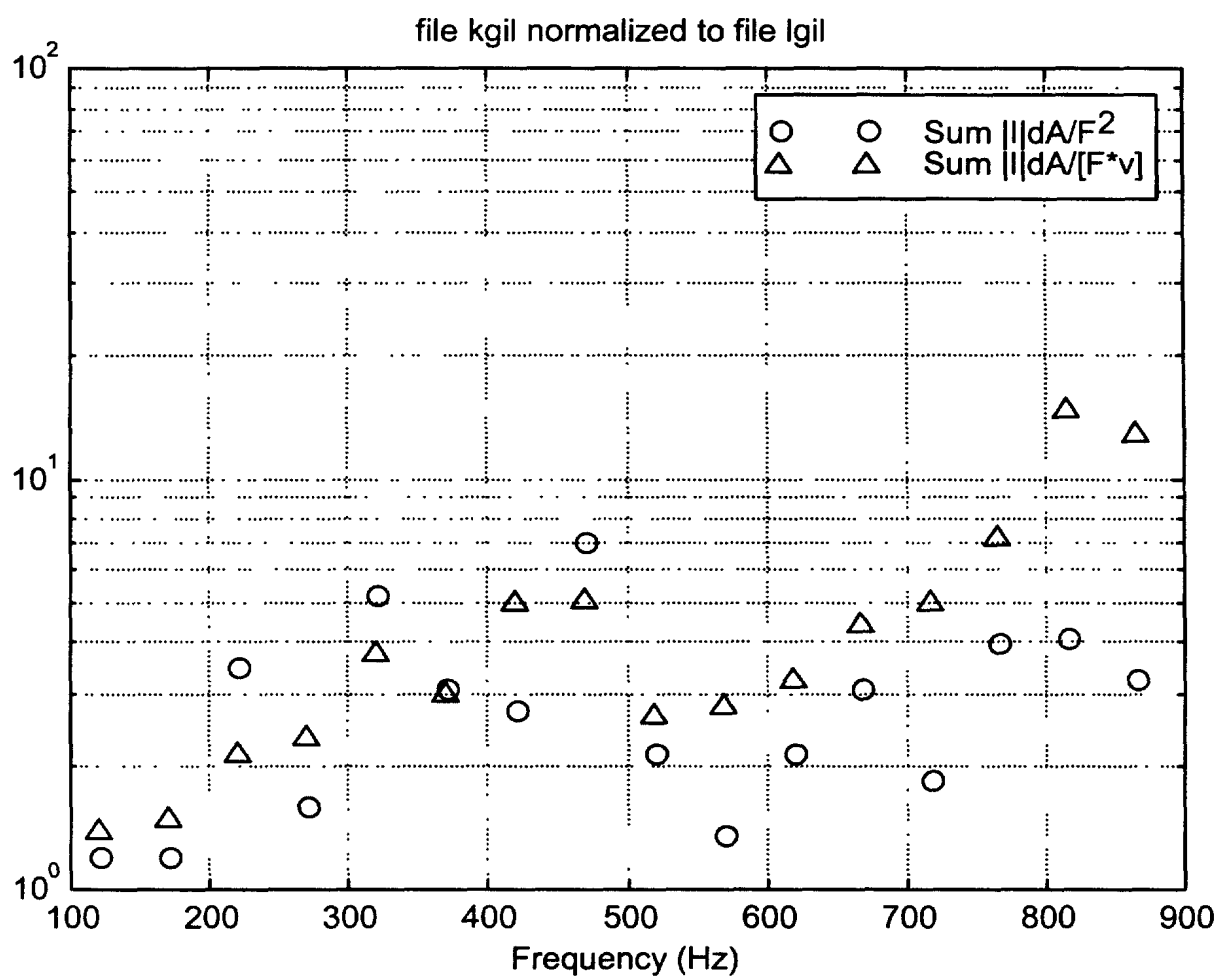


Plate K (3 mm bare steel) vs Plate L (3mm steel with 3 mm V710)

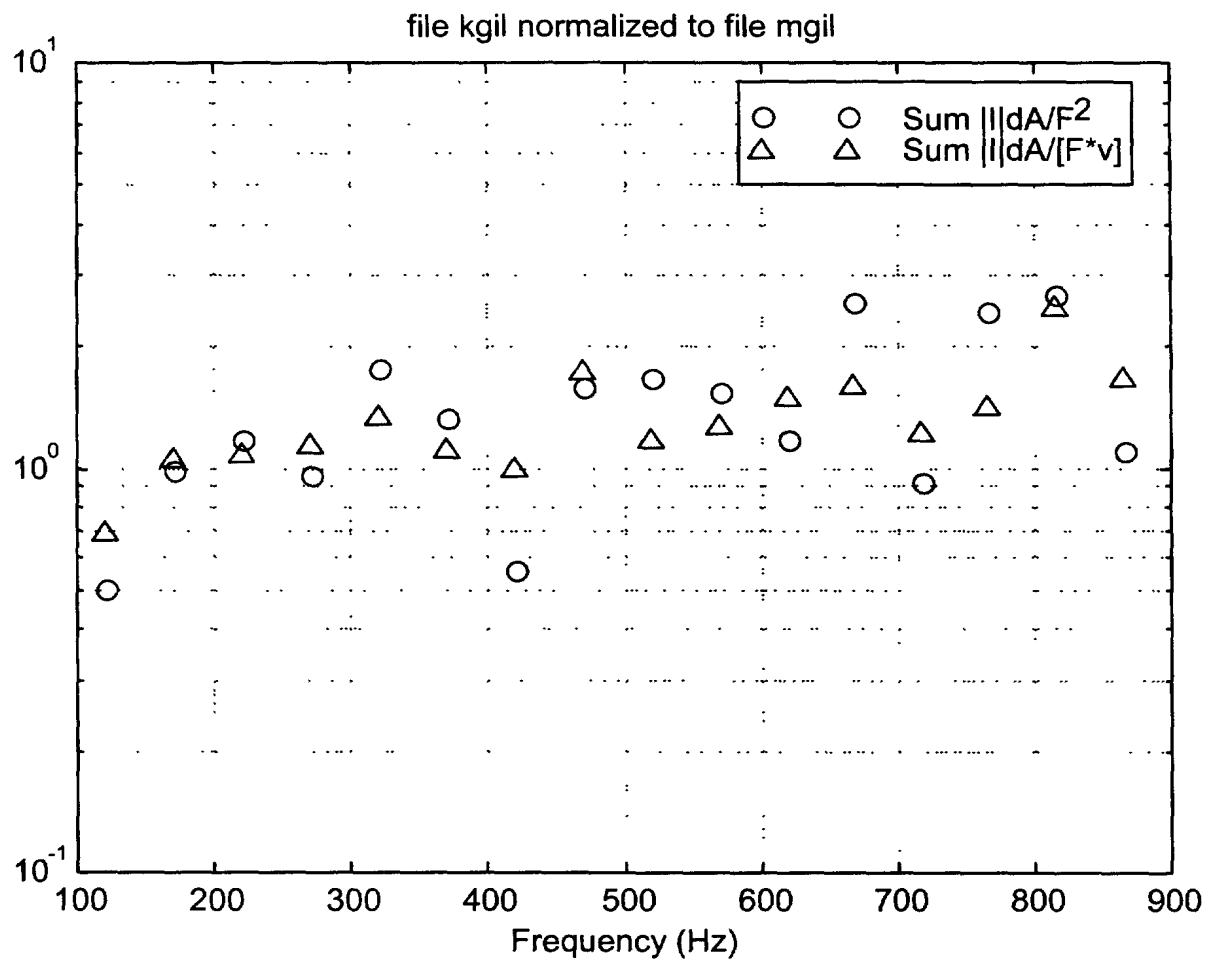


Plate K (3 mm bare steel) vs Plate M (3 mm steel with 3 mm C-1002)

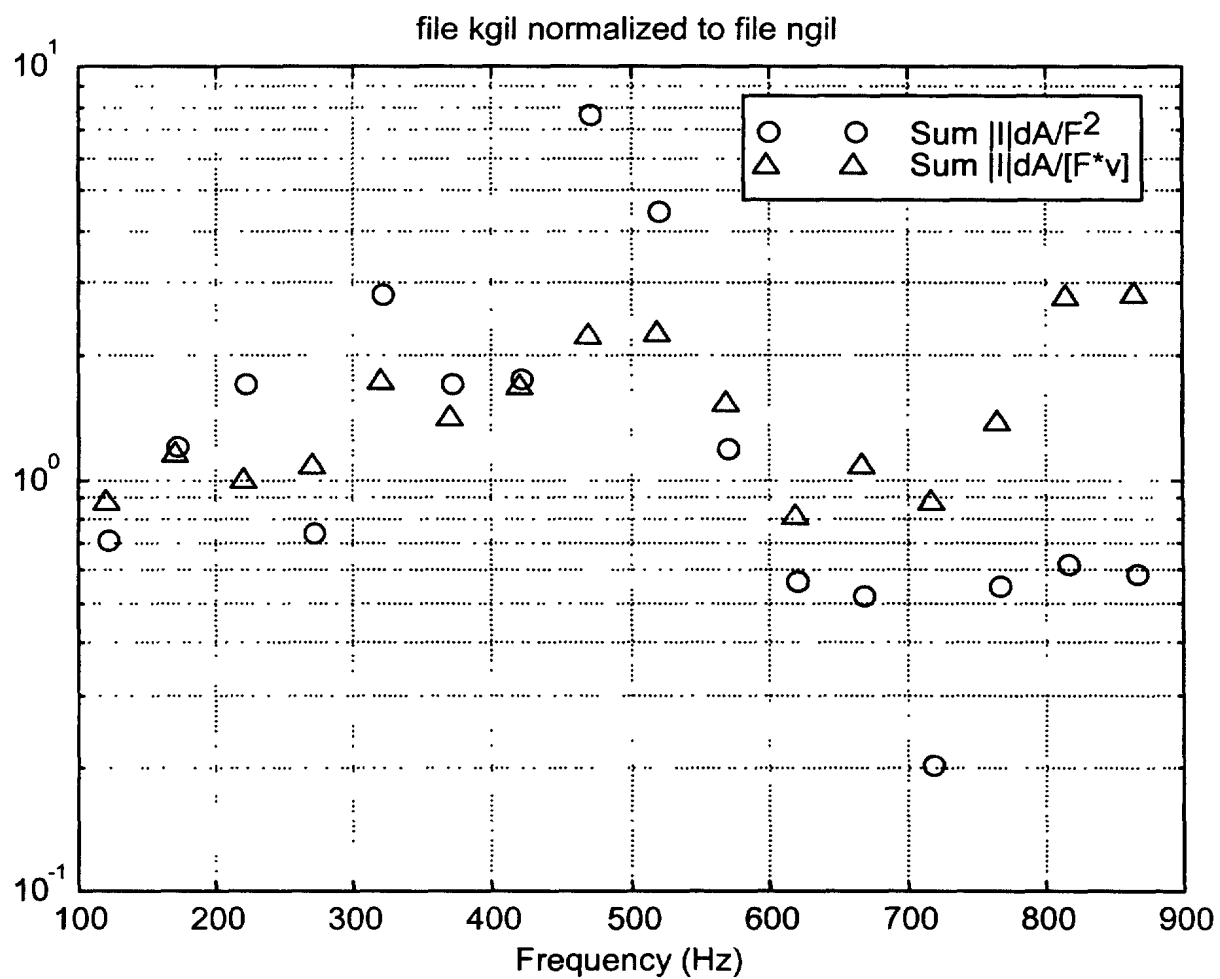


Plate K (3 mm bare steel) vs Plate N (3 mm steel with 12 mm VA80)

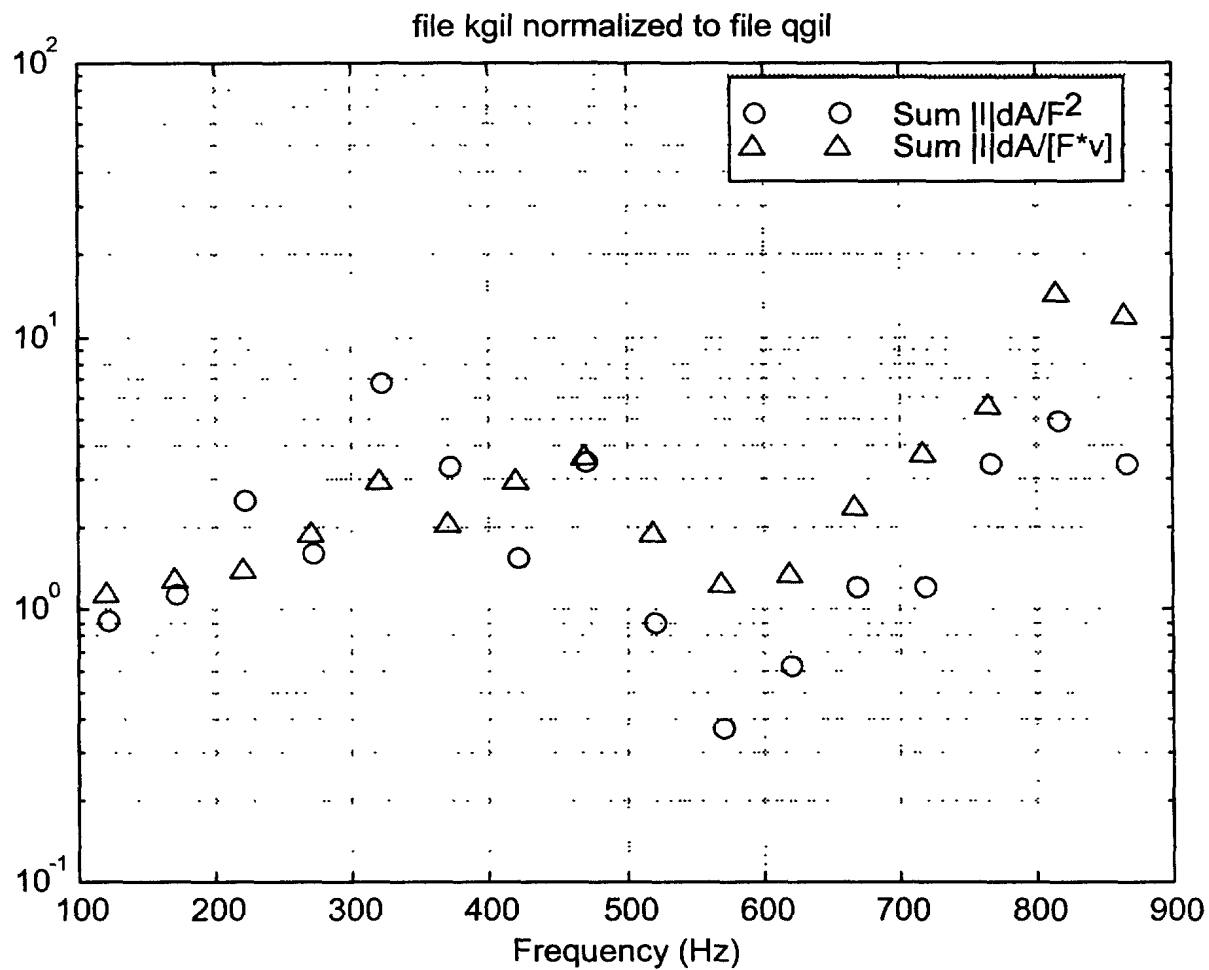


Plate K (3 mm bare steel) vs Plate Q (3 mm steel with 23 mm VA80)

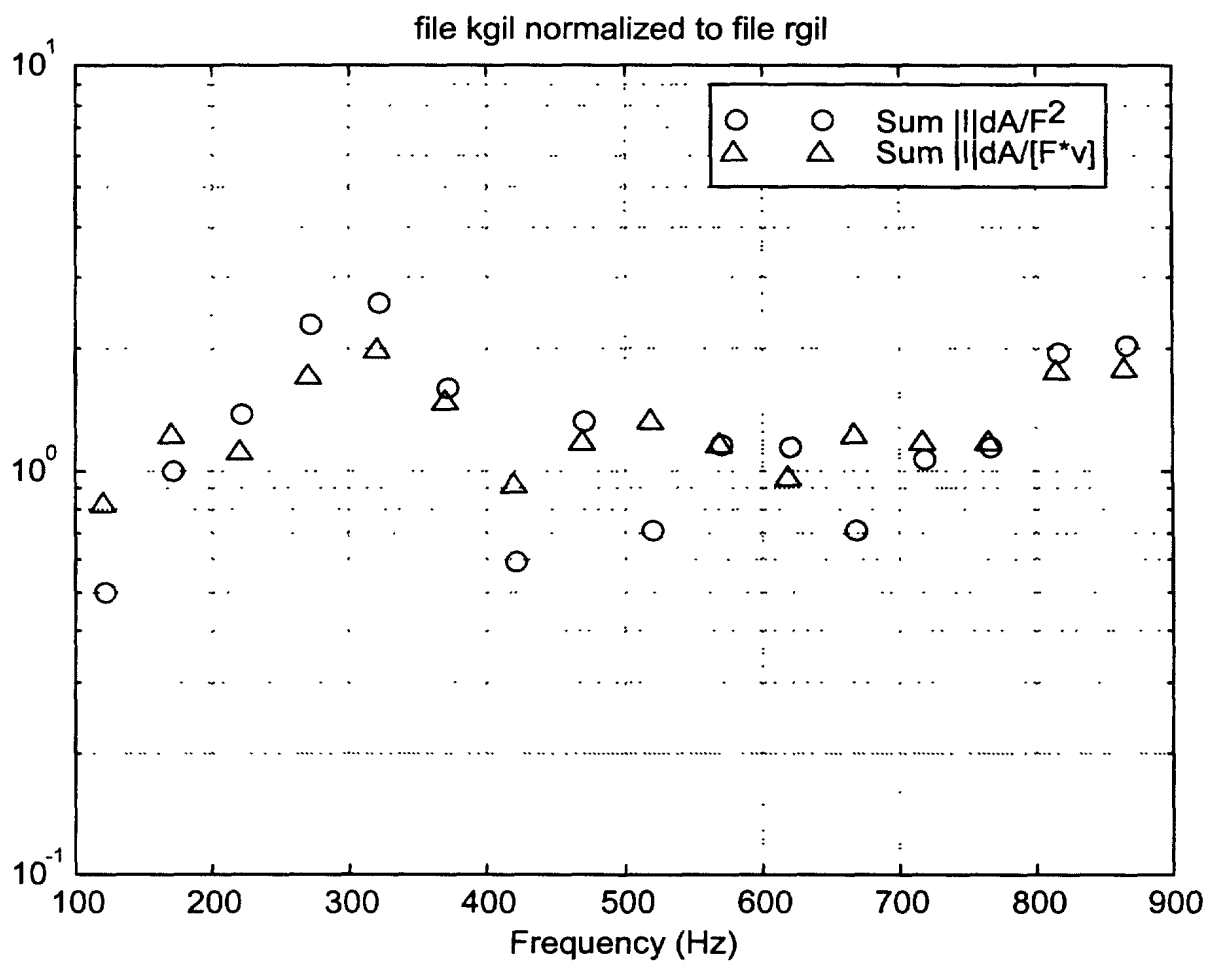


Plate K (3 mm bare steel) vs Plate R (3 mm steel with 3 mm C-1002 coating on air side of plate)

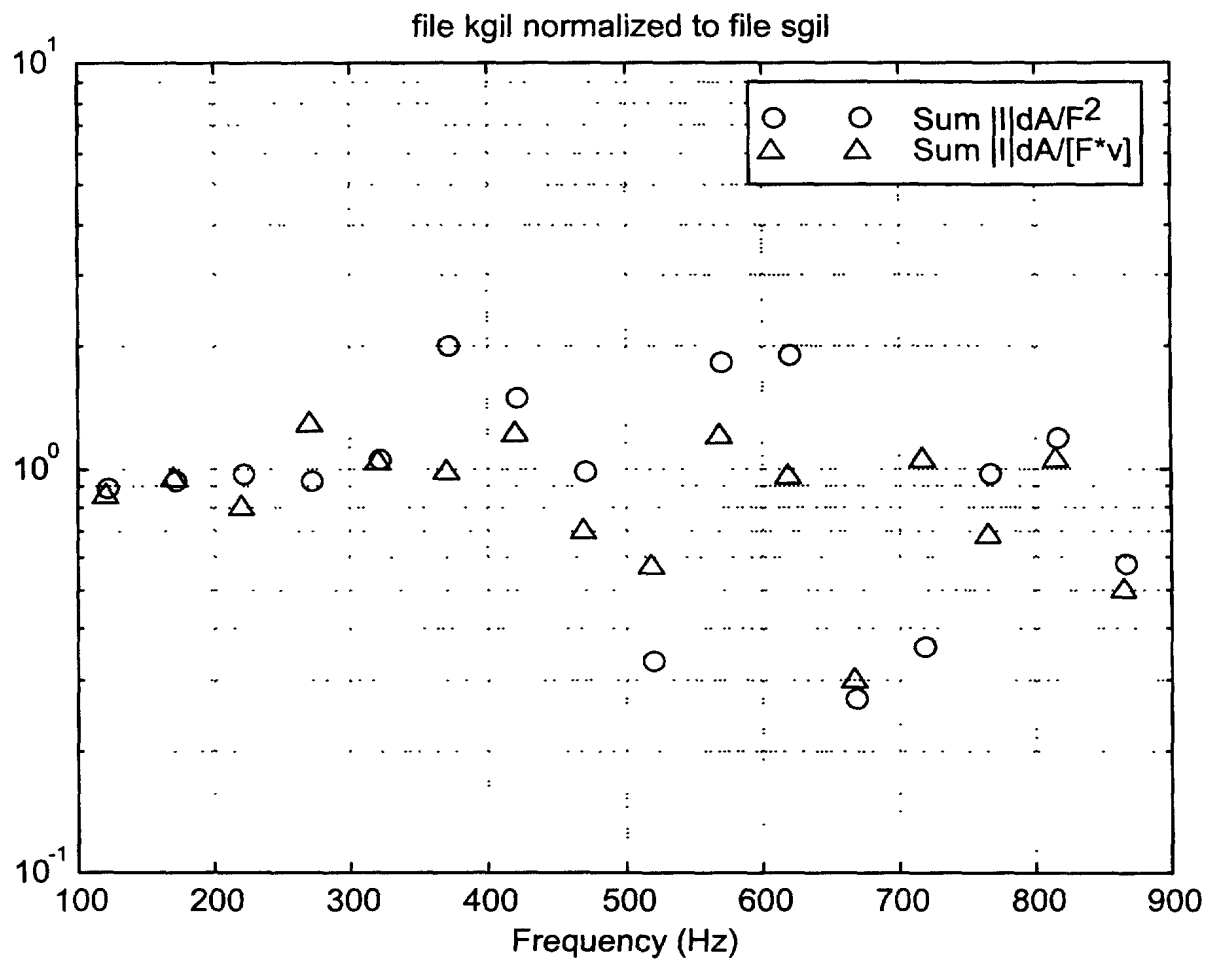
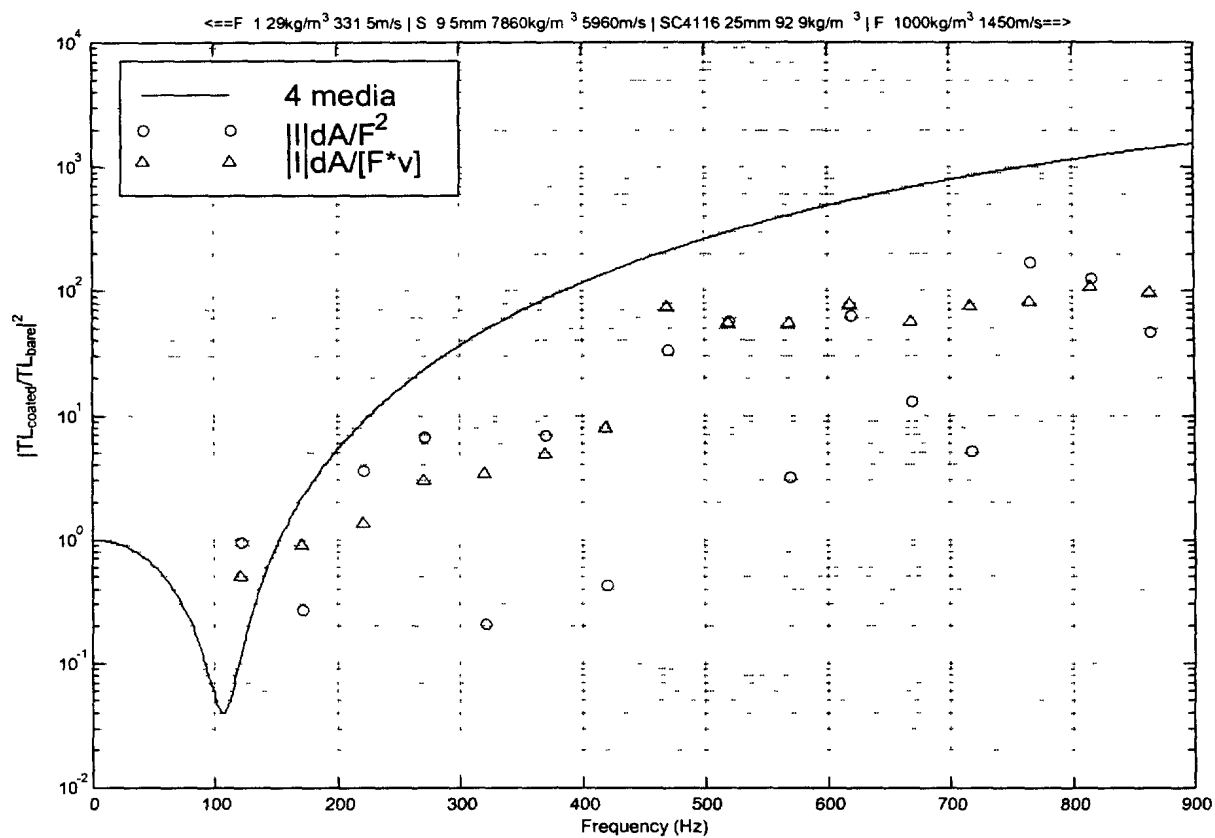
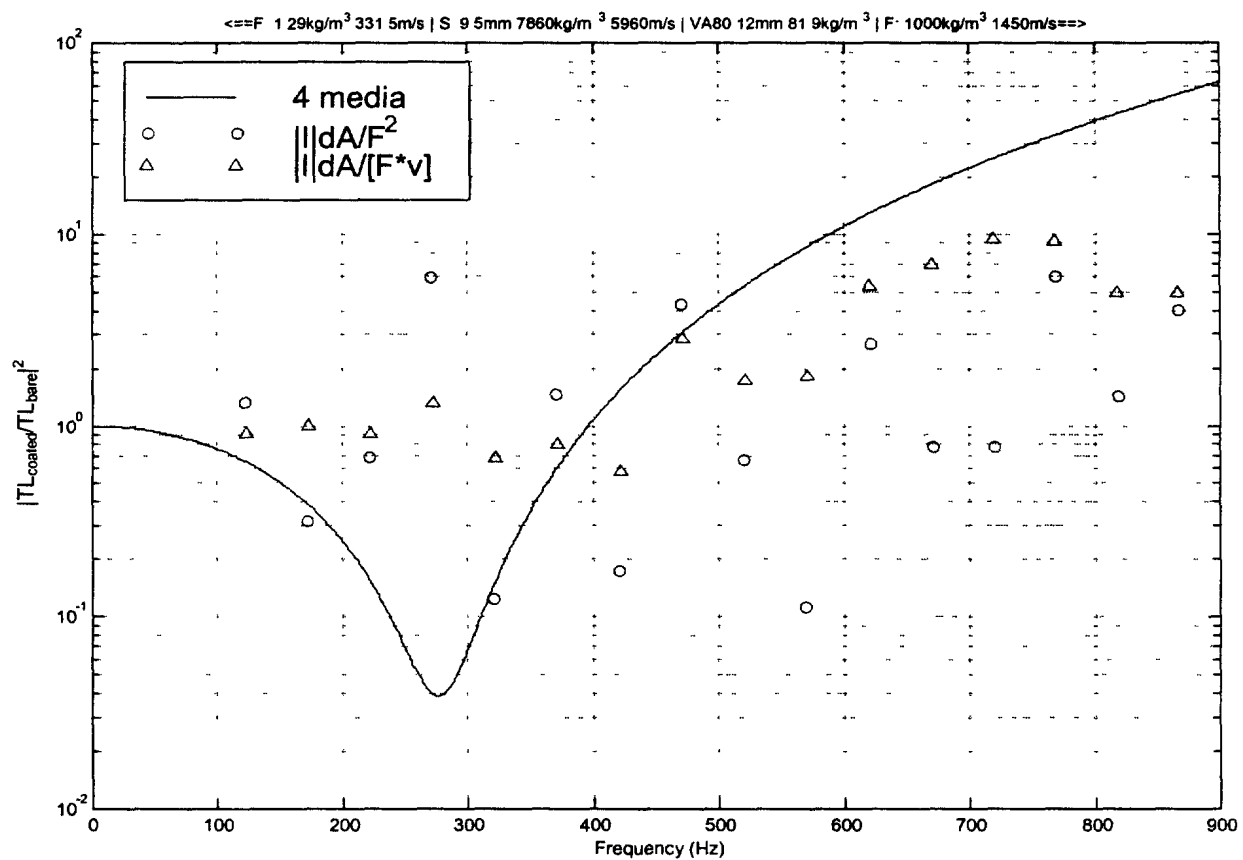


Plate K (3 mm bare steel) vs Plate S (3 mm steel with 3 mm V710 coating on air side of plate)

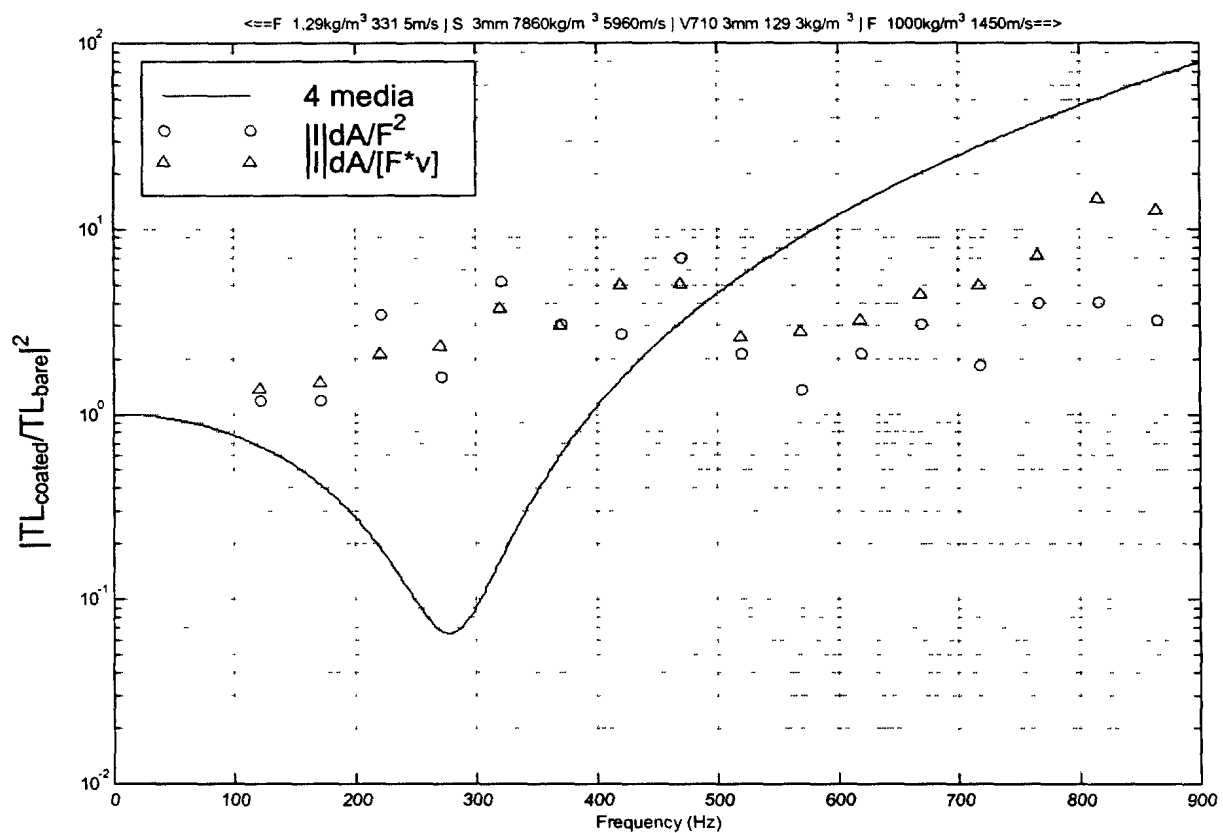
Appendix-G
Decoupling Performance: Prediction vs Calculated



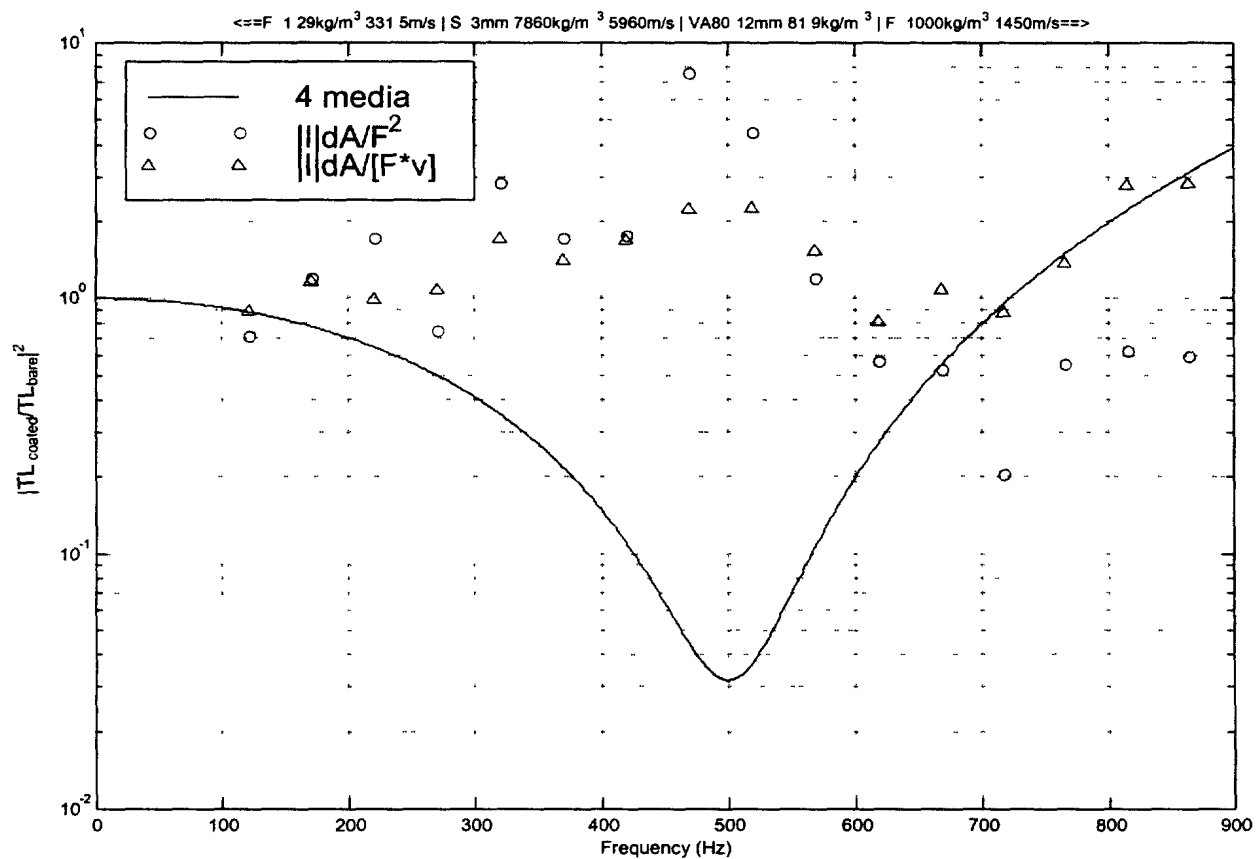
Decoupling Performance: 25mm SC4116 on 9.5mm plate



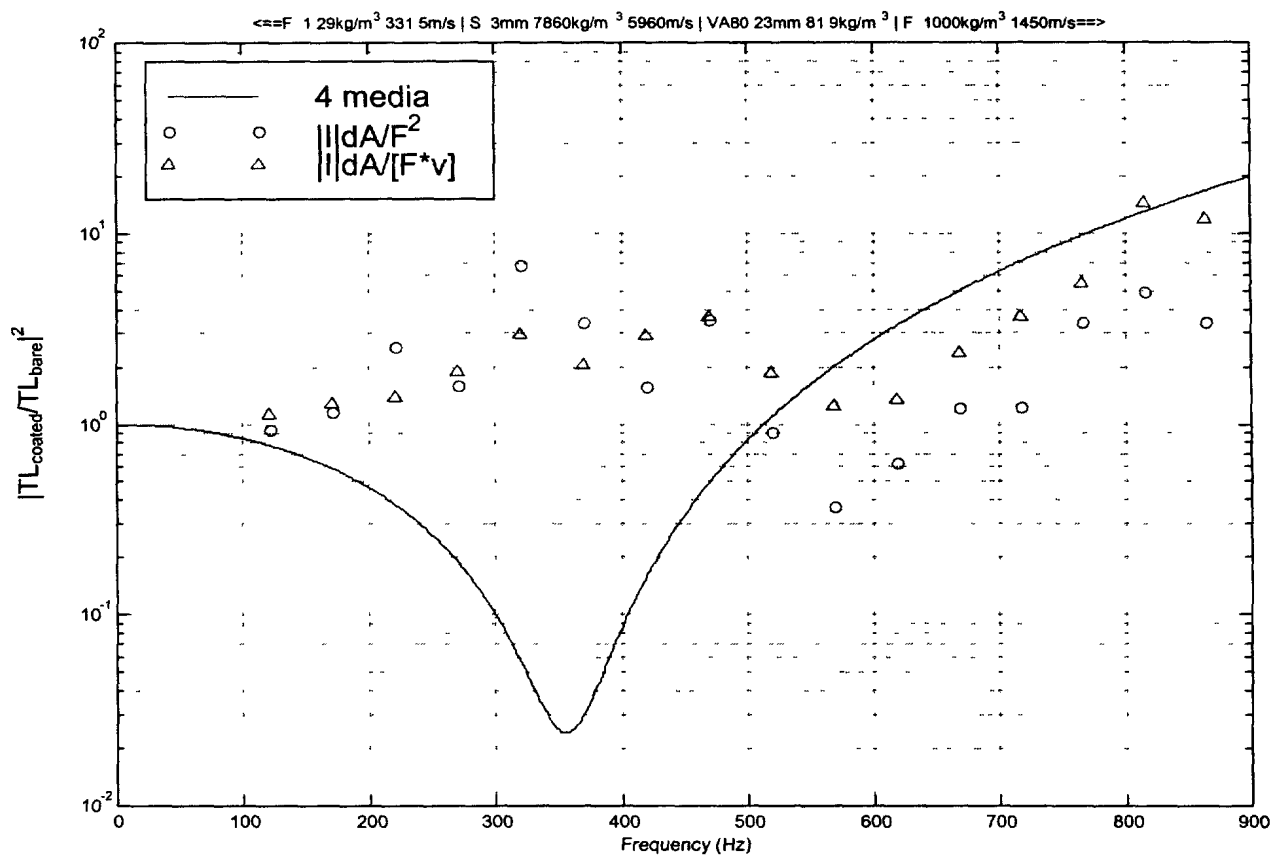
Decoupling Performance: 12mm VA80 on 9.5mm plate



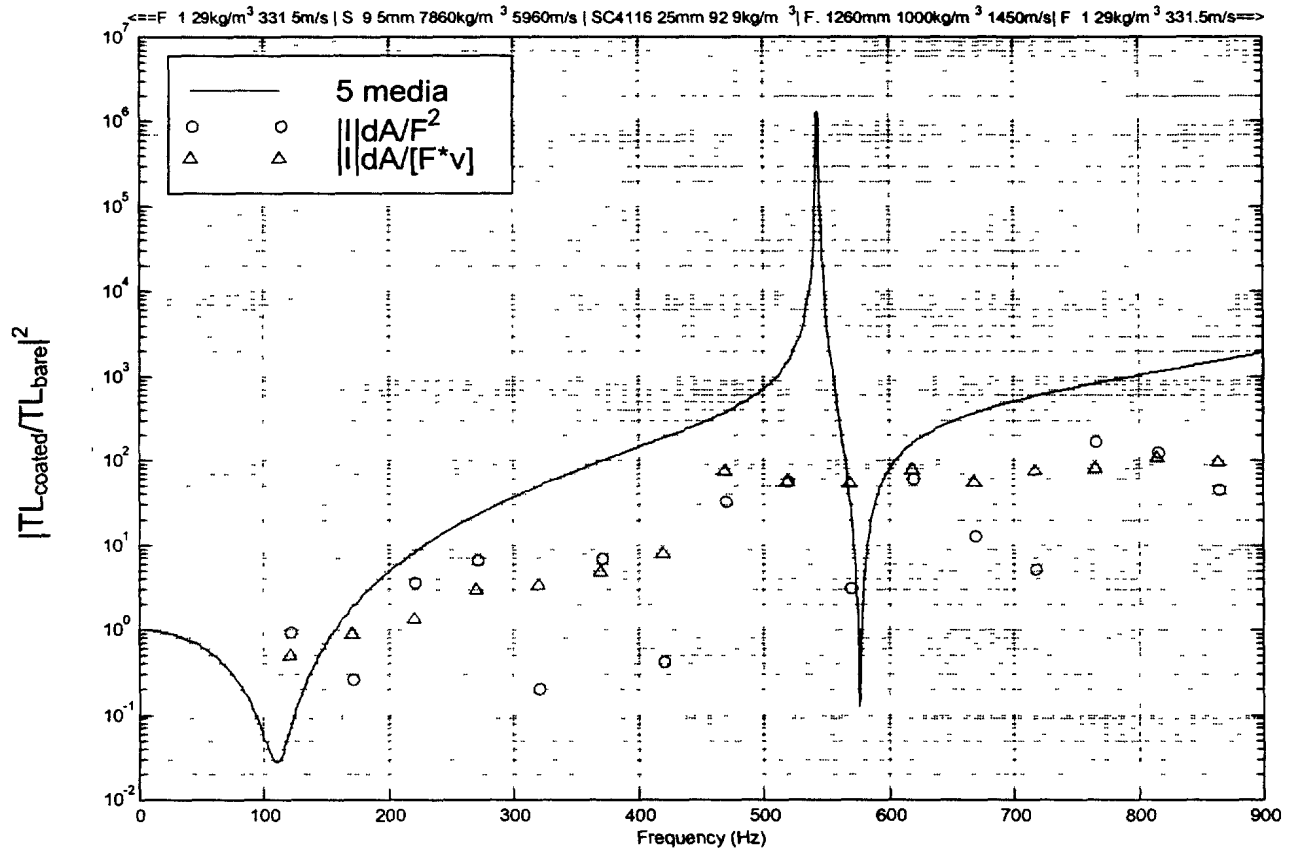
Decoupling Performance: 3mm V710 on 3mm plate



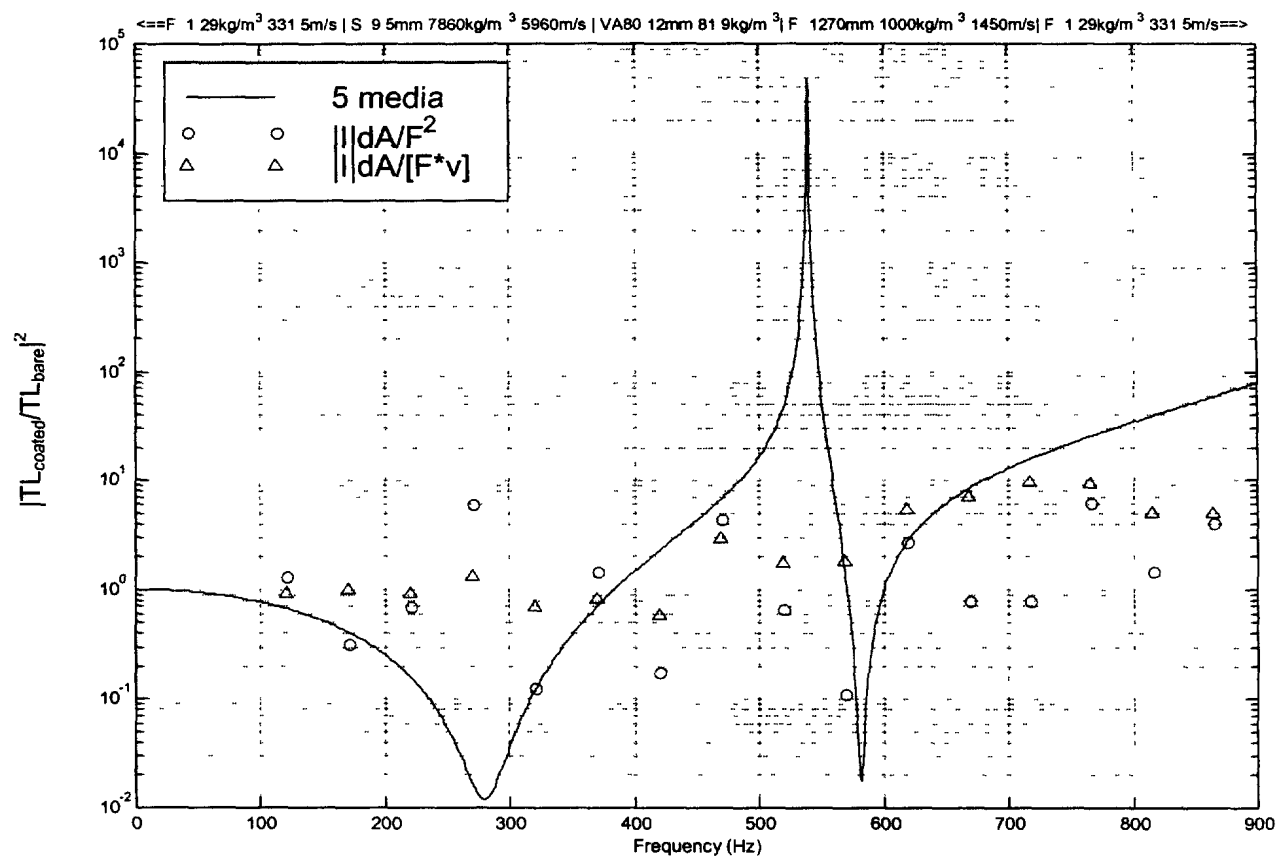
Decoupling Performance: 12mm VA80 on 3mm plate



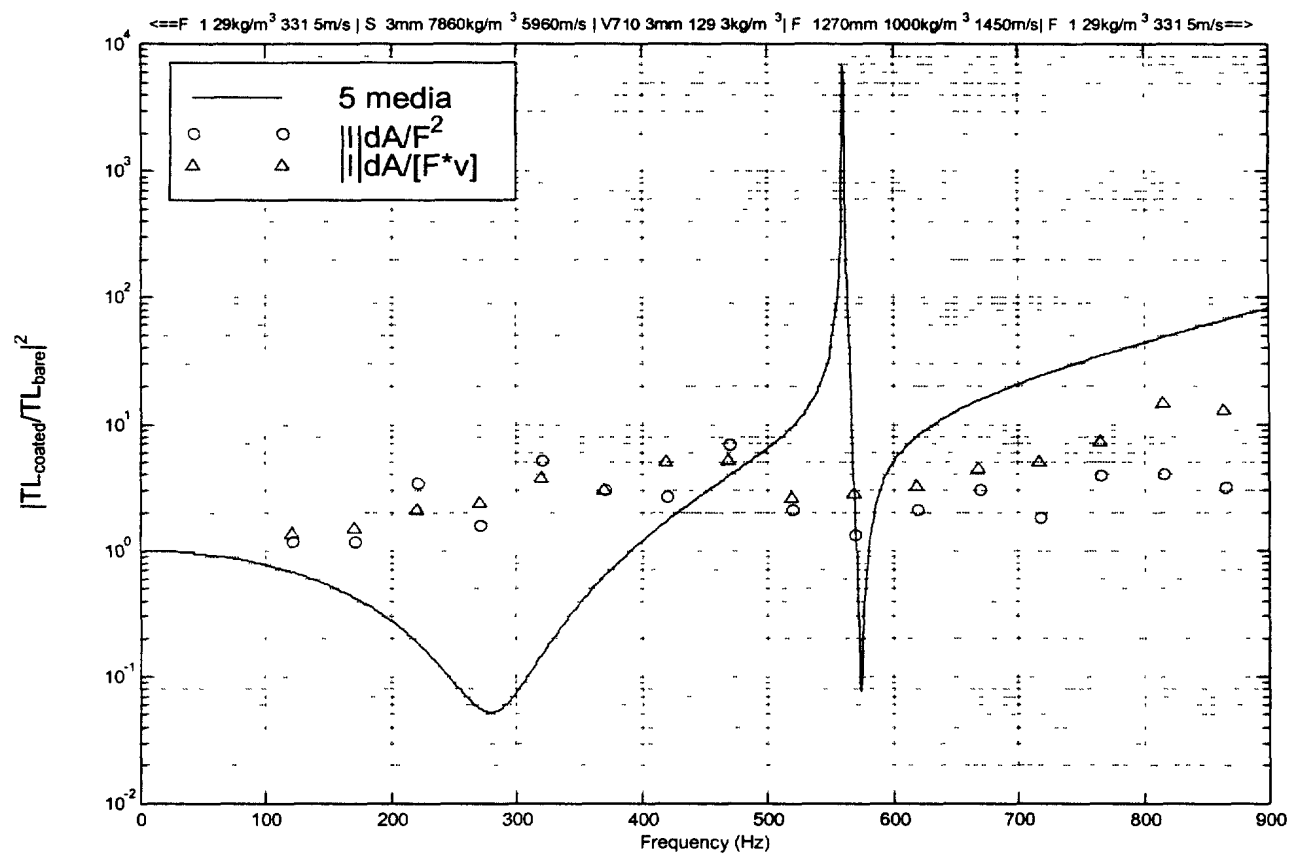
Decoupling Performance: 23mm VA80 on 3mm plate



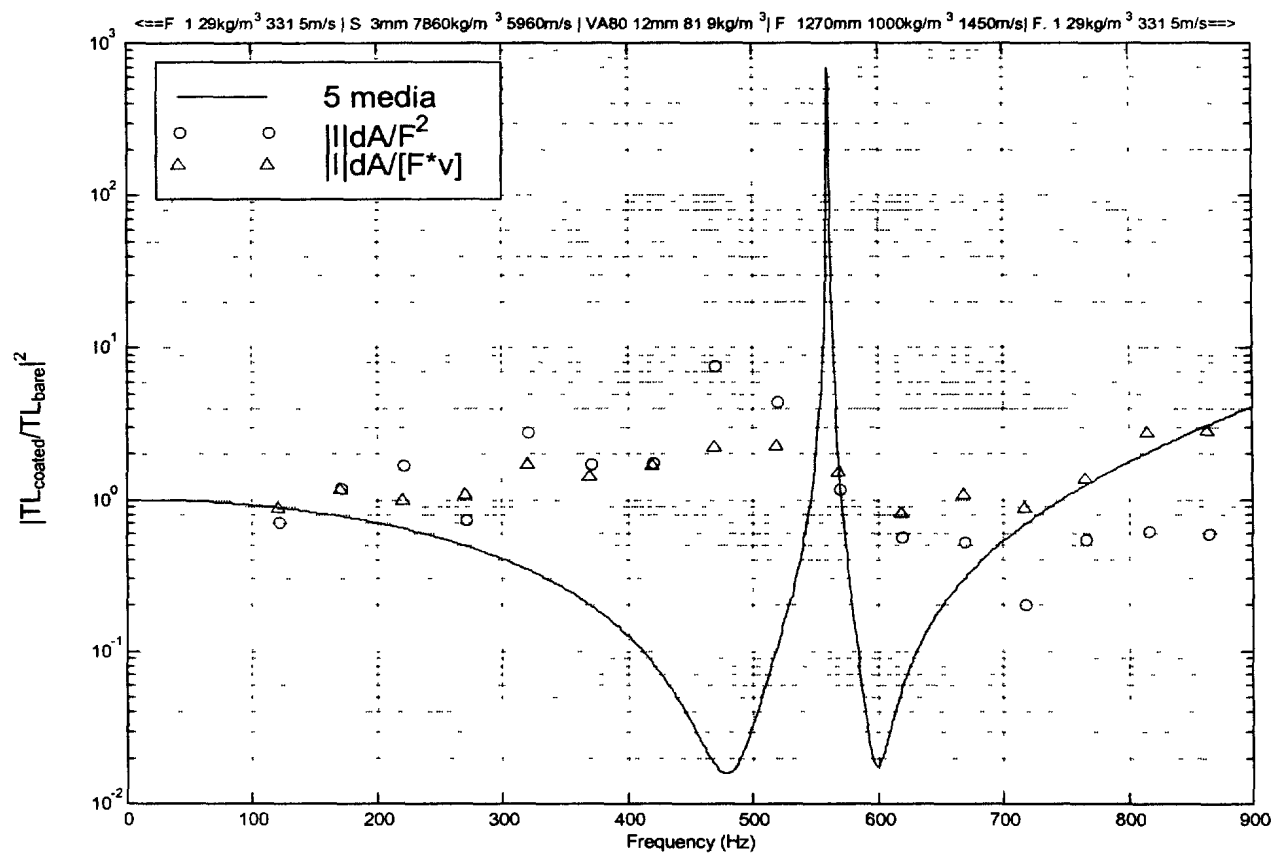
Decoupling Performance: 25mm SC4116 on 9.5mm plate



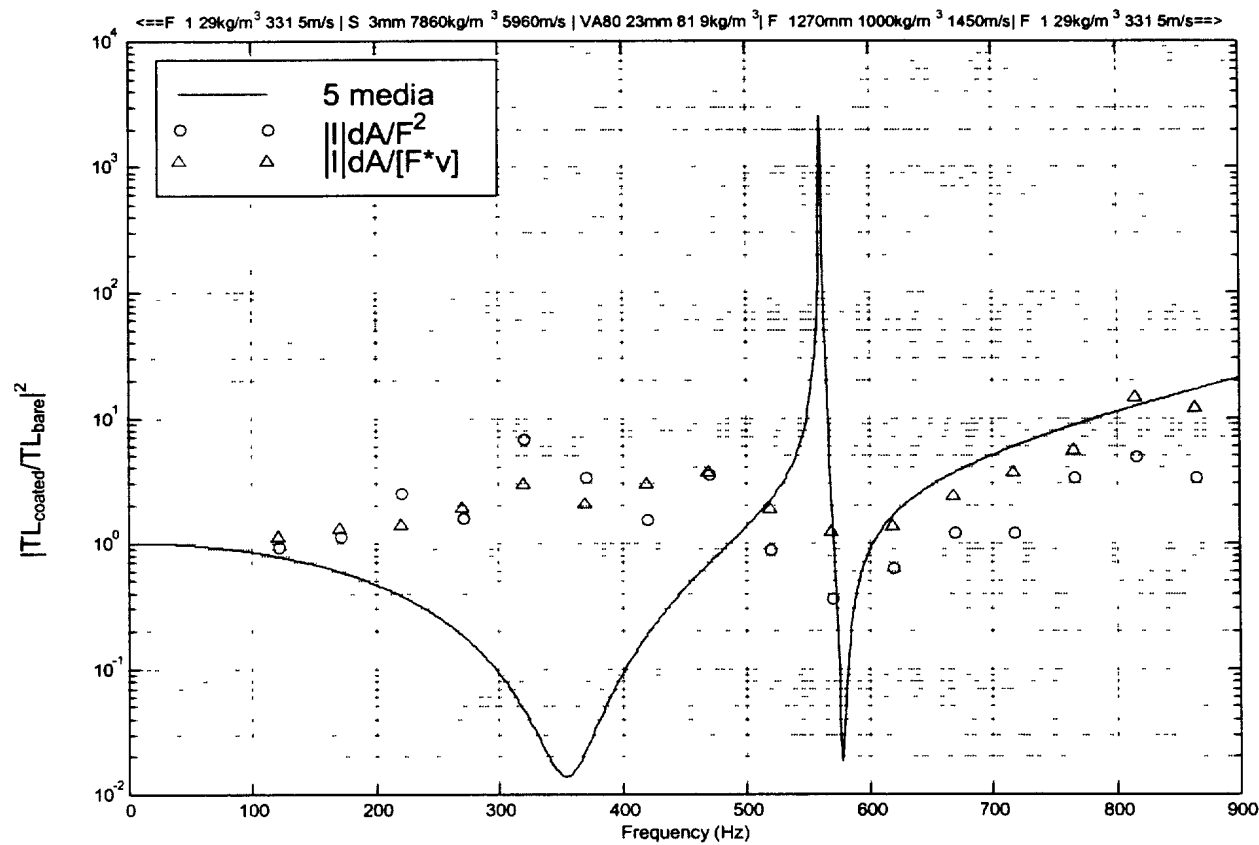
Decoupling Performance: 12mm VA80 on 9.5mm plate



Decoupling Performance: 3mm V710 on 3mm plate.



Decoupling Performance: 12mm VA80 on 3mm plate



Decoupling Performance: 23mm VA80 on 3mm plate

UNCLASSIFIED
SECURITY CLASSIFICATION OF FORM
(highest classification of Title, Abstract, Keywords)

DOCUMENT CONTROL DATA			
(Security classification of title, body of abstract and indexing annotation must be entered when the overall document is classified)			
1	ORIGINATOR (the name and address of the organization preparing the document. Organizations for whom the document was prepared, e.g. Establishment sponsoring a contractor's report, or tasking agency, are entered in section 8.) Guigné International Limited 685 St. Thomas Line Paradise, Newfoundland A1L 1C1	2	SECURITY CLASSIFICATION (overall security classification of the document including special warning terms if applicable) <p style="text-align: center; font-size: large;">Unclassified</p>
3	TITLE (the complete document title as indicated on the title page. Its classification should be indicated by the appropriate abbreviation (S,C,R or U) in parentheses after the title) Investigation of Decoupling Material Performance with a Transmission Loss Model and Acoustic Intensity Measurements		
4	AUTHORS (Last name, first name, middle initial. If military, show rank, e.g. Doe, Maj. John E.) K. Klein, Q. Liu, and J.Y. Guigné		
5	DATE OF PUBLICATION (month and year of publication of document) September 1999	6a	NO OF PAGES (total containing information. Include Annexes, Appendices, etc.) 127
		6b	NO OF REFS (total cited in document) 11
7	DESCRIPTIVE NOTES (the category of the document, e.g. technical report, technical note or memorandum. If appropriate, enter the type of report, e.g. interim, progress, summary, annual or final. Give the inclusive dates when a specific reporting period is covered.) DREA Contractor Report		
8	SPONSORING ACTIVITY (the name of the department, project office or laboratory sponsoring the research and development. Include the address.) Defence Research Establishment Atlantic P.O. Box 1012, Dartmouth, N.S. B2Y 3Z7		
9a	PROJECT OR GRANT NO. (if appropriate, the applicable research and development project or grant number under which the document was written. Please specify whether project or grant.) Project No. 1.g.h.14	9b	CONTRACT NO. (if appropriate, the applicable number under which the document was written) W7707-7-5409
10a	ORIGINATOR'S DOCUMENT NUMBER (the official document number by which the document is identified by the originating activity. This number must be unique to this document.)	10b	OTHER DOCUMENT NOS. (Any other numbers which may be assigned this document either by the originator or by the sponsor) <p style="text-align: center; font-size: large;">DREA CR 1999-127</p>
11	DOCUMENT AVAILABILITY (any limitations on further dissemination of the document, other than those imposed by security classification) <input checked="" type="checkbox"/> (X) Unlimited distribution <input type="checkbox"/> () Distribution limited to defence departments and defence contractors, further distribution only as approved <input type="checkbox"/> () Distribution limited to defence departments and Canadian defence contractors, further distribution only as approved <input type="checkbox"/> () Distribution limited to government departments and agencies, further distribution only as approved <input type="checkbox"/> () Distribution limited to defence departments, further distribution only as approved <input type="checkbox"/> () Other (please specify)		
12	DOCUMENT ANNOUNCEMENT (any limitation to the bibliographic announcement of this document. This will normally correspond to the Document Availability (11). However, where further distribution (beyond the audience specified in 11) is possible, a wider announcement audience may be selected.) <p style="text-align: center; font-size: large;">Unlimited</p>		

UNCLASSIFIED
SECURITY CLASSIFICATION OF FORM

13 **ABSTRACT** (a brief and factual summary of the document. It may also appear elsewhere in the body of the document itself. It is highly desirable that the abstract of classified documents be unclassified. Each paragraph of the abstract shall begin with an indication of the security classification of the information in the paragraph (unless the document itself is unclassified) represented as (S), (C), (R), or (U). It is not necessary to include here abstracts in both official languages unless the text is bilingual)

The complex dilatational moduli of three closed cell foam materials and one elastomeric material were determined by mechanical excitation of thin samples. The neoprene/EPT/SBR, polyvinylchloride, and ethylvinylacetate foams had moduli that ranged from 0.2 MPa to 3 MPa in the 100 – 900 Hz frequency range. The decoupling performance of these materials was then determined by applying them to steel substrates that were mechanically excited, and measuring the effect of the coatings on the radiated sound. Unlike previous studies where the test plates were supported at the corners and semi-submerged, in this study the plates were clamped at the edges and backed by an air filled concrete enclosure. This "concrete box" was submerged into a water filled tank and the radiated sound was determined by intensity mapping in the near field of the plate. Because the net radiated acoustic power was not uniformly positive across the frequency range studied (100 – 900 Hz), a quantity related to the near field acoustic

power, $\sum |\vec{I}| dA$, was used to quantify the effect of the coating. The experimental

decoupling behaviour of the coatings was compared to that predicted by a one dimensional transmission loss model for the 4 layer system: air/ steel/ coating/ water; or for the 5 layer system that included the finite dimensions of the water layer in the tank: air/ steel/ coating/ water/ air. Several of the substrate/ coating combinations were predicted to have large decoupling amplification peaks based on their measured material properties and the one dimensional model. Experimentally, these peaks were either much smaller than predicted or not observed at all. This discrepancy was explained by the fact that edges of the steel substrate were clamped, precluding a mass-spring resonance effect which is responsible for the amplification.

14 **KEYWORDS, DESCRIPTORS or IDENTIFIERS** (technically meaningful terms or short phrases that characterize a document and could be helpful in cataloguing the document. They should be selected so that no security classification is required. Identifiers, such as equipment model designation, trade name, military project code name, geographic location may also be included. If possible keywords should be selected from a published thesaurus e.g. Thesaurus of Engineering and Scientific Terms (TEST) and that thesaurus-identified. If it not possible to select indexing terms which are Unclassified, the classification of each should be indicated as with the title)

decoupling
damping
noise reduction
intensity
transmission loss

UNCLASSIFIED

SECURITY CLASSIFICATION OF FORM

The Defence Research
and Development Branch
provides Science and
Technology leadership
in the advancement and
maintenance of Canada's
defence capabilities.

Leader en sciences et
technologie de la défense,
la Direction de la recherche
et du développement pour
la défense contribue
à maintenir et à
accroître les compétences
du Canada dans
ce domaine.

#513477

CA001524



www.crad.dnd.ca